Thèse

Pour l'obtention du diplôme de

Docteur de l'Université Lille 1 – Sciences et Technologies

Ecole Doctorale : Sciences de la Matière, du Rayonnement et de l'Environnement

(ED SMRE)

Unité de catalyse et de la chimie du solide (UCCS UMR-8181)

Discipline : Molécules et Matière Condensée (N° d'ordre : 42387)

Maha AMMOURY

Synthèse de Propylène à Partir de l'Éthanol

Directeur de thèse : Mickaël CAPRON

Co-directeur de thèse : Benjamin Katryniok

Soutenance le 20 juin, 2017 devant la commission d'examen

Rapporteurs : **Pascal FONGARLAND** : Professeur au Laboratoire de Génie des Procédés Catalytiques (LGPC), Université Claude Bernard Lyon 1.

Franck RATABOUL : Chargé de Recherche CNRS à l'Institut de Recherche sur la Catalyse et l'Environnement de Lyon (IRCELyon), Université Claude Bernard Lyon 1.

Examinateurs : **Franck DUMEIGNIL** : Professeur à l'Unité de Catalyse et de Chimie du Solide (UCCS), Université Lille 1 - Sciences et Technologies

Thesis

To obtain the diploma of

Doctor of the University Lille 1 – Sciences and Technology

Doctoral School: Sciences of Matter, Radiation and Environment

(ED SMRE)

Unity of Catalysis and Solid State Chemistry (UCCS UMR-8181)

Academic Field: Molecules and Condensed Matter (Order N°: 42387)

Maha AMMOURY

Synthesis of Propylene from Ethanol

Thesis director : Mickaël CAPRON

Thesis Co-director : Benjamin Katryniok

Defense the 20th June, 2017 before the committee members

Referees: **Pascal FONGARLAND** : Professor at the Catalytic Process Engineering Laboratory (LGPC), University Claude Bernard Lyon 1.

Franck RATABOUL : CNRS Researcher at the Institute of Research on Catalysis and the Environment of Lyon (IRCELyon), University Claude Bernard Lyon 1.

Examiners : **Franck DUMEIGNIL** : Professor at the Unity of Catalysis and Solid State Chemistry (UCCS), University Lille 1 - Sciences and Technologies

Acknowledgments

I want to say I have a long list of thanks yous. This thesis was carried out among the heterogeneous catalysis team of the "Unité de Catalyse et de Chimie de Solide"-UCCS-UMR CNRS 8181. This research unity is directed by Prof Franck Dumeignil, professor at Université de Lille 1, that I thank him for welcoming me to his team and his laboratory.

I wanted to say thank you for Université de Lille 1 for financing the research project, "Synthesis of Propylene from Ethanol". Thanks also to École Centrale de Lille for taking a contribution in the financing.

I would also like to thank the jury members, Mr Pascal Fongarland, Professor at the LGPC, Mr Franck Rataboul, CNRS Researcher at IRCELyon, Mr Franck Dumeignil, Professor at the UCCS, for accepting to judge my work.

I want to say a big thank you to my supervisor in this project dr Mickaël Capron, associate professor at Université de Lille 1, and my co-supervisor dr Benjamin Katryniok, associate professor at Université de Lille 1. Being present since three years and a half in this lab, they allowed to valorize my knowledge, to make myself autonomous and ready for the future. I learned a lot from their wide scientific knowledge and experience. They also brought me a lot as a person by their humanitarian manners.

I got several valuable accompaniments during my thesis. Thanks for de dr Svetlana Heyte, a research engineer at Realcat platform-Lille, for helping me perform my experiments at Realcat. Here in between, I would like to thank the Realcat team headed by Prof Sébastien Paul, for giving me the opportunity to perform a part of my experiments there. Thanks to dr Marcia Araque-Marin for supervising part of my work. To drs Jérémy Faye and Guillaume Tesquet for their follow up of the start-up. Additionally, I would like to thank the International Joint Laboratory in Hokkaido University-Japan for realizing part of the experiments there, particularly I specify Prof Kenichi Shimizu and Mr Guillaume Pomalaza.

I would also like to express all my gratitude to all the engineers and the responsibles of the analysis techniques in our lab for their involvements, their skills and their extreme kindness. Thank you to Mr Jean-Charles Morin for the IR studies. To Mr Olivier Gardoll for the porosimetry and the TGA-MS analyses. To Mrs Pascale Dewalle for BET analyses. To Mrs Martine Trentesaux for the XPS analyses. To dr Joelle Thuriot for the XRF analyses. To Mrs Laurence Burylo for the XRD analyses. Without these people no project could be carried out properly so again, thank you.

I arrive to my PhD colleagues, who also carry out professional-quality work in their respective projects. We were working like a team in this international family. Anyway many of them became friends. You guys are amazing. I would like also to thank all the administratives and secretaries in the lab. To Mr David Porier, and Mrs Barbara Declerck, Virginie Buchet and Sandrine Breton.

Acknowledgments

Apart from the lab, I would like to thank the French government for all its facilitations to help me realize this thesis (residence cards, CROUS dormitory, CROUS restaurants…). Thanks also for the French people for their kind hospitality. It felt like home. I want to say also a big thank you to my loving family for their emotional support throughout my PhD. Finally, I would like to dedicate this thesis to my dad for supporting me in my early steps in the research domain.

Table of Contents

Table of Contents

Table of Contents

Introduction

Introduction

Propylene is the second most important starting product in the petrochemical industry – just after ethylene. It is used for the production of important chemicals such as polypropylene, propylene oxide, acrylonitrile, and acrylic acid etc. These four aforementioned chemical compounds are the main global propylene derivative markets, whereby polypropylene accounts for two thirds of the total demand of propylene. Polypropylene is a polymer used in plastic industry, as in packaging and labeling, textiles, and reusable containers etc.

Propylene is produced from fossil fuels, such as petroleum and natural gas. Hereby, propene is a byproduct of oil refining and natural gas processing – namely from the cracking units. During the oil refining process, larger hydrocarbon molecules are cracked into smaller ones in order to convert less valuable products into more useful and valuable ones. As a matter of fact, most of the gasoline/petrol is produced by cracking. Naphtha cracking is a type of oil refining process which is considered as a major source of propylene. In this process, the targeted product is ethylene, but propylene is formed as a co-product. In the separation section of steam cracking of naphtha, ethylene formed is 24% among all resulting products, while propylene percentage is 20%.

However, the demand for propylene derivatives is increasing worldwide. Meanwhile, petrochemical producers continue to shift to lighter steam cracker feedstocks than traditional oil refining cracks, resulting in relatively lower propylene yields. Also, other reasons for decreased production of propylene include the reduced motor gasoline demand. All these reasons are driving petrochemical industry leaders to look for alternative sources and technologies for its production, as well as to develop strategies to maximize profitability through downstream derivative markets. The solution of this problem lies in on-purpose production methods for propylene, including: olefin metathesis, propane dehydrogenation (PDH), methanol-to-propene (MTO) and ethanol-to-olefins (ETO).

According to the Petrochemical Special Report on European Petrochemical Outlook 2016 released on January 2016, Dow enterprise opened its PDH plant in Freeport, Texas in October 2015 as part of the move to produce more propylene in the US. In 2016 Russian propylene imports are expected to increase by 60,000-100,000 metric tons/year. Japan's Ministry of Economy, Trade and Industry in its latest forecast sees the Asian surplus increasing to 331,000 mt in 2016, 596,000 mt in 2017 and 901,000 mt in 2018. Also in China many new CTO/MTO plants (acronym, methanol and coal to olefins) are expected from 2016, producing another 1.3 million mt/year of propylene – these will be linked to PP (polypropylene) plants producing an equal amount of polyolefin. However, how many of these come online with crude oil at sub-$40/b remains to be seen.

But why do we need a price below $40/b?! An expert such as Paolo Moretti, former Purchasing Director at Dow Chemical and who understands the important relationship

between the value of crude oil and the price of many basic chemicals including ethylene and propylene. He wrote in his blog the following on why the price of crude oil had crushed since its relatively stable high of around $100 per barrel just a few years ago: “My own view is that global oil prices declined in order to delay Shale Gas (mainly in the U.S.) investments and further production.” (blog, 2016)

In 2016, crude oil price was predicted as 50 US$/BBL while that of ethylene 29-31 US$ cts/lb and that of propylene 34-39 US$ cts/lb. For 2017, they are predicted as: $60, $33-37 and $39-45 for crude oil, ethylene and propylene respectively. Moretti adds: “Let us be very clear that the prices of Ethylene and Propylene are driven by the feedstock but also by the supply-demand balance of each one, as well as other derivatives. For example, Ethylene pricing depends on demand for middle-distillate products like gasoline, diesel, and heating oil. Additionally, propane pricing represents a ceiling price for Ethane. As a result of all these drivers, Ethylene and Propylene prices have presented a delta (Propylene less Ethylene) between -$5 in 2000 to +$20 in 2011. Therefore, the prices may fluctuate much more than the predicted ones.” Predicting the future chemical prices is a thankless task, the blogger sums up (blog, 2016).

On-purpose propylene production processes are numerous and are applied worldwide. In China, Korea and India, these processes run in parallel with crackers leading to an increase in the production capacity of propylene in 2016. In the methanol-to-propene (MTP) process, synthetic gas (syngas) is converted to methanol, and then methanol converts to ethylene and/or propene. Synthetic gas is a fuel mixture consisting primarily of hydrogen and carbon monoxide. Another on-purpose production method is the ethanol-to-olefins conversion. Ethanol is more common in our lives than we may think. Most of the world’s ethanol is produced by fermentation of crops (93%) with synthetic ethanol (7%) being produced by direct catalytic hydration of ethene. In the latter process, ethanol is obtained by reacting ethene with steam, using phosphoric acid adsorbed on the surface of a solid (silica) as a catalyst in fixed bed reactors. The reaction is reversible and exothermic.

Ethanol can be produced synthetically by ethane hydration. Concerning this process, only 5% of the ethene is converted into ethanol at each pass through the reactor. By removing the ethanol from the equilibrium mixture, it is possible to achieve an overall conversion of 95%. According to an article amended in November 2013, the total annual production of synthetic ethanol is 850 000 tons in the world. The main uses of ethanol produced from ethene are as the chemical intermediate for: glycol ethers, ethanol amines (ethylamines) and ethyl propenoate. It is also used as a solvent in the manufacture of cosmetics, pharmaceuticals, detergents, inks and coatings. One of the main drawbacks of producing ethanol using ethene hydration is that ethene itself is a precious chemical as it is the most important starting product in the petrochemical industry, as it is used to make many polymers. Rather, bioethanol has become an important source of ethene nowadays, and not the reverse.

Ethanol can also be produced from crops. The fermentation of plant material (for example, barley and rice) is the route by which alcoholic drinks (e.g. beer, whiskey, gin and

vodka) are produced. Concerning the uses of bioethanol, the most important is the application as a fuel for cars but an increasing interest is also in the use as a feedstock for the synthesis of ethene by dehydration – the reverse reaction to the aforementioned hydration. Bioethanol produced has a very high purity, and is chemically indistinguishable from industrially-produced ethanol (*i.e.* ethanol produces from fossil resources). In the present work, we intended to convert ethanol to propylene using heterogeneous catalysts. There are many reasons why choosing bioethanol as the starting material:

- greater security of supply and less dependence on imports

- conservation of fossil fuels

- interest in environmental issues

- process of converting and burning bio-ethanol is carbon-neutral

- demand of ethanol as a substitute of gasoline is rapidly increasing

- demand of ethanol as a blend with gasoline

- innovative new industry offering potential for rural areas

- industrial ethanol production processes are costly

The European bioethanol production amounted to 1592 million liters in 2013. With 231 million liters, Germany is the leading producer. According to an ECN report, present cost for ethanol derived from sugar and starch crops is about 0.32-0.53€/liter, which makes bioethanol a cheap chemical. Basically, five steps are included in ethanol production composed of grinding, cooking, fermentation, distillation and water removal.

So, converting ethanol to propylene in one step is as killing two birds with one stone: From one hand, we are getting cheap ethanol and protecting the environment. From the other hand, we are producing a valuable platform molecule, namely propylene.

We will present in the following chapters of the manuscript a bibliographic review, experiments done, results obtained and results interpretation. Chapter 1 will be a bibliographic part. It sums up works that have been done by other researchers on the reaction of ethanol or ethene to propylene, olefins or aromatics products. It discusses all catalysts used in this reaction (mesoporous catalysts, ZSM-5 zeolites, SAPO-34 zeotypes…). The second chapter explains catalysts preparation methods and different set-ups and techniques used to test and characterize the catalysts, respectively.

The following two chapters are the results ones. Prescreening chapter is a preliminary study on supports to select the most appropriate ones. Some are commercial, and some are laboratory-made. It includes testing and characterization results as well. Raw supports were tested in both calcined and non-calcined states. The refined screening chapter includes a

study of further treatments done for the best-performing supports. These include impregnation, hydrothermal treatment etc. Every chapter is ended up by a conclusion to summarize the most important results. The manuscript is finish by an overall conclusion and perspectives, to ameliorate the catalysts and scale-up the reaction.

As a final remark, this project was done in collaboration between UCCS laboratory-Lille and the International Joint Laboratory-Hokkaido University-Japan.

blog, S. (2016, September 16). Thoughts on Predicting Crude Oil, Ethylene and Propylene Prices for 2017.

Chapter 1: Bibliography

Chapter 1. Bibliography

1.1. Catalysts Employed in the Ethanol-to-Propylene Reaction

The one-step conversion of ethanol or ethylene into propylene has caught a great attention in order to adjust the production of both olefins to the market requirements, since both molecules are the most important starting products in the petrochemical industry.

Three different mechanisms have been reported in literature:

a) The metathesis route has been suggested to occur over metallic catalysts (Ni, Mo, W) supported on different mesoporous materials (MCM-41, γ-Al_2O_3). It takes place in two consecutive steps: firstly, ethylene dimerizes into butenes and, secondly the butenes and ethylene undergo metathesis to form propylene.
b) The oligomerization-cracking route, which has been studied on acid microporous (HZSM-5, HX, HY, Hβ, HMOR, MCM-22, SAPO-34, SAPO-44, SAPO-18) and mesoporous (Al-SBA-15, Al-MCM-41) materials.

Other authors suggest a third mechanism to occur over microporous catalysts; i.e., the radical mechanism. It has been reported for ZSM-5 zeolites. Nevertheless, it occurs rather similar to the oligomerization-cracking route (*i.e.* hydrocarbon pool mechanism). Throughout this chapter, the difference between the three mechanisms will be explained.

1.1.1. Microporous Catalysts

Zeolites are well-defined microporous (<2 nm) crystalline aluminosilicate materials containing a one-, two-, or three-dimensional pore structure system. Zeolites are made by SiO_4 tetrahedra, which are connected via oxygen atoms. Pure siliceous zeolites are electrically neutral. An ion-exchangeable cationic site in the lattice is created through the substitution of a tetrahedrally coordinated silicon atom with a charge of 4^+ (Si^{4+}) by an atom with a charge of 3^+ (Al^{3+}) (J.A. Lercher, 2008). These sites are locations for redox and/or acid/base chemical reactions, depending on the nature of the charge balancing cations. In Figure 1.**1**, we see the kinetic diameter of zeolites, while in Table 1.1 we see examples of catalysts of different pore sizes of zeolites and their catalytic applications.

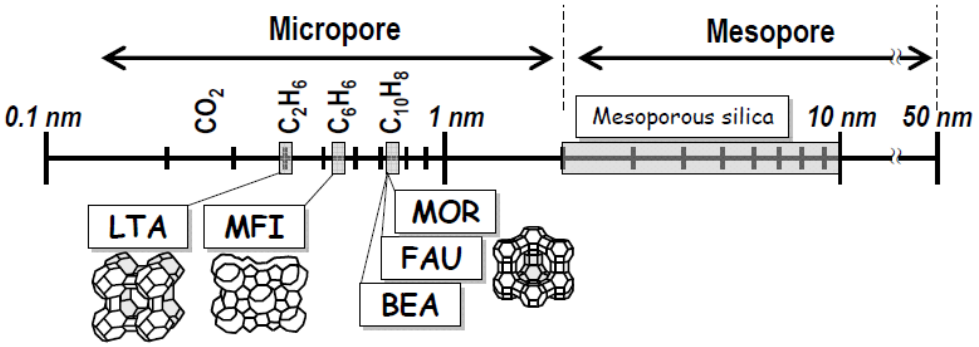

Figure 1.1. Kinetic diameter of some molecules and zeolites (T. Tago, 2010)

Table 1.1. Applications of zeolites and metallic catalysts in the chemical industry (D.C. Sherrington, 2001)

Zeolites	*Pore size(nm)*	*Catalysts*	*Applications*
8 Membered rings	0,3-0,45	A	n/iso butene separation, ion exchange
10 Membered rings	0,45-0,6	MFI	xylene isomerization, isomerization, dewaxing, methanol to olefins
		Ga_2O_3 -HMFI	aromatization
12 Membered rings	0,6-0,8	Y,Beta,FAU	cracking,isomerization, fluid catalytic cracking
		Pd/HFAU	isomerization aromatics
Metallic catalysts	>2nm	Fe_2O_3, Cr_2O_3,Pt	dehydrogenation, watergas shift reaction, …

On zeolites, different mechanisms are proposed for the ethanol-to-propylene reaction. Literature reports indicate that the distribution of products obtained in the zeolitic ethanol conversion is strongly dependent on the acidity as well as the channel structure of the zeolites. However, there are no reports concerning ethanol conversion on isomorphously framework-substitued zeolites, which show different acid strengths (Y. Furumoto N. T., 2012). By referring to D. Goto *et al.*, they consider that no matter what is the type of zeolite catalyst used, a general reaction mechanism occurs for the conversion of ethanol involving the following pathways: (1) the dehydration of ethanol into ethylene, (2) the oligomerization of ethylene into higher olefins, and (3) the cracking and/or aromatization of higher olefins. B. Lin *et al*. speculate that the cracking of the oligomeric intermediates may lead to the formation of propylene (B. Lin, 2009). This is called the "cracking mechanism" or the "oligomerization-cracking" mechanism. Since the cracking of light olefins proceeds at high temperatures, the thermal stability of zeolitic catalysts is a crucial factor (D. Goto, 2010). For this reason, we will discuss in this bibliographic chapter together the transformation of ethanol and ethylene knowing that the acidity needed to transform ethylene into higher olefin is enough to dehydrate the ethanol into ethylene.

1.1.1.a. ZSM-5

Among the microporous catalysts, ZSM5 like materials have been highly studied. The three-dimensional network in HZSM-5 zeolite is created by 10 ring channels running parallel (5.6 Å X 5.3 Å) intersected by 10 ring sinusoidal channels (5.5 Å X 5.1 Å) with an internal pore space of 6.36 Å [Figure 1.**2**;Figure 1.**3**]. It is an MFI structure-type zeolite; i.e., Mordenite Framework Inverted (zeolites). An outstanding feature of the microporous HZSM-5 is that it converts alcohol compounds to hydrocarbons. However, the same microporous structure causes the product selectivity discrimination to limit the carbon number to ~ C_{10} (J. Jae, 2011).

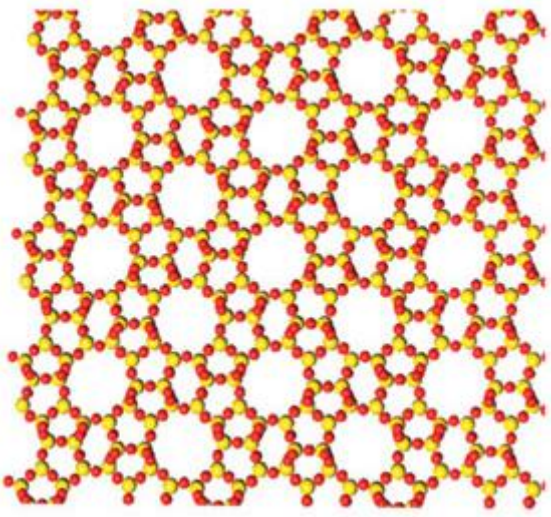

Figure 1.2. The molecular structure of MFI zeolite, showing well defined pores and channels in the zeolite. Yellow balls are Si and red balls are O atoms.

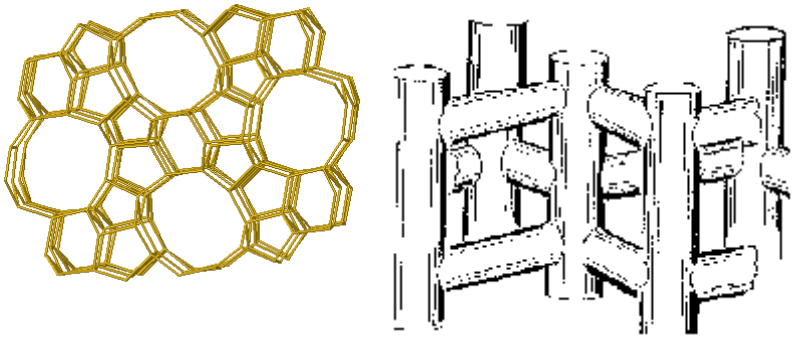

Figure 1.3. MFI structure (Commision, I.T.S. , 2012) (left), HZSM-5 structure (Conversion of ethanol to gasoline range hydrocarbons using a zeolite catalyst) (right)

The generally agreed route for the ethanol-to-hydrocarbons reaction over microporous materials (*e.g.* HZSM-5, HX, HMOR, HY, Hβ, MCM-22, SAPO-34, SAPO-44, SAPO-18) is the oligomerization-cracking one (E. Epelde, 2014). In the case of zeolite catalysts in general, ethylene formed undergoes disproportionation and condensation (K. Murata, 2008), and the ethyl group is added to the olefin chain. Among 11 kinds of molecular sieves examined by B. Lin *et al.*, H-ZSM-5 exhibited the highest activity for the direct conversion of ethylene to propylene (B. Lin, 2009). The conversion of ethylene was 58% and the selectivities to propylene and butenes were 42% and 21% respectively, over H-ZSM-5 at 450 °C. According to E. Epelde *et al*., the high performance of HZSM-5 zeolite in the light olefin production, is directly related to its moderate acidity and its three-dimensional porous structure, without cages in the intersections of the pores, facilitating the diffusion of the reactant and thus minimizing the retention of coke precursors (E. Epelde, 2014).

Murata *et al* go deeper in the understanding of mechanism taking place using these materials. To reach this goal, they used FT-IR spectroscopic measurements on H-ZSM-5 catalysts which allowed gaining more information about the reaction mechanism. They

evidence that propylene and butenes are formed as the main products from ethylene, while aromatics, propane, and butanes are mostly produced from these primary products. Among the products form, they also show the presence of aromatics such as benzene, toluene, and xylene (BTX), gasoline and kerosene range hydrocarbons (heavier products) and C_1-C_4 saturated hydrocarbons (K. Murata, 2008). Among these aromatics are alkylated benzene carbocations, which are active aromatic species that can release propylene through cracking. Hydrogenation of olefins gives C_1-C_4 saturated hydrocarbons, and other paraffins (Figure 1.4). It has to be noted that M. Inaba *et al.* proposed another reaction pathway whereby diethyl ether participated in the formation of olefins as well (Figure 1.5) (M. Inaba K. M., 2006).

There appears to be a correlation between ethylene selectivity and propylene selectivity, a weak reverse correlation between paraffin (alkanes) selectivity and propylene selectivity, and a reverse correlation between selectivity for aromatics and propylene selectivity (M. Inaba K. M., 2011). Deposited carbon and framework collapse suppress the formation of aromatics, and this suppression may result in: (1) increase in selectivity for C_{3+} olefins and propylene, and (2) decrease in the selectivity for C_{3+} olefins and propylene (M. Inaba K. M., 2011).

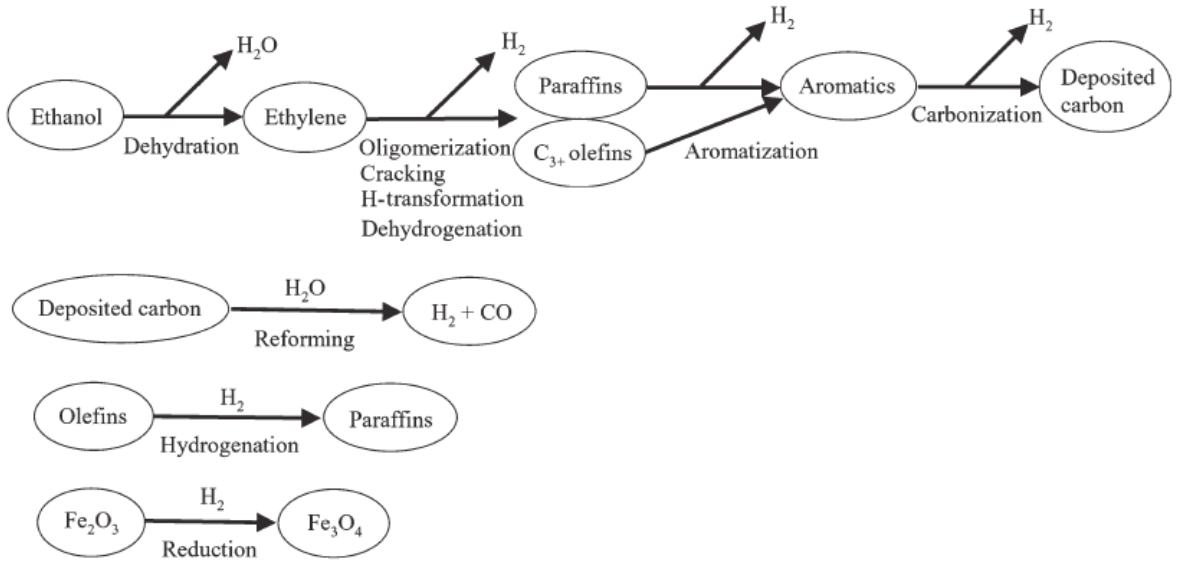

Figure 1.4. Supposed Reaction Pathway over ZSM-5 Catalysts (M. Inaba K. M., 2007)

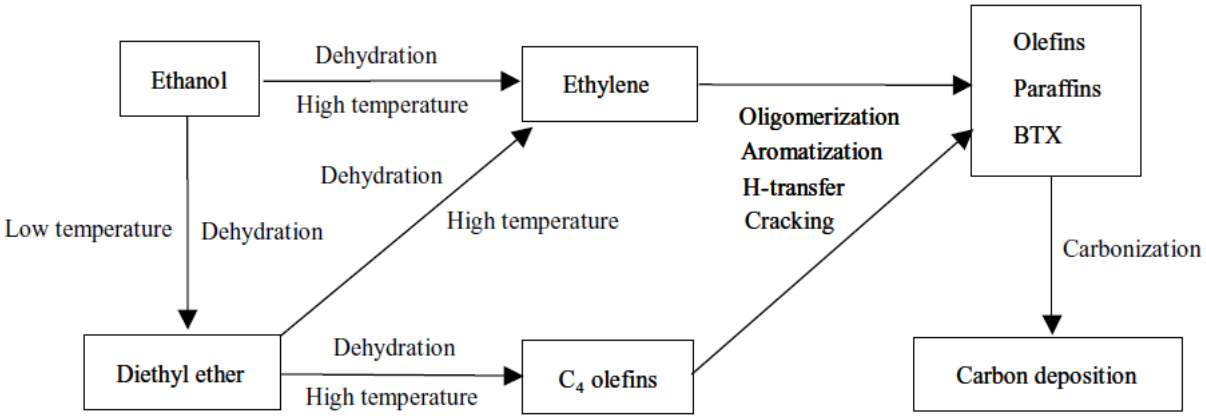

Figure 1.5. Supposed Reaction Pathway over ZSM-5 Catalysts (M. Inaba K. M., 2006)

Another mechanism proposed in literature for the direct conversion of ethylene or ethanol into propylene, without passing through the hydrocarbon pool mechanism was proposed by A. Takahashi *et al.* They used NH_4-ZSM-5 zeolites with Si/Al ratios of 80 (CBV 80) and 280 (CBV 280) obtained from Zeolyst International. Before the catalytic tests were performed, the NH_4-ZSM-5 samples were calcined in air at 600 °C for 4 h to obtain H-ZSM-5 samples. The authors examined the product distribution of the reaction over ZSM-5 for both Si/Al ratios as a function of contact time. At short contact times (W/F= 5.0 X 10^{-4} g cm^{-3} min), no ethers were observed and the main product was ethylene, whereby the latter decreased continuously with increasing contact time. On the other hand, the yields of propylene and butenes increased with increasing contact time. No aromatics or paraffins were produced at any contact time. The maximum propylene yield was 27% at W/F= 2.5 X 10^{-3} g cm^{-3} min. In contrast, the maximum of ethylene 39% was at W/F= 0.5 X 10^{-3} g cm^{-3} min (A. Takahashi W. X., 2013). These results indicate that over ZSM-5, ethanol was converted to propylene and butenes directly from ethylene, and not through the cracking of higher olefins and paraffins. In this mechanism, ethanol undergoes an intramolecular dehydration to yield ethylene. No ethers (e.g. diethyl ether) were observed, and ethylene was the only product, indicating that the initial reaction was not an intermolecular dehydration reaction, but rather intramolecular. Then, ethylene transforms to a carbene species via a π–complex on ZSM-5 (Eq. 1), and the carbene reacts with ethylene to form propylene (Eq. 2). Furthermore, ethylene also converts to butenes by dimerization (Eq. 3) (A. Takahashi W. X., 2013). Even though this mechanism is claimed in literature, the formation of a carbene species is worth of discussing.

$$C_2H_4 \rightarrow (CH_2)_2 \qquad \text{(Eq. 1)}$$

$$CH_2 + C_2H_4 \rightarrow C_3H_6 \qquad \text{(Eq. 2)}$$

$$2C_2H_4 \rightarrow C_4H_8 \qquad \text{(Eq. 3)}$$

Another totally different reaction pathway from ethanol to propylene was discussed by L. Pinard *et al*. (L. Pinard, 2013) They suggested that propylene formed in the ethanol-to-hydrocarbons reaction isn't the one formed by the direct dehydration of ethanol into ethylene, followed by the oligomerization and cracking of the latter to give propylene. They claimed that propylene is formed at the late stages of the reaction, once olefins cyclizes to give aromatics. The nature of the active species in the hydrocarbon pool mechanism is believed to be cationic. However, some authors argument that these are not only cationic, but also radical. The authors herein suggest the involvement of cationic free radical aromatics. It is thus called a "modified hydrocarbon pool" mechanism.

In order to prove the understanding on the hydrocarbon pool mechanism, several techniques were employed. EPR spectroscopy measurements indicate the presence of long live free radicals inside the zeolites. A pairing mechanism occurs on cationic free radical aromatics (Figure 1.**6**). Afterwards, these ionic polyalkylbenzene species would undergo a reaction of dealkylation of the ramifications before being dehydrogenated. Propylene and

butane are believed to be produced by the dealkylation process. They subsequently transform into the remaining products observed through conjunct polymerization (oligomerization, isomerization, cyclization and hydrogen transfer) for aromatic and paraffin formation. This suggests that the deactivation would not be due to external coke formation as postulated by others but by a change in the nature of coke – from active, radical, light coke to inactive larger polyaromatics.

In order to prove this mechanism, Pinard *et al*. tested the impact of the radical inhibitor hydroquinone on ethanol conversion, products distribution and "coke" formation. The addition of hydroquinone manifested itself in the form of increased polyaromatic formation, as well as a decrease in C3+ hydrocarbons yield and an increased ethylene yield – typical of ethanol-to-hydrocarbons reaction deactivation over ZSM-5.

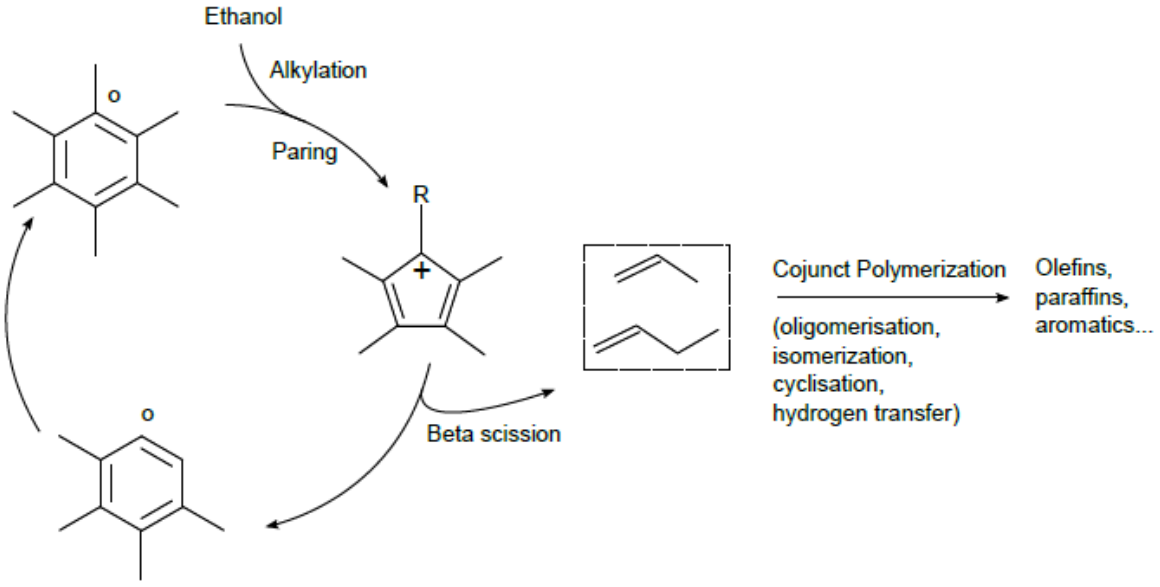

Figure 1.6. Hydrocarbon pool mechanism involving radicals, as proposed by Pinard *et al.* (L. Pinard, 2013)

- Acid strength and number of site:

A way to modify the acidity of the zeolites is to play on the Si/Al ratio. M. Inaba *et al*. examined the production of hydrocarbons from ethanol using zeolite catalysts, and found that H-ZSM-5 zeolite with a low Si/Al ratio favor the formation of higher hydrocarbons, such as BTX, at high selectivity, while other zeolites (H-mordenite, H-β and USY type zeolites) form ethylene exclusively (M. Inaba K. M., 2011). They cited back from the work of V.S. Nayak *et al.*, where the latter found that the conversion of m-xylene passes through a maximum at the Si/Al ratio of 17.2 due to a good balance of the strength and number of acid sites (Choudhary, 1982).

The change in the Si/Al ratio does have an effect on the acidity of the catalyst, and therefore this can divert catalytic test results. Many authors have discussed the effect of Si/Al ratio over the product distribution. To observe well this effect, the same contact catalyst should be studied in the same reaction temperature, catalyst mass and W/F… but with different Si/Al ratios in order to well estimate the effect the ratio has on ethanol conversion as well. Similarly, if we want to compare a doped catalyst with different Si/Al ratios, it must have the same percentage of doping and placed in the same reaction conditions so that one can properly evaluate the effect. Note that the overall acidity is a combination of the original acidity of the catalyst (determined by Si/Al ratio) plus extra treatments done for the support (doping, mild in situ treatment…).

E. Epelde *et al.* compared different raw H-ZSM-5 with SiO_2/Al_2O_3 ratios of 30, 80 and 280. For HZSM-5 (30) and at t_0, propylene yield was 98% and ethylene conversion was 98%. After 300 min, propylene yield increased to 22% while ethylene conversion decreased to 94%. For HZSM-5 (80), respective propylene yield and ethylene conversion were 19% and 91%. After 300 min, they became 25 and 77%, respectively. For HZSM-5 (280), they were originally 18 and 29% respectively, then they decreased into 12 and 18% respectively after 300 min from the beginning of the reaction (E. Epelde, 2014). We conclude that at t_0, HZSM-5 (80 and 280) showed higher propylene yields than HZSM-5 (30), while at t_{300min} it was higher for HZSM-5 (30 and 80) than for HZSM-5 (280). Besides, B. Lin *et al.* found that for 0.10g raw H-ZSM-5 at temperature of 450 °C and time on stream 1 h, as the Si/Al ratio increases from 38, 78, 102 up till 123, ethylene conversion decreases progressively from 58.0 to 9.6% while propylene selectivity fluctuates between 42.0 and 46% (B. Lin, 2009). This indicates that at these conditions, Si/Al ratio has an effect only on ethanol conversion and not on propylene selectivity.

Further and concerning the effect of SiO_2/Al_2O_3 ratio of raw HZSM-5 on propylene yield (temperature 500 °C, W/F= 0.0025 g_{cat}/ml/min), propylene yields for 50, 100, 150 and 200 are 28, 12, 4 and 3%, respectively (D. Goto, 2010). So, as the ratio increases, yield decreases till it reaches a stable value at the ratio of 150. For 0.5g of H-ZSM-5 at 450 °C according to K. Murata *et al.*, as ratio increases from 29 to 1900 passing through 68 and 190, ethanol conversion stays the same (around 100%), while propylene selectivity decreases from 24.4 to 1.89, passing through 12.6 and 10.6%. However, for 10wt% W/H-ZSM-5 (450 °C, 0.5g), as Si/Al_2 ratio increases from 25 to 50 to 80 to 150, ethanol conversion stays full while propylene selectivity increases from 25 to 28%, then it decreases back to 18 follwoed by 17% (K. Murata, 2008). So we deduce that there is no general rule to say that as the ratio increases the propylene selectivity decreases, but this rather a full package of all reaction conditions should be considered.

H. Xin *et al.* studied the catalytic dehydration of ethanol over post-treated ZSM-5 zeolites. The ascending order of Si/Al ratios (as measured by XRF and ICP-OES) for the samples being treated is as follows: 28 for the desilicated ZSM-5, 29 for the dealuminated ZSM-5 followed by desilication, 38 for the desilicated ZSM-5 followed by dealumination, 41 for the dealuminated ZSM-5 and 58 for the untreated ZSM-5. Ethanol conversion was maintained for all samples at 74% at t_0 and t_{133min}. For the desilicated sample, ethylene

selectivity was 17% at t_0 and became 14% at t_{133min}. The sample being desilicated from the originally dealuminated one showed 12% ethylene selectivity at t_0 and 8% at t_{133min}. In contrary, the sample being dealuminated from the originally desilicated one showed 5% ethylene at t_0 which roughly stayed constant at the end of the reaction (6%). Finally, the raw ZSM-5 of Si/Al ratio 58%, showed 7 and 8% ethylene selectivity at t_0 and t_{133min}, respectively. We conclude that in this case the higher is the Si/Al ratio, the lower the ethylene selectivity (H. Xin, 2014).

In the catalytic dehydration of ethanol over post-treated ZSM-5 at 200 °C and atmospheric pressure, diethyl ether and ethylene were two main products competitively formed . At the beginning of the reaction at 200 °C, parent ZSM-5, desilicated ZSM-5, dealuminated ZSM-5, desilicated followed by dealuminated ZSM-5, and dealuminated followed by desilicated ZSM-5 showed 7, 17, 5, 4 and 11% respective ethylene selectivities. The selectivity for the diethyl ether tended to deteriorate with decreasing catalytic Brønsted acidity. At 0.68 $mmolg^{-1}$ of weak acid sites, ethylene selectivity was 4%, while it increased to 14% at 1.1 $mmolg^{-1}$ amount (H. Xin, 2014).

As discussed before, dealumination and desilication treatments of ZSM-5 have a direct effect on varying the Si/Al ratio and the acidity as well, plus tuning the zeolite catalysts with hierarchically porous structure. Concerning the acidity section, the NH_3-TPD was used to calculate the total acidity of the hierarchical zeolites as being the NH_3 chemisorbed. The desilicated samples might include the bridge Al-OH-Si with weaker acidity in the low-crystallinity area. Desilication could also convert some of the strong Brønsted acid sites into sites of weaker acidity or modify the accessibility of these sites due to the partial removal of silica (H. Xin, 2014). In earlier studies, the Si/Al ratio had a relation with total acidity for microporous zeolites. The total acid number was 1.55 mmol g^{-1} for ZSM-5, more than the treated samples, except for ZSM-deSi (1.80 mmol g^{-1}). The ratios of weak acid sites to strong acid sites were calculated. Overall, desilication could increase the ratio of weak acid sites to strong ones. From the activation energies (kcal/mol) for the ethanol to ethylene and diethyl ether reactions on Brønsted acid site of Al- and B-ZSM-5 models, the authors found that the formation of ethoxide intermediate was the rate determining step for producing ethylene (H. Xin, 2014).

Several strategies have been tested to suppress the formation of propylene and butene from ethene, like adding phosphorus over ZSM-5 catalysts to decrease the acidity of the active sites of the zeolites (A. Takahashi W. X., 2012), and reduce the acidity of H-[Al]-ZSM-5 through introduction of alkaline earth metal cations such as Ca^{2+} (H. Oikawa, 2006). According to M. Inaba *et al.*, Ga- or noble metal-modified H-ZSM-5 zeolite catalysts showed higher selectivity for BTX, while Fe or Cr- loading raised the selectivity for C_{3+} olefins ($C^{'}_{3}$-$C^{'}_{7}$) (M. Inaba K. M., 2011; M. Inaba K. M., 2009). M. Inaba *et al.* found that framework collapse of the zeolite support, due to dealumination of the zeolite framework during the reaction, may also be considered a cause of catalytic deactivation and change of products selectivities, since the zeolite acidity essential for this reaction is imparted by Al atoms incorporated into the zeolite framework.

They also found that the decrease in the solid acidity caused by aluminum atoms incorporated in the zeolite framework, due to framework collapse may lead to a decrease in the formation of aromatics. Additionally, they found that the NH_3 desorption peak at 400 °C refers back to solid acidity. Calcination at higher temperatures may cause framwework collapse. H-ZSM-5 (500) and P/H-ZSM-5 catalysts which possess more acidic sites than H-ZSM-5 (700), Fe/H-ZSM-5 and (Fe and P)/H-ZSM-5 catalysts (revealed by a sharp NH_3 desorption peak), showed an increase in propylene selectivity (M. Inaba K. M., 2011). However, in an earlier study for M. Inaba *et al.*, they considered that deposited carbon blocks the acidic sites of the zeolite and inhibit the aromatics formation, leading to an enhancement of ethylene formation (M. Inaba K. M., 2009).

K. Murata *et al*. previously added additives for accelerating the disproportionation and condensation of ethylene (K. Murata, 2008). So, the acidity of the metal selected should be adjusted in the range of giving early-stage olefins (C_3-C_4). The obtainment of ethylene is a good sign, but sometimes H-ZSM-5 gives only ethylene in high yields. The majority of research done so far attributes high yields in the ethanol-to-propylene to the Brønsted acidity, whereby low acid density is favorable. K. Inoue *et al*. found that in the initial stage of ethanol introduction, ethylene production by dehydration was increased in La- and Mg-co-modified H-ZSM-5 with lower surface acidity, whereas the formation of aromatics by oligomerization-cracking increased in un-modified H-ZSM-5 with higher surface acidity. Used H-ZSM-5 with Si/Al_2 ratio of 150. 32% propylene was obtained with La- and Mg-co-modified H-ZSM-5. The number of acid sites and the acid strength (surface acidity) decreased in the order of unmodified, La-modified, and La- and Mg-co-modified H-ZSM-5 (K. Inoue K. O., 2010). According to E. Epelde *et al.*, ethylene conversion needs a high density of sites with high acid strength, but at the same time, this property favors hydrogen transfer and secondary reactions in which paraffins, heavy olefins, aromatics and coke are formed (E. Epelde, 2014).

For Ga-ZSM-5 (29), respective percentages of ethanol conversion, $C_{3+olefins}$ selectivity and BTX selectivity are 93, 11 and 74%. For Fe-ZSM-5 (29) they are 97, 30 and 51% respectively. While for Cr-ZSM-5 (29), they are 94, 18 and 42%, respectively (M. Inaba K. M., 2006). They carried out the universal NH_3-TPD analyses to measure the acidity of the zeolite supports. They found that modest solid acidity of the zeolite is essential for the formation of higher hydrocarbons, but not of ethylene. This is because it enhances a set of reactions like oligomerization, aromatization and H-transfer reactions. They also found that some metals, like Au, decrease solid acidity so this in turn suppresses the transformation of hydrocarbons into deposited carbon. While other metals increase solid acidity thus enhancing carbon deposition.

Earlier studies have revealed that saturated hydrocarbons such as propane are the major products with aromatics over unmodified H-ZSM-5, while Zn- and Ga- doping lead to increased selectivity for aromatics (K. Murata, 2008). They claimed that excess P impregnated over H-ZSM-5 support (5 wt%) destroyed Brønsted sites in the H-ZSM-5, consequently resulting in increased ethylene selectivity and decreased propylene selectivity. They also reported that the high percentage of Brønsted sites in the total number of acid sites of H-ZSM-5 (29) as being 94% and estimated by pyridine adsorption, is required for

propylene formation. However, they did not test this themselves. They only performed an NH_3-TPD study proving that the total acid amount of (La and W)/H-ZSM-5 is less than that of W/H-ZSM-5 resulting in higher propylene selectivity upon co-impregnation (higher than 20%).

K. Murata *et al.* reported the highest propylene selectivity was obtained at H-ZSM-% with Si/Al_2 ratio of 29, and the selectivity decreased at H-ZSM-% with higher Si/Al_2 ratio (weak surface acidity) (K. Murata, 2008). According to K. Inoue *et al.*, increasing the Si/Al_2 ratio reduces the surface acidity on H-ZSM-5. Besides, they deduced that the total surface acidity and acid strength distribution on H-ZSM-5 decrease after La introduction. The decrease in acidity results in the decrease of coke formation during the reactions and the increase of the catalyst stability. Additionally, the ethylene production was promoted in lower surface acidity (La/Al_2 ratio: 4 and 6), whereas higher surface acidity (La/Al_2 ratio: 0 and 1) lead to the production of more propane, C_4 and aromatics. Therefore, the highest propylene selectivity was obtained in the moderate surface acidity (La/Al_2 ratio: 2.2). In La-modified H-ZSM-5 (Si/Al_2 ratio: 280) modified at a molar ratio of La to Al_2 of 2.2, the propylene selectivity was 31% at 0.1 MPa, 550 °C and was higher than those of non-modified catalysts. The propylene selectivity remained high (24%) even after 28 h-reaction (K. Inoue M. I., 2010).

- Deactivation and regeneration:

It is always better to increase the lifetime of the catalyst by avoiding its deactivation, rather than performing regeneration procedures which can be damaging for the structure and acidic sites of the catalyst. For instance, Au/H-ZSM-5 catalyst can partially inhibit carbon deposition during the reaction, thus maintaining constant catalytic activity for BTX formation (M. Inaba K. M., 2006). S.K. Saha *et al*. found that the incorporation of Zn and Ga also increases the yield of gasoline and kerosene range hydrocarbons (heavier products), besides increasing the life of the catalyst (Sivasanker, 1992; M. Inaba K. M., 2009).

In 2007, M. Inaba *et al*. reported that the catalyst deactivation by carbon deposition on the catalyst and in the framework could cause the collapse of the zeolite (M. Inaba K. M., 2007). In 2009, M. Inaba *et al*. considered that carbon deposition and framework collapse could be the cause for the change in selectivity of products and showed that low Fe-loading could inhibit carbon deposition and framework collapse to some degree, and – at higher reaction temperature – could enhance the formation of olefins in the ethanol-to-propylene reaction over ZSM-5 catalysts (M. Inaba K. M., 2009). Both, carbon deposition and framework collapse of zeolite support can be suppressed in some degree (M. Inaba K. M., 2009).

In 2011, M. Inaba *et al*. mediated the discussion of the effect of the framework collapse. They claim that it can have a positive or negative effect. Their study suggests that the cause of changed selectivity for each product may be carbon deposition and framework collapse during the reaction. The deposited carbon and framework collapse suppress the

formation of aromatics, and this suppression increases or decreases the selectivity of C_{3+} olefins and propylene (M. Inaba K. M., 2011). Phosphorus-modified HZSM-5 (Ga) showed a good catalytic activity and stability because of the suppression of carbonaceous species. This is due to the reduction in the number of strong acid sites. At 500 °C, the ethanol conversion was 100%. The propylene and butane yields increased with an increase in the P/Ga ratio, whereas the ethylene yield increased monotonously with the P/Ga ratio, indicating that the oligomerization of ethylene produced by the dehydration of ethanol was suppressed by phosphorus modification by the reduction in the number of strong acid sites. Propylene yield reached a maximum of 28% at the P/Ga ratio of ca. 0.3 (Y. Furumoto Y. H., 2011).

It frequently happens that ethanol dehydrates into ethylene, but the reaction stops at this step instead of going further. Y. Furumoto *et al*. reported an HZSM-5(Fe) catalyst which yielded exclusively ethylene instead of propylene for all Si/Fe_2O_3 ratios (Y. Furumoto Y. H., 2011). However, there have been many reports that modified zeolite catalysts have a superior effect on the production of ethylene from ethanol (K. Inoue K. O., 2010). In general, catalysts showing higher initial selectivity for propylene exhibited a steeper decrease in propylene selectivity with time on-stream (M. Inaba K. M., 2011).

Since zeolites are irreversibly deactivated during the reaction, investigations have been conducted with the goal of improving the catalyst stability (A. Takahashi W. X., 2012). Due to the poor catalyst stability and resistance to coke formation of the H-ZSM-5 zeolites, this catalyst is insufficient for industrialization until now (T. Meng, 2012). Carbon deposition, which was the main cause of the deactivation of the phosphorus-modified zeolites was suppressed by H_2O produced during the dehydration of ethanol, according to A. Takahashi *et al.* (A. Takahashi W. X., 2012). M. Inaba *et al*. showed that the catalytic performance of Fe and/or P-modified H-ZSM-5 zeolite catalysts was regenerated by calcination in flowing air (M. Inaba K. M., 2011). Another used Fe-ZSM-5 catalyst could be regenerated by air treatment at 500 °C, but the degree of regeneration depended on the kind of iron starting materials and the calcinations temperature in the preparation method (M. Inaba K. M., 2007). An $FeCl_3$-based catalyst, calcined at 700 °C, and catalysts calcined at 900 °C (irrespective of iron source) can be almost completely regenerated, while $Fe(NO_3)_3$- or $Fe_2(SO_4)_3$- based catalyst, calcined at 700 °C, cannot be completely regenerated by this treatment.

Nevertheless, one cannot discuss the coke formation independently from the propylene formation for the ethanol-to-propylene reaction. It has been suggested that the pathway to coke formation on oxides and sulfides, starting from olefins or aromatics, may involve: (a) dehydrogenation to olefins; (b) olefin polymerization, (c) olefin cyclization to form substituted benzenes, and (d) formation of polynuclear aromatics from benzene. These mechanisms proceed via carbonium ions intermediates and accordingly they are catalyzed by Brønsed acid sites. In case of the ethanol-to-propylene reaction, one can speculate that the reactive intermediates combine, rearrange and dehydrogenate into coke-type structures via carbonium ions type reactions (P. Forzatti, 1999). So, the cracking mechanism of the ethanol-to-propylene reaction over ZSM-5 catalyst is the same as that for the coke formation reaction,

and it occurs on the same type of active sites (Brønsted acid sites) with the same type of intermediates (carbonium ions).

During the ethanol-to-propylene reaction, an equilibrium is reached between the rate of coke production and the rate of coke removal by disproportionation so that steady-state conditions, corresponding to a certain level of coke present on the catalyst surface, are eventually reached. Otherwise, if the rate of coke deposition is higher than that of coke removal, a suitable regeneration procedure must be applied. (P. Forzatti, 1999).

The high rate of coking requires frequent high temperatures for catalyst regeneration. The H-ZSM-5 zeolite is also amenable to regeneration by simply burning the catalyst at around 500 °C in air or oxygen atmosphere to remove the coke deposits. The high temperature treatment can potentially lead to the irreversible loss of catalytic activity and ultimately reduce the overall catalyst lifetime. According to K.K. Ramasamy *et al.*, the H-ZSM-5 zeolite can be easily regenerated after deactivation due to coke deposition. However, long catalytic life-time is still advantageous in negating the cost of frequent interruption for catalyst regeneration or replacement and the permanent loss of catalytic activity due to dealumination or other irreversible structural damage from frequent high-temperature regeneration conditions. (K.K. Ramasamy, 2014).

- "Textural" properties:

In order to study more systematically the influence of the textural parameters, T. Meng *et al.* prepared three ZSM-5 zeolites with different crystal sizes. The acidic properties were very similar, but their textural properties are strongly influenced by the crystal size. The small-sized H-ZSM-5 shows higher propylene selectivity and better stability. With the crystallite size decreasing, the surface area, pore volume and pore diameter of the H-ZSM-5 increase. Hence the authors concluded that the higher propylene selectivity and better stability were due to its larger pore volume, more secondary pores, shorter channels, and reduced diffusion paths, which shows low formation rate of coke, low diffusion resistance, and high ability to tolerate the coke (T. Meng, 2012).

1.1.1.b. SAPO-34

The synthesis of new 8-membered ring zeolites are important for catalytic studies, owing to the shape selectivity imposed by their narrow pores (Q. Zhu, 2009). Other types of protonated zeolites or zeotype materials utilized for the ethanol-to-propylene reaction are 8-membered ring zeolites, like SAPO-34. The distribution of products obtained in the zeolitic ethanol conversion process is strongly dependent on the acidity as well as the channel structure of the zeolites (Y. Furumoto N. T., 2012). SAPO-34, a small pore silico-aluminophosphate, with large cavities (6.7 Å X 10.9 Å) interconnected through small windows (3.8 Å X 3.8 Å) is currently one of the archetypal industrial methanol-to-olefins catalysts (Q. Qian, 2014), but it is also used for ethanol-to-olefins reactions. Zeolites with an

8-membered ring pore system, such as SAPO-34 and LEV, selectively convert ethanol to propylene. However, these zeolites are rapidly deactivated by carbon deposition (A. Takahashi W. X., 2012).

H. Oikawa *et al*. contributed the high yield of propylene in the conversion of ethylene and ethanol over SAPO-34, to the reason that the pore size of SAPO-34 is comparable to the kinetic diameter of propene (H. Oikawa, 2006). They postulated a reaction mechanism for the ethene to propene reaction over SAPO-34. According to this "carbenium ion mechanism" (Figure 1.7) for propene formation in the conversion of ethene, the fission of a carbon-carbon bond in the β-position of the hexyl carbenium ion (2) and/or the 4-methyl-2-pentyl carbenium ion (4) is an important reaction in the selective synthesis of propene. In the latter reaction for the formation of 4, the tertiary carbenium ion of 3 should be converted to the secondary carbenium ion of 4. The formation of 2 via 1 presumably proceeds more easily than 4 via 3 (H. Oikawa, 2006).

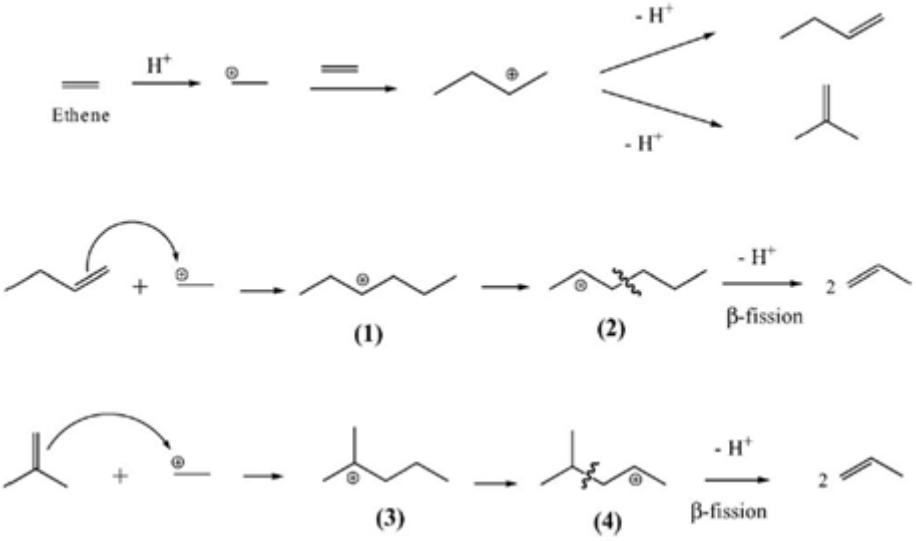

Figure 1.7. Reaction Scheme of Carbenium Ion Mechanism over SAPO-34 Solid Acid Catalyst (H. Oikawa, 2006)

Further, SAPO-34 molecular sieve affords high propylene yield, but ethanol is not converted in full, and the interconnected-cage structure of SAPO-34 affords higher trapping of coke precursors. According to H. Oikawa *et al.* and T. baba, ethene conversion at 450 °C over SAPO-34 is 71.2%, while the propylene yield is 52.2% (H. Oikawa, 2006) (Baba). According to C. Duan *et al.*, ethanol conversion at isothermal fixed-bed reactor is 100%; however, zero propylene yield was obtained. Reaction conditions were: 500 °C, 0.1 MPa and 0.5g catalyst (C. Duan X. Z., 2013) (C. Duan X. Z., 2011).

Another type of advanced catalyst is HZSM-5/SAPO-34 catalyst prepared by hydrothermal synthesis and physical mixture. Ethanol to propylene over these as-prepared catalysts was investigated under different reaction conditions. Synergetic effect of HZSM-5 with SAPO-34 occurred on HZSM-5/SAPO-34 catalyst, which modified its properties and

catalytic reactivity. The concentration and the strength distribution of acid sites were closely relative to the catalytic reactivity of HZSM-5/SAPO-34 catalyst (C. Duan X. Z., 2013).

1.1.1.c. H-SSZ-13, CHA and MTF zeolites

The aluminosilicate H-SSZ-13 analogue to SAPO-34 with stronger acidity and 8-membered ring windows was scarcely studied in the ethanol-to-propylene conversion (W. Dai X. S., 2014; W. Dai B. T.). It has been reported that SSZ-13 displays higher acid strength than SAPO-34 in alcohol-to-olefins conversion. As a consequence, ethene is supposed to be rapidly oligomerized and converted into naphthalene-based carbenium ions, playing a significant role in the ETP reaction. Polyalkylnaphthalene are rapidly formed on dealuminated SSZ-13. The cracking of polyalkynaphthalene likely results in the formation of propylene (W. Dai B. T.).

The reaction mechanism over HSSZ-13 is illustrated in Figure 1.8. (i) After starting the ethene conversion, a rapid oligomerization occurs (proven by FTIR) leading to the formation of dienes, aromatics, and polycyclic aromatics (evidenced by UV/Vis). Polyalkylnaphthalenes as the major detected organic species play a key role in the active period of the catalyst, while these species strongly decrease upon the catalyst deactivation (GC-MS). (iii) Already in the active period of the catalyst, a rapid and strong decrease in the density of accessible Brønsted acid sites occurs, while the number of naphthalene-based carbenium ions increases (detected by ^{1}H MAS NMR). (iv) Caused by the accumulation of large polycyclic aromatics (UV/Vis, GC-MS), a blocking of the catalysts pores occurs. Consequently, neither Brønsted acid sites nor catalytically active carbenium ions are accessible for further reactants (^{1}H MAS NMR). This leads to a strong deactivation of the deAlH-SSZ-13 material (W. Dai X. S., 2014).

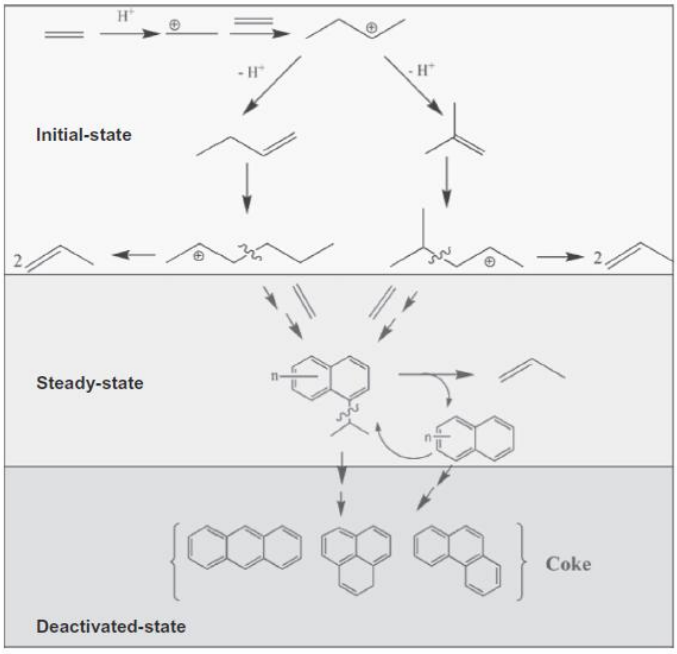

Figure 1.8. Reaction Mechanism over H-SSZ-13 (W. Dai X. S., 2014)

Other types of 8-ring zeolites employed in the alcohol transformations are CHA and MTF zeolites. It is noted that the pores of both zeolites are large enough for small organic chemicals such as methanol, ethanol and ethylene to diffuse into. The dehydration product of ethanol is ethylene, and further transformation of ethylene to higher olefins readily occurs on acid catalysts. Ethanol is readily transformed into olefins on H/CHA whereas only dehydration reaction of ethanol occurs on H/MTF (Q. Zhu, 2009).

1.1.2. Mesoporous Catalysts

Over mesoporous catalysts, the metathesis route mechanism is commonly suggested. The olefin produced firstly is ethylene. It then dimerizes and oligomerizes readily to various olefins on mesoporous catalysts. Afterwards, the as-formed olefins undergo metatheses over to produce propylene.

To better understand the behavior of alcohols on mesoporous catalysts, Ph. de Werbier *et al.* have studied the transformation of the C2 alcohol on Fischer-Tropsch catalysts, namely cobalt deposited on alumina. On this type of metallic catalysts deposited on an acidic support, pure ethanol can undergo three types of reactions, namely dehydration into ether and/or into olefin, dehydrogenation into aldehyde and condensation into higher hydrocarbons. While it is not possible to dissociate the last two reactions, the dehydration can be avoided by adding water to the feed (Ph. de Werbier, 1988). According to M. Iwamoto *et al.*, it takes place by the following two steps (Figure 1.9): (i) the dimerization of ethylene to butenes and, (ii) the metathesis of butenes and ethylene to form propylene (Iwamoto, 2011). The use of ^{13}C enriched ethanol over Co/Al_2O_3 shows that the methyl group of the alcohol molecule participates mainly in the chain growth (Ph. de Werbier, 1988).

As an example for mesoporous catalysts, MCM-41 is active in the dehydration of EtOH to yield ethylene (Iwamoto, 2011). It is important to note that exceptionally over MCM-41 (also Al-SBA-15), both oligomerization-cracking and/or metathesis mechanisms can occur. The metathesis route has been studied over metallic catalysts (Ni, Mo, W) supported on different mesoporous materials (γ-Al_2O_3, MCM-41) (M. Taoufik, 2007).

In case of nickel on silica (Ni-MCM-41), two possible reaction routes are suggested to form ethene from ethanol. One is the dehydration route via diethylether as intermediate. The other is a complicated route described in Figure 1.**10** which go through acetaldehyde and ethylacetate as intermediates. The reaction rate of the latter route is slower than that of the former, since the formation of acetaldehyde was observed in a wide range space velocity values (Iwamoto, 2011).

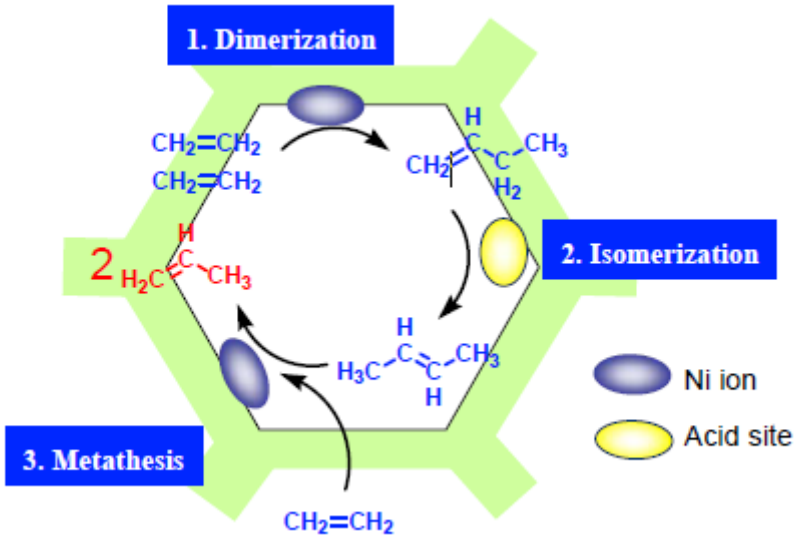

Figure 1.9. Proposed reaction mechanism for the conversion of ethene to propene on Nickel ion-loaded MCM-41 (Iwamoto, 2011)

$$2CH_3CH_2OH\ (EtOH) \rightarrow CH_3CH_2OCH_2CH_3\ (DEE) + H_2O \quad (1)$$

$$CH_3CH_2OCH_2CH_3 \rightarrow CH_2{=}CH_2\ (C2^{=}) + CH_3CH_2OH \quad (2)$$

$$2CH_2{=}CH_2 \rightarrow CH_2{=}CHCH_2CH_3\ (C4^{=}) \quad (3)$$

$$CH_2{=}CHCH_2CH_3 \rightarrow CH_3CH{=}CHCH_3\ (C4^{=}) \quad (4)$$

$$CH_3CH{=}CHCH_3 + CH_2{=}CH_2 \rightarrow 2CH_2{=}CHCH_3\ (C3^{=}) \quad (5)$$

$$CH_3CH_2OH \rightarrow CH_3CHO + H_2 \quad (6)$$

$$CH_3CHO + CH_3CH_2OH \rightarrow CH_3COOCH_2CH_3\ (ETA) + H_2 \quad (7)$$

$$2CH_3CHO \rightarrow CH_3COOCH_2CH_3\ (ETA) \quad (7')$$

$$CH_3COOCH_2CH_3 \rightarrow CH_3COOH + CH_2{=}CH_2 \quad (8)$$

$$CH_3COOCH_2CH_3 + H_2O \rightarrow CH_3COOH + CH_3CH_2OH \quad (8')$$

$$CH_3COOH + CH_3CH_2OH \rightarrow CH_3COOCH_2CH_3 + H_2O \quad (9)$$

$$CH_3COOH + H_2 \rightarrow CH_3CHO + H_2O \quad (10)$$

Figure 1.10. The reaction routes for the formation of $C2^{=}$ from EtOH on Ni-MCM-41 (Iwamoto, 2011)

Several mesoporous catalysts have been employed in the ethanol-to-propylene reaction and high selectivities of propylene were obtained, even twice than that obtained over H-ZSM5. The main drawback is the rather low ethanol conversion. A.S. Frey *et al*. has prepared MCM-48 by four synthesis routes. They reported propylene selectivity of 56% for ethene conversion of 40%. More recently, Perea *et al*. disclosed that the ethene conversion can be improved to about 80% over Ni/Al MCM-41 with few acid sites (W. Dai X. S., 2014). Ni/Al MCM-41 was synthesized at different Si/Al ratios tested in the direct conversion of

ethene to propene. The highest conversion was obtained for the Si/Al ratio of 60 (76%). Respective propylene selectivity was 36% (L.A. Perea, 2013).

1.2. An Overview of Some Catalytic Performances

Here we display some catalytic results for different types of catalysts found in literature (Table 1.**2**;Table 1.**3**). Note that the catalytic performance is dependent on a combination of reaction conditions, plus physical and textural properties of the catalyst itself. But here, we can have a global view and constitute a rough estimation of the performance of each category of catalysis.

Table 1.2. Different catalysts cited in literature and their catalytic performance

No	Category	Catalyst	Ethanol Conversion (%)	Propylene selectivity (%)	Reference
1	ZSM-5s with different Si/Al_2 ratios	H-ZSM-5 (29)	98.2	24.4	(K. Murata, 2008)
2		H-ZSM-5 (30)	100	10.9	(Z. Song, 2009)
3		H-ZSM-5 (68)	99.8	12.6	(K. Murata, 2008)
4		H-ZSM-5 (80)	100	16.9	(Z. Song, 2009)
5		H-ZSM-5 (190)	99.7	10.6	(K. Murata, 2008)
6		H-ZSM-5 (280)	100	3.2	(Z. Song, 2009)
7		H-ZSM-5 (1900)	100	1.86	(K. Murata, 2008)
8	Metal-modified ZSM-5s	Re-ZSM-5	99.9	14.8	(K. Murata, 2008)
9		Mo-ZSM-5	99.1	14.0	(K. Murata, 2008)
10		P-ZSM-5	99.8	13.2	(M. Inaba K. M., 2011)
11		Fe-ZSM-5	94.9 at t0, 100 after 420 min	13.2 at t0, 31 after 420 min	(M. Inaba K. M., 2011)
12		Cr-ZSM-5	93	24	(K. Inoue M. I., 2010)
13		Fe-ZSM-5	83	22	(K. Inoue M. I., 2010)
14		Zr-ZSM-5	82	26	(K. Inoue M. I., 2010)
15		La-ZSM-5	94 at t0, 98 after 28.2h	30 at t0, 24 after 28.2h	(K. Inoue M. I., 2010)
16		Ce-ZSM-5	93	27	(K. Inoue M. I., 2010)
17		W-ZSM-5	83	27	(K. Inoue M. I., 2010)
18		Sr-ZSM-5	100	32	(C. Duan X. Z., 2013)
19		Ga-ZSM-5	100	23.4	(C. Duan X. Z., 2013)
20	Metal-modified ZSM-5s with different wt%	W-ZSM-5 (0 wt%)	100	8.69	(K. Murata, 2008)
21		W-ZSM-5 (5 wt%)	99.8	8.76	(K. Murata, 2008)
22		W-ZSM-5 (10 wt%)	98.2	24.4	(K. Murata, 2008)
23		W-ZSM-5 (20 wt%)	51.1	7.20	(K. Murata, 2008)
24		Fe-ZSM-5 (1 wt%)	97 at t0, 100 after 7h	9 at t0, 11 after 7h	(M. Inaba K. M., 2009)
25		Fe-ZSM-5 (10	97 at t0, 99	9 at t0, 8 after	(M. Inaba K. M.,

		wt%) at 400 °C reaction	after 7h	7h	2009)
26		Fe-ZSM-5 (10 wt%) at 450 °C reaction	95 at t0, 100 after 7h	16 at t0, 9 after 7h	(M. Inaba K. M., 2009)
27	Bi-metallic Modified ZSM-5s	La (1)/W-ZSM-5	94-95	21-23	(K. Murata, 2008)
28		La (5)/W-ZSM-5	96.9	16.5	(K. Murata, 2008)
29		P (1)/W-ZSM-5	97.8	29.5	(K. Murata, 2008)
30		P (5)/W-ZSM-5	100	0.22	(K. Murata, 2008)
31		B (1)/W-ZSM-5	100	7.13	(K. Murata, 2008)
32		Mg (1)/W-ZSM-5	34.4	4.79	(K. Murata, 2008)
33		Fe/P-ZSM-5	99.7 at t0, 100 after 420 min	18.3 at t0, 33 after 420 min	(M. Inaba K. M., 2011)
34		P/Fe-ZSM-5	97.8	17.2	(M. Inaba K. M., 2011)
35		Fe-P-ZSM-5	98.6 at t0, 100 after 420 min	11.5 at t0, 34 after 420 min	(M. Inaba K. M., 2011)
36	Impact of Fe precursor for Fe-ZSM-5	Fe $(NO_3).9H_2O$ (500 °C Cal . Temp.)	100	9.5	(M. Inaba K. M., 2007)
37		Fe $(SO_4)_3.nH_2O$ (500 °C Cal . Temp.)	99.6	10.0	(M. Inaba K. M., 2007)
38		$FeCl_3.6H_2O$ (500 °C Cal . Temp.)	99.6	9.0	(M. Inaba K. M., 2007)
39		$FeC_2O_4.2H_2O$ (500 °C Cal . Temp.)	95.6	12.0	(M. Inaba K. M., 2007)
40		$FePO_4.nH_2O$ (500 °C Cal . Temp.)	95.60	8.1	(M. Inaba K. M., 2007)
41	Mesoporous catalysts	Co/Al_2O_3	28	35	(Ph. de Werbier, 1988)
42		Ni-MCM-41	57 after 1h, 58 after 4h	24 after 1h, 24 after 4h	(Iwamoto, 2011)
43		$W(H)_3/Al_2O_3$	42	95	(M. Taoufik, 2007)
44		Ni/AlMCM-41	88 at t0, 60 after 60h	27 at t0, 44 after 60h	(L.A. Perea, 2013)
45		Ni/AlMCM-48	40	56	(A.S. frey, 2012)
46	Other catalysts	SAPO-34	100	0	(C. Duan X. Z., 2013)
47		SAPO-34	7.9	79.5	(H. Oikawa, 2006)
48		HZSM-5/SAPO-34	100	34.5	(C. Duan X. Z., 2013)
49		H-MOR (18.3)	100	0	(K. Murata, 2008)
50		USY (6.3)	100	2.67	(K. Murata, 2008)
51		γ-Al_2O_3	100	0.47	(K. Murata, 2008)

Table 1.3. Different catalysts cited in literature and their catalytic performance

No.	Category	Catalyst	Reaction Temperature (°C)	Time-on-stream	Reference
1	ZSM-5s with different Si/Al_2 ratios	H-ZSM-5 (29)	450	t0	(K. Murata, 2008)
2		H-ZSM-5 (30)	400	30 min	(Z. Song, 2009)
3		H-ZSM-5 (68)	450	t0	(K. Murata, 2008)
4		H-ZSM-5 (80)	400	30 min	(Z. Song, 2009)
5		H-ZSM-5 (190)	450	t0	(K. Murata, 2008)
6		H-ZSM-5 (280)	400	30 min	(Z. Song, 2009)
7		H-ZSM-5 (1900)	450	t0	(K. Murata, 2008)
8	Metal-modified ZSM-5s	Re-ZSM-5	450	t0	(K. Murata, 2008)
9		Mo-ZSM-5	450	t0	(K. Murata, 2008)
10		P-ZSM-5	450	t0	(M. Inaba K. M., 2011)
11		Fe-ZSM-5	450	t0 and 420 min	(M. Inaba K. M., 2011)
12		Cr-ZSM-5	550	t0	(K. Inoue M. I., 2010)
13		Fe-ZSM-5	550	t0	(K. Inoue M. I., 2010)
14		Zr-ZSM-5	550	t0	(K. Inoue M. I., 2010)
15		La-ZSM-5	550	t0 and 28.2h	(K. Inoue M. I., 2010)
16		Ce-ZSM-5	550	t0	(K. Inoue M. I., 2010)
17		W-ZSM-5	550	12 min	(K. Inoue M. I., 2010)
18		Sr-ZSM-5	550	t0	(C. Duan X. Z., 2013)
19		Ga-ZSM-5	500	t0	(C. Duan X. Z., 2013)
20	Metal-modified ZSM-5s with different wt%	W-ZSM-5 (0 wt%)	450	t0	(K. Murata, 2008)
21		W-ZSM-5 (5 wt%)	450	t0	(K. Murata, 2008)
22		W-ZSM-5 (10 wt%)	450	t0	(K. Murata, 2008)
23		W-ZSM-5 (20 wt%)	450	t0	(K. Murata, 2008)
24		Fe-ZSM-5 (1 wt%)	400	t0 and 7h	(M. Inaba K. M., 2009)
25		Fe-ZSM-5 (10 wt%) at 400 °C reaction	400	t0 and 7h	(M. Inaba K. M., 2009)
26		Fe-ZSM-5 (10 wt%) at 450 °C reaction	450	t0 and 7h	(M. Inaba K. M., 2009)
27	Bi-metallic Modified ZSM-5s	La (1)/W-ZSM-5	400	26 h	(K. Murata, 2008)
28		La (5)/W-ZSM-5	450	t0	(K. Murata, 2008)
29		P (1)/W-ZSM-5	450	t0	(K. Murata, 2008)
30		P (5)/W-ZSM-5	450	t0	(K. Murata, 2008)
31		B (1)/W-ZSM-5	450	t0	(K. Murata, 2008)
32		Mg (1)/W-ZSM-5	450	t0	(K. Murata, 2008)
33		Fe/P-ZSM-5	450	t0 and 420 min	(M. Inaba K. M., 2011)
34		P/Fe-ZSM-5	450	t0	(M. Inaba K. M., 2011)

35		Fe-P-ZSM-5	450	t0 and 420 min	(M. Inaba K. M., 2011)
36	Impact of Fe precursor for Fe-ZSM-5	Fe $(NO_3)_3.9H_2O$ (500 °C Cal . Temp.)	400	t0	(M. Inaba K. M., 2007)
37		Fe $(SO_4)_3.nH_2O$ (500 °C Cal . Temp.)	400	t0	(M. Inaba K. M., 2007)
38		$FeCl_3.6H_2O$ (500 °C Cal . Temp.)	400	t0	(M. Inaba K. M., 2007)
39		$FeC_2O_4.2H_2O$ (500 °C Cal . Temp.)	400	t0	(M. Inaba K. M., 2007)
40		$FePO_4.nH_2O$ (500 °C Cal . Temp.)	400	t0	(M. Inaba K. M., 2007)
41	Mesoporous catalysts	Co/Al_2O_3	200	t0	(Ph. de Werbier, 1988)
42		Ni-MCM-41	400	1h and 4h	(Iwamoto, 2011)
43		$W(H)_3/Al_2O_3$	150	120 h	(M. Taoufik, 2007)
44		Ni/AlMCM-41	450	t0 and 60h	(L.A. Perea, 2013)
45		Ni/AlMCM-48	350	4 h	(A.S. frey, 2012)
46	Other catalysts	SAPO-34	500	3 h	(C. Duan X. Z., 2013)
47		SAPO-34	450	1 h	(H. Oikawa, 2006)
48		HZSM-5/SAPO-34	550	t0	(C. Duan X. Z., 2013)
49		H-MOR (18.3)	450	t0	(K. Murata, 2008)
50		USY (6.3)	450	t0	(K. Murata, 2008)
51		γ-Al_2O_3	450	t0	(K. Murata, 2008)

As we can see from the tables above, zeolites generally show 100% of ethanol conversion, which is higher than that of mesoporous catalysts employed for the same reaction (low down to 28%). This full conversion can be maintained for up to 28h (as in the case of La-ZSM-5). However, mesoporous catalysts show higher selectivities for propylene than zeolites (maximum of 56% for Ni/AlMCM-41 versus maximum of 30% at t_0 for La-ZSM-5). Reaction temperatures range of the reaction for both categories is the same (350-550 °C), indicating that both are resistant to high temperatures as high as 550 °C. Note that alumina-doped catalysts such as $W(H)_3/Al_2O_3$ and Co/Al_2O_3 formed 95 and 35% of propylene at relatively low temperatures (150 and 200 °C, respectively). Both categories of catalysts can show generally a remarkable increase in propylene selectivity with time-on stream. It is certain that for the same catalyst, other reaction conditions which are not mentioned here can affect the pathway of the reaction.

1.3. Conclusion

These works show the complex relationship between the catalyst performance and properties (porous structure and acidity): ethylene/ethanol conversion needs a high density of sites with high acid strength, but at the same time, this property favors secondary and hydrogen transfer reactions in which paraffin, heavy olefins, aromatics and coke are formed. Furthermore, the attenuation of hydrogen transfer reactions by using catalysts with severe

shape selectivity (such as SAPOs) favors the retention of coke in its cages, which are characteristic of the porous structure of these catalysts.

Whenever employing a catalyst in an ethanol-to-propylene reaction, a balance between four indices should be kept in mind for the best catalyst choice, which are: ethanol conversion, propylene selectivity, catalyst stability and catalyst hydrothermal stability. According to K.K. Ramasamy *et al.*, among all zeolite catalysts tested, the H-ZSM-5 zeolite provides a suitable compromise among activity, shape selectivity to produce hydrocarbons smaller than carbon number C_{10} (gasoline range), slow deactivation by coke formation from alcohol functional group as well as better hydrothermal stability (K.K. Ramasamy, 2014).

The transformation of ethylene/ethanol for producing propylene is a highly complex process that involves different individual reactions, whose development is affected by catalyst deactivation. As a consequence, product distribution evolves with time on stream and the propylene yield reaches a maximum that is dependent on catalyst properties (topology and acidity) (E. Epelde, 2014).

1.4. References

(s.d.). Récupéré sur http://wwwchem.uwimona.edu.jm/lectures/synfuel.html

A. Takahashi, W. X. (2012). Effects of added phosphorus on conversion of ethanol to propylene over ZSM-5 catalysts. *Applied Catalysis A: General*, 162-167.

A. Takahashi, W. X. (2013). Difference between the mechanisms of propylene production from methanol and ethanol over ZSM-5 catalysts. *Applied Catalysis A: General*, 380-385.

A.S. frey, O. H. (2012). Comparison of differently synthesized Ni(Al)MCM-48 catalysts in the ethene to propene reaction. *Microporous and Mesoporous Materials*, 164-171.

B. Lin, Q. Z. (2009). Catalytic Conversion of ethylene to propylene and butenes over H-ZSM-5. *Ind. Eng. Chem. Res.*, 10788-10795.

Baba, T. (s.d.). Catalytic propylene production from ethylene using zeolite catalysts.

Bioethanol. (s.d.). Consulté le 03 14, 2014, sur CropEnergies AG: http://www.cropenergies.com/en/Bioethanol/

C. Duan, X. Z. (2011). Hydrothermally synthesized HZSM-5/SAPO-34 composite zeolite catalyst for ethanol conversion to propylene. *Catal Lett*, 1821-1827.

C. Duan, X. Z. (2013). Comparative studies of ethanol to propylene over HZSM-5/SAPO-34 catalysts prepared by hydrothermal mixture and physical mixture. *Fuel Processing Technology*, 31-40.

Choudhary, V. N. (1982). Isomerization of m-xylene on H-ZSM-5. part I: Influence on catalytic activity and selectivity of Si/Al ratio, degree of cation exchange, deammoniation on conditions and poisoning of stronger acid sites. *Applied Catalysis*, 333-352.

Commision, I.T.S. . (2012). *Database of zeolite structure*.

Conversion of ethanol to gasoline range hydrocarbons using a zeolite catalyst. (s.d.). Récupéré sur http://wwwchem.uwimona.edu.jm/lectures/synfuel.html

Costigan MJ, H. L. (2013). The Isothermal Displacement Calorimeter: Design Modifications for Measuring Exothermic Enthalpies of Mixing. *Aust. J. Chem* , doi: 10.1071/CH 9802103.

D. Goto, Y. H. (2010). Conversion of ethanol to propylene over HZSM-5 type zeolites containing alkaline earth metals. *Applied Catalysis A: General* , 89-95.

D.C. Sherrington, A. K. (2001). Influence of zeolite composition on catalytic activity . *Supported Catalysts and Their Applications*, 55-67.

E. Epelde, A. A. (2014). Modifications in the HZSM-5 zeolite for the selective transformation of ethylene into propylene. *Applied Catalysis A: General*, 17-25.

E. Rossetto, M. C.-G. (2010). Ethylene oligomerization using nickel-rmbeta-diimine hybrid xerogels produced by the sol-gel process. *Applied Catalysis A, General*, doi: 10.1016/j.apcata.2012.09.024.

F.J. Machado, C. L. (2002). The transformation of n-butane over Ga/SAPO-11: the role of extra-framework gallium species. *Applied Catalysis a-General*, 241-252.

Fundamental issues of catalytic conversion of bioethanol into butadiene. (s.d.). *Applied Catalysis A*, Manuscript Number: APCATA-D-14-00200.

H. Oikawa, Y. S. (2006). Highly selective conversion of ethene to propene over SAPO-34 as a solid acid catalyst. *Applied Catalysis A: General*, 181-185.

H. Xin, X. L. (2014). Catalytic dehydration of ethanol over post-treated ZSM-5 catalysts. *Journal of Catalysis*, 204-215.

Iwamoto, M. (2011). One step formation of propene from ethene or ethanol through metathesis on nickel ion-loaded silica. *Molecules*, 7844-7863.

J. Jae, G. T. (2011). Investigation into teh shape selectivity of zeolite catalysts for biomass conversion. *Journal of Catalysis*, 257.

J.A. Lercher, A. J. (2008). Catalytic test reactions for probing the acidity and basicity of zeolites. *Molecular Sieves-Science and Technology* , 153.

J.R. Sohn, S. L. (2007). Effect of TiO2-ZrO2 composition on the catalytic activity of of supported NiSO4 for ethylene oligomerization. *Applied Catalysis A: General*, 27-34.

K. Inoue, K. O. (2010). Metal modification effects on ethanol conversion to propylene by H-ZSM-5 with Si/Al2 ratio of 150. *Reac Kinet Mech Cat*, 477-489.

K. Inoue, M. I. (2010). Conversion of ethanol to propylene by H-ZSM-5 with Si/Al2 ratio of 280. *Cata Lett*, 14-19.

K. Murata, M. I. (2008). Effects of Surface Modification of H-ZSM-5 catalysts on direct transformation of ethanol into lower olefins. *Journal of the Japan Petroleum Institute* , 234-239.

K.K. Ramasamy, H. Z. (2014). Conversion of ethanol to hydrocarbons on hierarchical HZSM-5 zeolites. *Catalysis Today*, 103-110.

L. Pinard, K. B. (2013, 12). On the involvement of radical coke in ethanol conversion to hydrocarbons over HZSM-5 zeolite. *Catalysis Today*, 57-64.

L.A. Perea, T. W.-M. (2013). Alumino-mesostructured Ni catalysts for the direct conversion of ethene to propene. *Journal of Catalysis*, 154-168.

Lei Z, W. H. (2002). Influence of salt added to solvent on extractive distillation. *Chem Eng J.*, 149. Doi: 10.1016/S13 85-8947 (01) 00211-X.

Lide, D. (2000). *CRC Handbook of Chemistry and Physics 81st edition.* CRC press. ISBN 0-8493-0481-4.

M. Inaba, K. M. (2006). Ethanol conversion to aromatic hydrocarbons over several zeolite catalysts. *React.Kinet.Catal.Lett.*, 135-142.

M. Inaba, K. M. (2007). Production of olefins from ethanol by Fe-supported zeolite catalysts. *Green Chem.*, 638-646.

M. Inaba, K. M. (2009). Effect of Fe-loading and reaction temperature on the production of olefins from ethanol by Fe/H-ZSM-5 zeolite catalysts. *React Kinet Catal Lett* , 19-26.

M. Inaba, K. M. (2011). Production of olefins from ethanol by Fe and/or P-modified H-ZSM-5 zeolite catalysts. *J Chem Technol Biotechnol*, 95-104.

M. Itakura, I. G. (2011). Synthesis of high-silica CHA type zeolite by interzeolite conversion of FAU type zeolite in the presence of seed catalysts. *Microporous and Mesoporous Materials*, 91-96.

M. Taoufik, E. L.-C. (2007). Direct transformation of ethylene into propylene catalyzed by a tungsten hydride supported on alumina:trifunctional single-site catalysis. *Angew. Chem. Int. Ed.*, 7202-7205.

Marrison, R. T., & Boyd, R. N. (1972). *Organic Chemistry (2nd ed.).* Allyn and Bacon, inc. ISBN 0-205-08452-4.

Mills GA, E. E. (1987). Alcohols as Components of Transportation Fuels. *Annual Review of Energy*, 47. doi: 10.1146/annurev. eg. 12.110187.000403.

P. Forzatti, L. L. (1999). Catalyst deactivation. *Catalysis Today*, 165-181.

Ph. de Werbier, J. C. (1988). Selective transformation of ethanol into propene on cobalt catalysts. *Catalysis Letters 1*, 169-176.

Q. Qian, J. R.-M.-T. (2014). Single-catalyst particle spectroscopy of alcohol-to-olefins conversions: Comparison between SAPO-34 and SSZ-13. *Catalysis Today*, 14-24.

Q. Zhu, J. K. (2009). Catalytic activities of alcohol transformations over 8-ring zeolites. *Top Catal*, 1272-1280.

Redmond, W. M. (2008). Alcohol. *Microsoft ® Student 2009 [DVD]*.

S. Ilias, A. B. (2014). The mechanism of aromatic dealkylation in methanol-to-hydrocarbons conversion on H-ZSM-5: What are the aromatic precursors to light olefins? *Journal of Catalysis*, 6-16.

Sansare, V. C. (1984). Conversion of ethanol to aromatics on H-ZSM-5 in a pulse microreactor. *Applied Catalysis*, 147-159.

Sivasanker, S. S. (1992). Influence of Zn- and Ga- doping on the conversion of ethanol to hydrocarbons over ZSM-5. *Catalysis Letters*, 413-418.

Stevens, S. (2011-2012). *Transformation of bioethanol into hydrocarbon on modified ZSM-5*. Department of Chemical engineering and technical chemistry-Ghent University, Netherlands.

T. Meng, D. M. (2012). The effect of crystal sizes of HZSM-5 zeolites in ethanol conversion to propylene. *Catalysis Communications*, 52-57.

T. Tago, T. M. (2010). Zeolite nanocrystals-synthesis and applications. *Nanocrystals*, 326.

T. Yamazaki, N. K. (2009). Synthesis of light olefins from bioethanol over Ni-MFI catalysts. *Journal of the Japan Petroleum Institute* , 239-247.

W. Dai, B. T. (s.d.). Direct transformation of ethylene into propylene on H-SSZ-13.

W. Dai, X. S. (2014). Verifying the mechanism of ethene-to-propene conversion on zeolite H-SSZ-13. *Journal of Catalysis*, 10-20.

W. Phongsawat, B. N. (2012). Production of propylene from an unconventional metathesis of ethylene and 2-pentene over Re2O7/SiO2-Al2O3 catalysis. *Journal of Natural Gas Chemistry*, 83-90.

Windholz, M. (1976). *The Merck index: an encyclopedia of chemicals and drugs (9th ed.).* Rahway, N.J., U.S.A: Merck. ISBN 0-911910-26-3.

Y. Furumoto, N. T. (2012). Conversion of ethanol to propylene over HZSM-5(Ga) co-modified with lanthanum and phosphorus. *Applied Catalysis A: General*, 137-144.

Y. Furumoto, Y. H. (2011). Effect of acidity of ZSM-5 zeolite on conversion of ethanol to propylene. *Catalysis A: General*, 262-267.

Z. Song, A. T. (2009). Production of propylene from ethanol over ZSM-5 zeolites . *Catal Lett*, 364-369.

Chapter 2: Catalyst Preparation and Experimental Techniques

Chapter 2. Catalyst Preparation and Experimental Techniques

2.1. Catalyst Synthesis

2.1.1. Metal-modified ZSM-5 zeolites & mesoporous catalysts

CBV 5524G ZSM-5 (SiO_2/Al_2O_3 ratio 50, surface area 425 m^2/g) is a Zeolyst International product, while Siral-1 silica alumina (Si/Al ratio 0.01, surface area 280 m^2/g) is a SASOL product. Each of these commercial supports was dried at 100 °C, before being calcined at 500 °C for 2 h. Afterwards, it was impregnated with a selected metal, dried at 70 °C and again at 78 °C. Before use, the sample was calcined at 500 °C for 5 h. The impregnation was performed using a suspension of the solid support with a solution of a the corresponding metal salt. The resulting material was then activated.

The metals selected for impregnation cover different categories of the periodic table: alkaline earth metals, transition metals, post-transition metals and lanthanides. A specific mass of the metal precursor and volume of water were selected to be mixed with a defined mass of the support in order to obtain 10 wt% of the metal on the support. The impregnation procedure involves physically mixing of the three components together: metal precursor, support and water. The metal precursors used were sulfate, nitrate and chloride salts of metals. The aim behind using different types of salts was to study whether or not the metal precursor type had an influence. Below (Table 2.4) is a table showing the prepared impregnated catalysts:

Table 2.4. Table showing 3 batches of CBV 5524G and Siral-1 impregnated catalysts, with metal and metal precursor types

Impregnated Metals	Metal Precursor	Catalyst Support
Mg-	Magnesium nitrate hexahydrate	+CBV5524G
		+Siral-1
W-	Ammonium metatungstate hydrate	+CBV5524G
		+Siral-1
La-	Lanthanum (III) nitrate hexahydrate	+CBV5524G
		+Siral-1
Fe-	Iron (III) nitrate nonahydrate	+CBV5524G
		+Siral-1
Bi-	Bismuth (III) nitrate peentahydrate	+CBV5524G
		+Siral-1
Ag-	Silver nitrate	+CBV5524G
		+Siral-1
Ni-	Nickel (II) nitrate hexahydrate	+CBV5524G
		+Siral-1
Al-	Aluminum nitrate nonahydrate	+CBV5524G
		+Siral-1
Co-	Cobalt (II) nitrate hexahydrate	+CBV5524G
		+Siral-1

Ce-	Cerium (II) nitrate hexahydrate	+CBV5524G
		+Siral-1
Sn-	Tin (II) chloride dihydrate	+CBV5524G
		+Siral-1
Mo-	Ammonium molybdate dihydrate	+CBV5524G
		+Siral-1
Ca-	Calcium nitrate tetrahydrate	+CBV5524G
		+Siral-1
Sr-	Strontium nitrate	+CBV5524G
		+Siral-1
Ba-	Barium nitrate	+CBV5524G
		+Siral-1
Cr-	Chromium (III) nitrate monohydrate	+CBV5524G
		+Siral-1
Cu-	Copper (II) sulfate pentahydrate	+CBV5524G
		+Siral-1
Ru-	Ruthenium (III) chloride hydride	+CBV5524G
		+Siral-1
Zr-	Zirconyl nitrate hydrate	+CBV5524G
		+Siral-1

2.1.2. Post-treated ZSM-5 zeolites & Siral-1 mesoporous catalysts

2.1.2.a. Via hydrothermal treatment

Hierarchical mesoporous zeolite can be generated via hydrothermal treatment using the dry gel procedure (HTS). This method is partially adopted from the work of K. K. Ramasamy *et al.* (K.K. Ramasamy, Conversion of ethanol to hydrocarbons on hierarchical HZSM-5 zeolites, 2014). Typically, for the synthesis used in this study, 2.5g of the commercial CBV 5524G or Siral-1 were placed in a Teflon-lined autoclave, and 2.5g of water was added to create steam during the hydrothermal synthesis conditions. The autoclave was then placed in a thermostatic bath set at 180 °C and kept up to 5 days for vapour-assisted hydrothermal crystallization. The final paste-like material was then dried at 110 °C in an oven overnight, then calcined at 500 °C for 20 h in a static air atmosphere. The final synthesized hierarchical mesoporous catalyst was smoothly crushed. The solvent evaporation procedure not only induces mesoporosity within the framework of the zeolite, but also generates nano-size zeolite crystals.

In total, six samples were obtained: raw CBV 5524G (commercial), CBV 5524G after autoclave plus 110 °C, CBV 5524G after autoclave followed by 100 °C followed by calcination, raw Siral-1, Siral-1 after autoclave plus 110 °C, Siral-1 after autoclave followed by 110 °C followed by calcination. These six catalysts were characterized and tested.

2.1.2.b. Via dealumination post-treatment

The post-treatments of the parent ZSM-5 zeolite included dealumination and desilication, following the work of H. Xin *et al.* (H. Xin, 2014). Dealumination was done with oxalic acid, and desilication with sodium hydroxide.

The dealumination treatment of the zeolite was carried out in an aqueous 0.5 M oxalic acid solution. To this end, 1.0g of the sample was reacted in 50 mL of oxalic acid solution in a flask. The mixture was transferred to Teflon container, heated to 120 °C, and kept at this temperature for 2 h. The resulting solid was separated by filtration and washed extensively with deionized water. The solid product was dried overnight at 100 °C and subsequently calcined in static air at 550 °C for 5 h (ramp rate 1 °C min^{-1}). The suffix –deAl refers to the sample being dealuminated by oxalic acid. The sample dealuminated from ZSM-5 was referred as ZSM-deAl.

The same dealumination procedure was also performed for Siral-1.

2.1.2.c. Via desilication post-treatment

The desilication treatment of the zeolites was performed in an aqueous 0.2 M NaOH solution. To this end, 3.3g of the sample was vigorously stirred in 100 mL of NaOH solution for 30 min at 65 °C. Subsequently, the reaction was quenched by submersion of the flask in an ice-water bath, followed by filtration and thorough washing with deionized water. The solid product was dried overnight at 100 °C and converted into the H-form by three consecutive exchanges in 1 M NH_4NO_3 solution (1g of zeolites was vigorously stirred in 30 mL of NH_4NO_3 solution) and subsequent calcination in static air at 550 °C for 5 h (ramp rate 1 °C min^{-1}). The suffix –deSi refers to the sample being desilicated by NaOH. The sample after desilication of ZSM-5 was referred as ZSM-deSi.

The same desilication procedure was also performed for Siral-1.

2.1.3. Na-exchanged CBV 3024E

To diminish the amount of acid sites of ZSM-5, NH_4 was exchanged for sodium following an ion-exchange procedure that involved mixing the zeolite with different amounts of NaCl in deionized water, followed by three days of continuous stirring. The resulting mixture was centrifuged for 10 minutes at 4000 RPM and washed with more deionized water for a total amount of 5 times. This was followed by drying the white paste overnight resulting in white powder, independent of NaCl amount.

2.1.4. Synthesized SAPO zeotypes

This work was done in collaboration with the International Joint Laboratory in Japan. Different zeotypes prepared include: SAPO-11, SAPO-34, SAPO-39 and SAPO-41.

2.1.4.a. Dry-Gel Conversion (DGC) of SAPO-34

SAPO-34 was synthesized by dry-gel conversion following the work of Nishiyama *et al.* (N. Nishiyama, 2009) (Y. Hirota, 2010). Catapal B. (Sasol), 20% colloidal silica solution from Nissant Chemical Industries, LTD. (SNOWTEX O) and an aqueous solution of phosphoric acid with a concentration of 88wt.% (Tokyo Chemical Industry) were used as respective sources of aluminium, silica and phosphorous. Tetraethylammonium hydroxide (TEAOH) produced by Tokyo Chemical Industry was used as SDA to obtained the desired silicoaluminophosphate. The molar ratio used was Al_2O_3, 1.0; P_2O_5, 0.3; SiO_2, 1.0; TEAOH, 7; H_2O, 77.

In a typical synthesis, TEAOH (7.220 mL) was mixed with distilled water (10 ml) in a beaker using a magnetic stirrer. To this mixture, Catapal B. (1.245 g) was slowly added and stirred at 250 rpm until a milky white suspension mixture was obtained. With continued stirring, phosphoric acid (1.20 mL) was added drop-wise to the latter at a rate of one drop each five seconds. This was followed by one hour of stirring, very slightly decolorizing the mixture. At the same drop-rate, colloidal silica (0.7 mL) was added to the beaker while stirring, which was continued for 1 hour. Afterwards, the mixture was poured into a ceramic plate and placed in a drying oven for 12 hours. This led to the formation of the dry-gel, a brittle, mildly transparent, white solid. The dry-gel was finely grounded and 1.50 g of it was placed in a 50 mL Teflon-lined auto-clave, to which 10 g of deionized water was added separately in a quartz tube. The autoclave was placed in an oven at 180 °C and crystallization was conducted for 24 hours. Once cooled, the product – brownish solution with a white precipitate – was washed with deionized water and centrifuged at 4000 rpm for 10 minutes three times. The resulting wet white powder was dried overnight in an oven at 90 °C. This afforded 1.077 g of white solid, which was labeled DGC-SAPO-34-BC. Part of the solid was grounded and calcined at 500°C for 12 hours, with a temperature increase ramp of 0.3 °C per minute. The resulting powder was labeled DGC SAPO-34-AC.

2.1.4.b. Hydrothermal Synthesis (HT) of SAPO-34 and SAPO-41

SAPO-34 was hydrothermally synthesized in accordance to the work of Prakash *et al.* (Unnikrishnan, 1994). Numerous other methods are available for the hydrothermal synthesis of SAPO-34 and the choice of using this particular one results from the availability of certain regents. Catapal B. (Sasol), fumed silica (Sigma-Aldrich) and an aqueous solution of phosphoric acid with a concentration of 85wt.% (Wako) where used as respective sources of aluminium, silica and phosphorous. Morpholine (Tokyo Chemical Industry) served as the structure directing agent (SDA) for the formation of the desired silicoaluminophosphate. The molar ratio used was Al_2O_3, 1.0; P_2O_5, 1.0; SiO_2, 1.0; Morpholine, 2; H_2O, 66. In a typical synthesis, water (6.040 g) was mixed with phosphoric acid (5.661 g) in a glass beaker using a magnetic stirrer until homogenization. To this mixture, Catapal B. (3.077 g) was slowly added, followed by 3.330 g of water. The mixture was stirred overnight at room temperature, resulting in an opaque, milky white mixture. To this intermediate mixture was added morpholine (3.888 g) until a single, yellowish white and opaque phase was obtained. Fumed silica (1.377 g) was slowly added and left to stir for 7 hours. The resulting mixture was transferred to a 50 ml Teflon-lined stainless steel autoclave and aged for 24 hours at 30 °C

without agitation. Following this, the autoclave was put in an oven at 200 °C for 24 hours. After this period, the autoclave was quenched in cold water. The product was rinsed with deionized water and separated by centrifugation at 4000 RPM for 10 minutes; this process was repeated 3 times. The resulting white, paste-like substance was dried overnight at 90 °C. This yielded 2.443 grams of dried solid. The dried substance (labeled HT-SAPO-34-BC) was grounded and calcined at 500 °C for 12 hours, with a temperature increase ramp of 0.3 °C per minute. The resulting powder was labeled HT-SAPO-34-AC.

SAPO-41 was hydrothermally synthesized following the instructions outlined in the publication of Ma *et al.* (Y. Ma, 2006). The particularity of this reaction is the simultaneous sources of phosphorous: phosphoric acid (H_3PO_4) and phosphorous acid (H_3PO_3) to ensure reproducibility. The regents used were phosphoric acid 85wt.% wt (Wako Pure Chemical Industries, Ltd.), dipropylamine (DPA) from Wako Pure Chemical Industries as SDA, 20% colloidal silica solution (SNOWTEX O) from Nissan Chemical Industries, LTD. and Catapal B (72% Al_2O_3) from Sasol as aluminum source. In a typical synthesis, Catapal B (2.607 g) was mixed with deionized water (23.405 mL) in a glass beaker using a magnetic stirrer for 30 minutes. A white suspension was obtained. Separately, using a Teflon-lined spatula, H_3PO_3 (1.532 g) was dissolved in 7.8 mL of deionized water and mixed together with H_3PO_4 (2.50 ml) until clear. Drop-wise, the H_3PO_4/H_3PO_3 solution was added to the Catapal B mixture at a rate of 1 drop every 5 seconds, with continuous stirring at 300rpm. After 1 hour, DPA (10 mL) was slowly added to the mixture while stirring, which was continued for one more hour. The yellowish white mixture that resulted was transferred into a 50 mL Teflon-lined autoclave. Crystallization was done at 200 °C for 24 hours. After this period, the autoclave was quenched. The mixture in the autoclave consisted of a transparent orange liquid phase and a white precipitate. The precipitate was washed with deionized water and separated by centrifugation at 4000 rpmfor 10 minutes; this process was repeated 5 times. The resulting white paste was dried overnight at 90 °C. This yielded 0.838 g of fine, white powder, labeled HT-SAPO-41.

2.2. Characterization Techniques

The synthesized solids were characterized by a set of physico-chemical techniques, allowing to better understand their structure, their properties and their reactivity.

2.2.1. Textural characterizations

The characterizations were performed on Tristar II 3020 apparatus or a 3 Flex of Micrometrics for specific surface area and porosity measurements. The specific surface area (S_{BET}) was obtained using the BET method and the pore distribution was calculated according to the Barret-Joyner-Halenda (BJH) formula. The total pore volume (Vp) was determined on the isotherms at a relative pressure (P/P^0) of 0.995.

2.2.2. XRD

The X-rays diffraction is a technique allowing the determination of the nature of crystalline phases comprising the catalyst but also the evaluation of the crystallites size. These characterizations were realized on a D8 Advanced Bruker AXS diffractometer equipped with a goniometer of θ/θ type (fixed sample). The source of X-rays is a copper anticathode characterized by a wavelength λ equals to 1.5406 Å corresponding to the Cu-$K_{\alpha 1}$ line. The diffractograms are registered in an angular range 2θ between 5 and 60°, with an angle step of 0.02 and an acquisition time of 0.5s per step.

The reprocessing of diffractograms is executed on EVA software (Diffrac-plus), owning a very detailed database of thousands of crystalline phases, plus commonly called JCPDS file (Joint Committee on Powder Diffraction Standard). These files are employed for identifying the phases contained in every catalyst. Furthermore, thanks to the Debye-Scherrer law, the crystallites size can be estimated from the diffractograms by the following formula (Scherrer, 1918):

$$t_p = \frac{K\lambda}{\beta\, Cos\theta}$$

where t_p: mean size of the ordered (crystalline) domains (unit in nm)

K: dimensionless shape factor equal to 0.89 (unitless)

λ : X-ray wavelength equals to 0.15406 nm (unit in nm)

β: line broadening at half the maximum intensity (FWHM) [unit in radians]

θ: Bragg angle (unit in degrees or radians, since the Cosθ corresponds to the same number)

The way to get FWHM (standard) is to run a reference sample on the instrument with the same parameters as for the unknown sample. The standard will enable us to subtract the instrumental broadening, so that the remaining broadening can be related to size (and microstrain). So,

FWHM (structure) = FWHM (observed) – FWHM (standard)

Instrumental contributions arise from factors such as the following: misalignment of the diffractometers, axial divergence of the incident/diffracted beams etc.

2.2.3. XPS

XPS, or X-ray photoelectron spectroscopy, is an analysis technique employed for determining the chemical composition of the surface of our materials (up to 10 nm of depth) but also the nature, and more particularly the oxidation degrees in which the elements are found.

The principle (Figure 2.**11**) of this analysis is to irradiate the sample thanks to the monochromatic X-rays having a specific energy hν [where h is Planck's constant ($6.626 . 10^{-3}$ J.s), and ν is the irradiation frequency] in a sealed chamber under vacuum (10^{-7} Pa). The irradiation of an element will generate photoelectrons having a kinetic energy E_{kin} characteristic of the orbital energy involved. The number of electrons ejected as well as their kinetic energy will be registered by the detectors and the XPS spectrum corresponds thus to a plot of the number of electrons detected as a function of their binding energy (BE). The energetic balance of the XPS analysis can be therefore written:

$$BE = h\nu - E_{kin} - W_f,$$

where W_f is a work function.

Thanks to data tables in literature, every peak can be attributed, providing information on the atom analyzed and the bond in which it is involved, etc… The integration of the corrected peaks of the cross section relative to each element allows an atomic semi-quantitative analysis on the surface of samples. The reprocessing of XPS data was carried out via CasaXPS software.

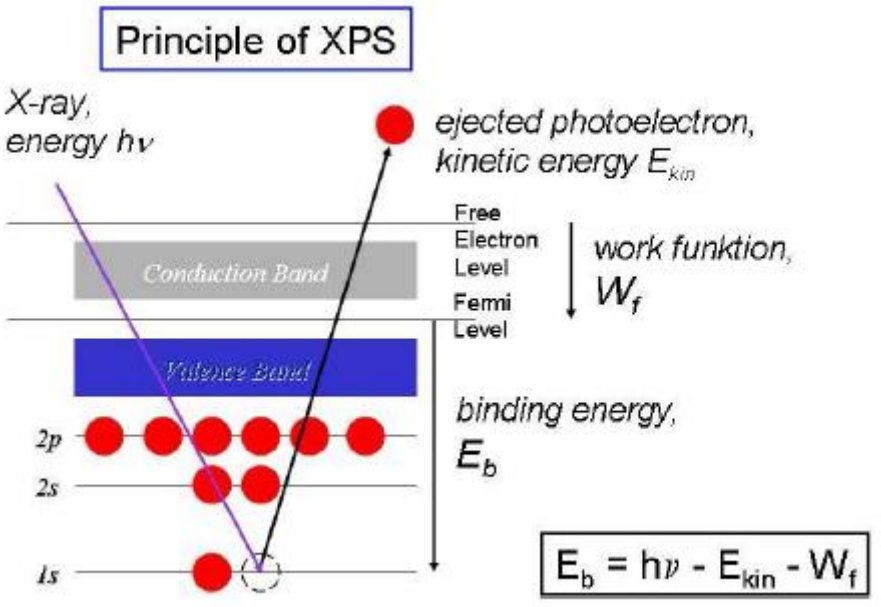

Figure 2.11. Principle of XPS analysis (htt1)

The XPS analyses were performed on a VG ESCALAB 220XL spectrometer, using a radiation source of aluminum of 1486.6 eV energy (Al-$K_{\alpha 1}$).

2.2.4. TGA and TGA-MS

The thermogravimetry is a technique where the loss of sample mass is represented as a function of time or temperature under controlled atmosphere. In order to improve the

visibility of mass losses, the derivative of the thermogravimetry (DTG) is frequently plotted. TGA was performed on an instrument allowing the measurement of mass loss of type SERATAN 92-16. The sample is deposed in an alumina crucible previously weighed. The analyses are performed between 25 and 800 °C, with a ramp of 10 °C/min under a flow of 20 mL/min of argon. An OMNISTAR mass spectrometer was placed at the outlet of the TGA to analyze the nature of the desorbed species.

2.2.5. TPR-MS

Temperature-programmed reduction (TPR) is a characterization technique for heterogeneous catalysts to find the most efficient reduction conditions. An oxidized catalyst is submitted to a flow of a reducing gas (*i.e.* H_2) along with a programmed temperature rise, thus allowing to follow the reduction of the sample as a function of temperature. Due to the quantification of the hydrogen consumption, this type of analysis also offers the possibility to know the amount of metal oxide MO that can be reduced:

$$MO_{(s)} + H_{2(g)} \rightarrow M_{(s)} + H_2O_{(g)}$$

The total flow was fixed at 50 mL/min of hydrogen in helium, with a 5% hydrogen concentration, and the heating rate chosen is 10 °C/min. A pretreatment under argon at 600 °C is carried out to eliminate the water traces and the physisorbed species. The apparatus over which we performed the experiments is a Micrometrics AutoChem III.

Other TPR-MS characterizations were conducted in the International Joint Laboratory-Japan, in an IR system connected with a capillary line to MS spectrometer (ANELVA M-200QA-F). The capacity of the retained hydrocarbon species to generate olefins in absence of ethanol was evaluated by first protonating the Na-exchanged ZSM-5 zeolite at 500 °C under a flow of helium, after which the ETH reaction was conducted for 10 minutes at 250 °C with a feed of 12% EtOH/He at a flow rate of 30ml/min. Following this, the catalysts were quickly cooled down. The temperature was then increased to 475 °C under helium to expel the lighter hydrocarbons into the MS spectrometer.

2.2.6. *In situ* UV/Vis Spectroscopy

Diffuse reflectance UV/Vis measurements were made using a UV/Vis diffractometer (JASCO V-550) equipped with an *in situ* flow cell having a quartz window. The cell has a heating system inside and is connected to a gas flow system. A thermocouple located under the bed of the sample cell was used to measure the local temperature. This gas flow allows an ethanol/nitrogen mix or pure nitrogen to go through the catalyst. UV/Vis spectra were recorded during the ethanol-to-olefins reaction. This technique is well-adapted to detect the presence of conjugated hydrocarbons. Absorbance was measured using the Kubelka Munk theory of reflectance.

The catalysts were first activated under nitrogen flow at 450 °C for 1 hour. UV/Vis spectra were then recorded during the ethanol-to-olefins reaction over H-ZSM-5 at 300 °C and a concentration of 12% EtOH, and after the feed was switched to nitrogen feed. Another similar procedure was performed at 450 °C. Also, this was performed over the different ion-exchanged ZSM-5 catalysts at 450 °C reaction temperature. On the other hand, similar tests were also applied for the SAPO-34 samples at 350 °C and 12% EtOH feed to measure the effect of crystal size. A UV/Vis experiment was done with the nano-sized SAPO-34, first during the ethanol-to-olefins reaction at 350 °C for a feed of 12% EtOH, then using a feed of 1% ammonia.

2.2.7. Inductively coupled plasma mass spectrometry (ICP-MS)

This elemental analysis allows to detect metals and several non-metals composing the catalyst, along with their mass fraction (wt.%). ICP-MS has many advantages over other elemental analysis techniques such as atomic adsorption and optical emission spectrometry, including ICP Atomic Emission Spectroscopy (ICP-AES). An ICP-MS combines a high temperature ICP (Inductively Coupled Plasma) source with a mass spectrometer. The ICP source converts the atoms of the elements in the sample into ions. These ions are then separated and detected by the mass spectrometer.

The concentration of sodium in each prepared samples of ion-exchanged CBV 3024E was calculated using inductively coupled plasma on-line with an MS spectrometer (ICP-MS). For samples that have particulate matter, a process known as sample digestion may have to be carried out before it can be pipetted and analyzed. A small amount of each ion-exchanged sample was dissolved in sulfuric acid and a small volume was introduced in the ICP MS machine – a Shimadzu ICPE-9000 – providing the quantity of sodium in ppm for each solution. With the amount of ion per weight of catalyst, it was possible to determine the degree of ion exchange and the Na/Al ratio. This technique was done with collaboration with the International Joint Laboratory.

As a rule, acid digestion procedures are employed for the determination of elements in solids subsequent to sampling and mechanical sample preparation in order to completely transfer the analytes into solution so that they can be introduced into the determination step (ICP-MS) in the liquid form. The goal of every digestion process is therefore the complete solution of the analytes and the complete decomposition of the solid while avoiding loss or contamination of the analyte. In this context, wet chemical digestions utilizing various mineral acids (e.g. H_2SO_4) is carried out in either an open system, that is, under atmospheric pressure, or in closed vessels. Regarding the chemistry of acid digestion, sulfuric acid is a non-oxidizing acid. The boiling point of 98% H_2SO_4 is 340 °C. It is effective for the digestion of minerals. Naturally the employed vessels must be resistant to acids used.

2.2.8. Pyridine FTIR

The acid sites are generally characterized by adsorption of ammonia (NH_3) and the basic sites by adsorption of carbon dioxide (CO_2). While ammonia (Kinetic diameter

approximately 3.57 Å) can have access to almost all the acid sites in the microporous zeolites, pyridine with kinetic diameter of almost 5.85 Å may not approach to the acid sites situated in relatively small pores (Masih, 2010). But when desiring to distinguish between Lewis and Brønsted acids sites, pyridine is a good choice as a probe molecule. However, its relatively large size (0.57 nm) restricts its use to zeolites with large pores and some zeolites with intermediate-size pores. It is a relatively strong base (pKa= 5.2) which: First, is protonated on Brønsted sites (forming a pyridinium ion). Second, it is coordinated to the Lewis sites. Third, it forms hydrogen bonds with less acidic OH groups (silanols). All these modes of adsorption are illustrated in Figure 2.**12**. To these modes of chemical adsorption, is added a physical adsorption which must be removed (by heat treatment) for not to be hindered. The pyridine adsorption can be done in two ways: standard additions (accurate method but quite tedious) or saturation of the sample. The experimentation by transmission infrared spectroscopy (IR) allows highlighting the types of bonds present within the analyzed sample thanks to the characteristic bands of these ones.

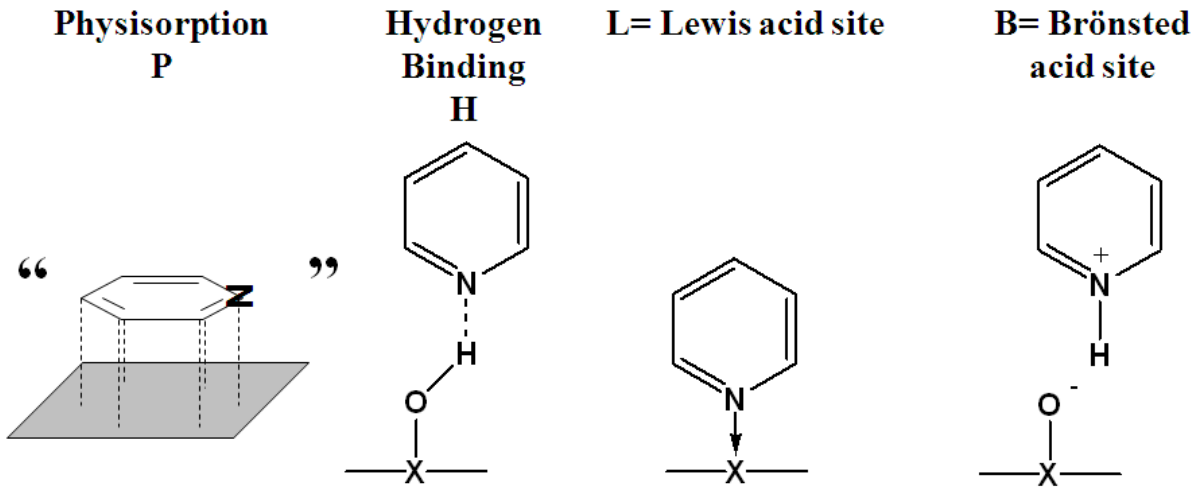

Figure 2.12. Pyridine modes of adsorption

In the procedure that we adapted, pellets were prepared firstly by grinding a mixture of catalyst and of dry potassium bromide (KBr) with a 1% of mass percentage of the catalyst. Afterwards, pellets of 30mg are formed using a press and placed in the sample holder of the IR spectrometer. Then, all samples were heated at 450 °C under high vacuum (10^{-6} mbar) for 2 hours. An average of 64 scans is recorded between 400 and 4000 cm^{-1} at room temperature and under vacuum, by a Nicolet 460 Fourier Transform IR Spectrometer. Pyridine adsorption was performed at room temperature at 1.2 mbar at equilibrium for 30 minutes. Then the molecule was desorbed under vacuum, first at 150 °C for 15 minutes, then at 250, then 350 and finally at 450 °C (Figure 2.**13**).

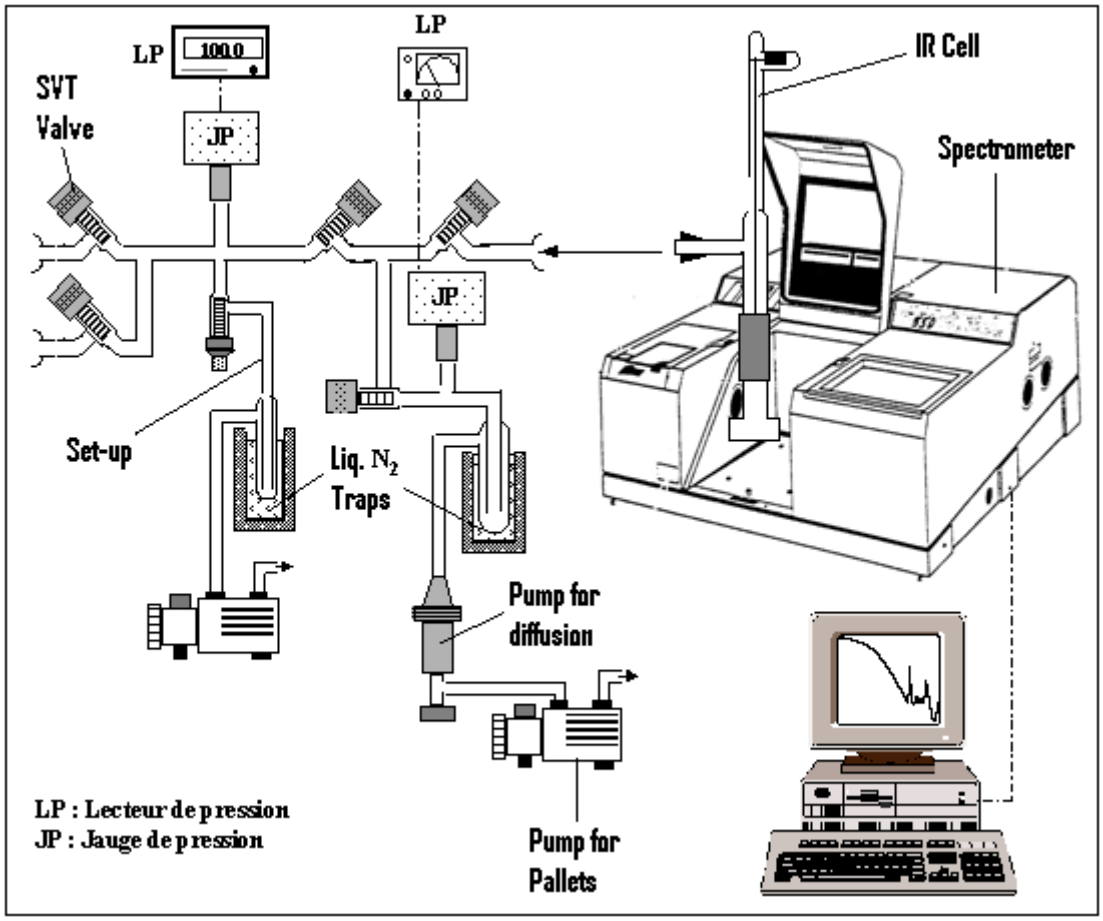

Figure 2.13. Adsorption of probe molecules followed by IR spectroscopy under dynamic vacuum

2.2.9. NH_3-TPD

The measure of the acidity of the samples was determined by a thermal desorption method of ammonia probe molecule using a TCD detector. The principle of the method is to adsorb a probe molecule selectively on acidic sites then follow the desorption of the latter. The strength of sites can be determined from desorption temperature since the stronger the sites are the more energy should be provided to desorb the probe molecule. On the other hand, the quantity of the sites can be calculated by measuring the area of desorption peaks.

15mg of the catalyst was degassed under helium (27 mL/min) at 250 °C (10 °C/min) for 2 h in order to remove and desorb species. It was then cooled at 130 °C, before being flushed with ammonia at 130 °C. After the purge, the desorption of ammonia was performed with a temperature ramp of 10 °C/min up to 700 °C for 15 min. The molecules of desorbed NH_3 are detected and quantified by a TCD detector. The calibration of their response was performed by injecting 1 mL pulses of helium/ammonia mixture. The number of sites is obtained by integrating the response of the TCD signal and then applying to it the determined response factor. The thermograms obtained are initially subtracted from a blank test in order to correct the drift of the baseline. Finally, they are smoothed for greater clarity when several thermograms are superimposed.

2.3. Apparatus Description

2.3.2. FLOWRENCE T1220 platform description

Some ZSM-5 and SAPO-34 zeolites were tested on a AVANTES Flowrence T1220 apparatus using the REALCAT platform. It allows the parallel testing of up to 16 catalysts in a same experiment. The reactors are divided into four different blocks, allowing to vary the parameters of each block the way one wants, as reaction temperature for example. Next to rapid screening of catalyst libraries, the high throughput approach allows the simultaneous optimization of the reaction conditions like GHSV, reactant concentration and reaction temperature etc. In this approach, the fixed-bed catalyst is sandwiched between two layers of carborandum. Ethanol mixed with diluent gas (He and N_2) flows through the reactors. The outlet of each and every reactor is connected to GC online analysis. The total gas flow rate was fixed to a GHSV of 25215 mL/g_{cat}.h during the reaction, and the gas composition was kept as 0.0125 mL/min of liquid ethanol, and 21 mL/min of helium/krypton taken as a carrier gas (also because one reactor).

Concerning the on-line GC analysis on a FLOWRENCE® Reactor system-T1220, the GC built-up consists of: a side_TCD, injectors, purge and splits, pneumatics injectors, pneumatics detectors, pneumatic Aux EPC, electronics, actuator controls, detector boards, injector boards and key path. The set-up has three separation channels, with three column sets: PPQ/PPQ, DB-624/DB-624 and HayeSep Q/Molsieve. The selection of the columns is based on the analyte list: all permanent gases (He, H_2, N_2, CH_4 and CO), alkanes or alkenes (C1-C3, CO_2) and several classes (oxygenates). For the Agilent 7890A GC conditions, the oven program is as follows: 40 °C (2 min) → at 20 °C/min → 132 °C.

All channels of the GC are equipped with back-flush valves to shorten analysis time. The front TCD analyses CO_2 and hydrocarbons, with the separating columns being two PPQ at constant pressure. The carrier gas here is He at constant pressure (Split, 250 µL loop). On the other hand, the back FID channel in the GC is dedicated to detect oxygenates. Columns used are DB-624 (2m, 0.25 mm) and DB-624 (28m, 0.25 mm). The carrier gas here is He at constant pressure (Split, 250 µL loop). The third detector used is Aux TCD for permanent gases, where the columns used are HayeSep Q and Molecular Sieve. The carrier gas here is Ar (Splitless, 250 µL loop). So in the case of the ethanol-to-olefins reaction, ethanol peak appears on the back channel

2.3.3. Multi-Valve reactor system description

As a second catalytic test device, a homemade multi-valve reactor was employed (Figure 2.**14**). Four liners (consequently four reactors) are comprised in this system. The stacking of every liner is as follows: starting from the bottom, 100mg carborandum SiC (1.19 mm particle diameter), then 100mg SiC 0.5 mm, 100mg SiC 0.25 mm, and 100mg SiC 0.125 mm consequently. Then, we deposit the catalyst (active phase, xxmg). Afterwards, we deposit the inverse of the aforementioned stacking of SiC. That is, 100mg SiC 0.125 mm, then 100mg SiC 0.25mm, then 100mg SiC 0.5mm finally SiC 1.19mm.

Liners are placed in their proper positions inside the reactors, in the heating oven. The flow of He/Kr used for almost all reactions was 21 mL/min per reactor, so 84 mL/min as total flow for four reactors. The He/Kr flow rate was kept fixed, and varying the flow rate of liquid ethanol depends on the desired percentage of ethanol in the gaseous phase (based on calculations). In our experiments performed on this apparatus, only two concentrations of ethanol were used in the gaseous phase: 20 and 50%. Ethanol used is: Ethanol puriss, p.a., AC reagent, absolute- ≥ 99.8%, Fluka. The temperature of the whole equipment maintained at 100 °C in order to avoid the condensation of ethanol and products. The transfer line is heated up to 150 °C. This transfer line conducts the products formed in the reaction from the exit of reactors to the GC.

The analytical system is composed of an Agilent 7890A chromatograph equipped with a "valve box" (Figure 2.**14**) heated at 120 °C, which analyses the gases coming from the reactors in a sequential way. It is this "valve box" that allows selecting the reactor using a multi-position valve (1 → 8). It allows also, via a fine adjustment, toggling polar molecules and apolar molecules towards the appropriate columns and detectors. In our case, this switching time is 2.3 minutes, inducing an ideal separation of the compounds.

The GC oven contains 3 columns, each playing a specific role. The reaction mixture passes first through a Restek STABILAX-DB column (15 m X 0.25 mm X 0.5 μm) which leads to a separation of polar and apolar compounds. These latter (Kr, ethylene, propylene, butane, BTXs…) are sent to another Agilent HP-PLOT/Q column (30 m X 0.25 mm X 1 μm) to be separated and analyzed by a thermal conductivity detector (TCD). The polar products (ethanol, acetaldehyde…) are meanwhile oriented to another column, a Phenomenex-Zebron ZB-Bioethanol (30 m X 0.25 mm X 1 μm), then analyzed using a flame ionization detector (FID).

The reprocessing of analyses is possible through Chemstation software, where the integration of peaks corresponding to the reaction products is carried out. The performance of the catalyst was calculated as follows:

Ethanol conversion (%): $X= \frac{n0-n\ X100}{n0}$

where n^0 is the initial number of moles of ethanol and n is the number of unconverted ethanol.

The initial number of moles of ethanol is calculated as follows:

$n_0= A_0$ EtOH * Rf of EtOH

where Rf is the response factor of ethanol, derived from previous calibrations and A_0 is the peak area viewed on FID for ethanol initially introduced in the system.

The selectivity for every product formed is as follows:

Selectivity to product (%): $S = \frac{nCx * nx}{nCEth\ (n0 - n)}$

where n_{CX} is the number of carbons in the product x, n_x is the number of moles of the formed product x, and n_{CEth} is the number of carbon atoms in one ethanol molecule (i.e., 2).

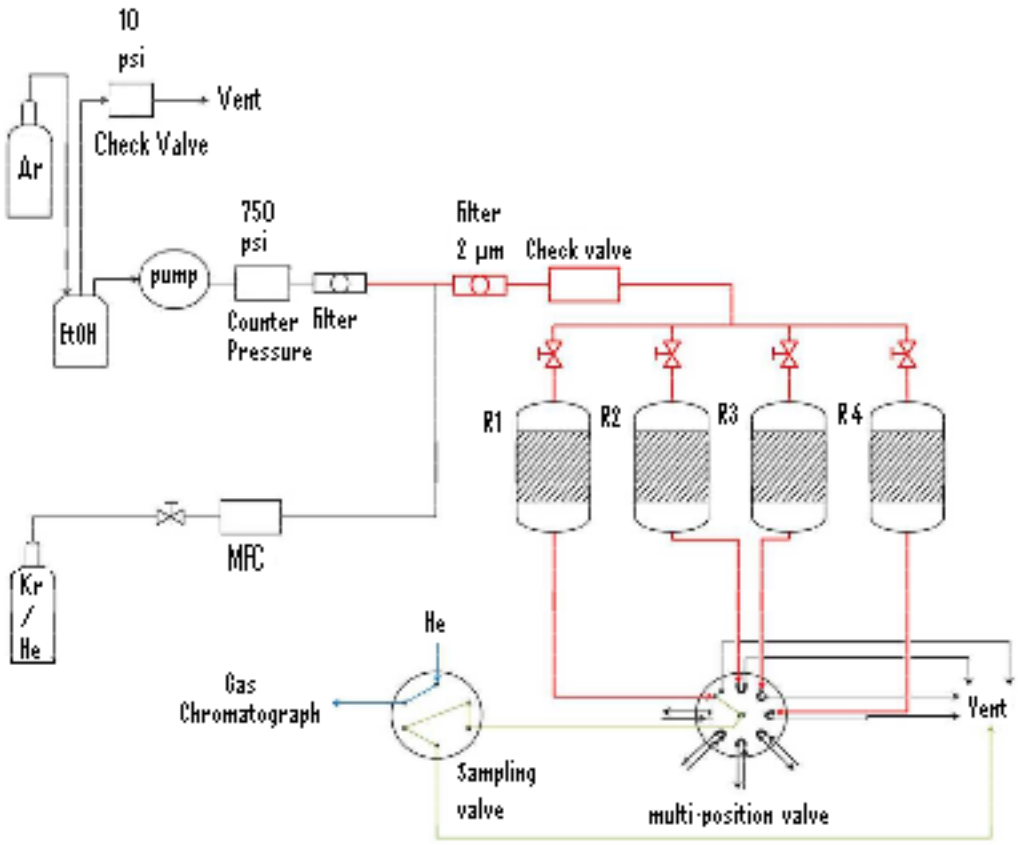

Figure 2.14. Scheme of Multi-Reactors catalytic system (Tesquet, 2013)

2.3.4. GC-MS apparatus

A GC-MS setup was employed to indentify the products formed in the ETP reaction (GC, Agilent Technologies, 7890A GC System, MS: Agilent Technologies 5975C VL MSD with Triple-Axis Detector with was a Zebron ZB-BIOETHANOL 44m; 291 µm; 13.5 µm column).

Catalytic test of ethanol conversion into propylene was performed using a classical fixed bed reactor. Before the experiment, 50 mg of the catalyst were mixed with 50 mg of SiC (Ø= 0.125 mm), in order to homogenize the temperature inside the catalytic bed. On top of this mixture, place 125mg SiC (same particle size). The catalyst used for this test was tungsten-doped CBV5524G.

The catalytic tests were carried out in a glass reactor consisting of a 10 mm diameter tube connected on line with a GC-MS apparatus, which enabled analysis runs every 20 min. The reaction was performed at dynamic temperatures from 250 to 350 °C under atmospheric pressure. 5-7 injections were performed for each of the temperature steps. The total gas flow rate was fixed to a GHSV of 25215 mL/g_{cat}.h during the reaction, and the gas composition was kept as 0.0125 mL/min of liquid ethanol, and 21 mL/min of helium/krypton taken as a carrier gas (also because one reactor). These conditions are the same as those on the GC-Multi-Valve Reactor System, and as Flowrence T1220 in order to mimic the same test. The final list of definitive products formed in the ETP reaction could be obtained in combination of two softwares: GC-MS Data Analysis and le WebBook de Chimie NIST (online), by referring to the molecular weight of products identified at a specific recuperation time.

2.3.4.a. Products identified on GC-MS apparatus

All authors dealing with the ethanol-to-propylene reaction cited the products formed based on their own reaction conditions. Some discussed light olefins, while others focused on aromatics. We wanted to verify this using the GC-MS setup. The catalyst tested was W+CBV50 (50mg) at 350 °C. 21 ml/min He and 0.0125 ml/min EtOH were used per reactor. This catalyst was chosen for the GC-MS test since it is one of the best performing catalysts in terms of propylene yield. Here is a list of the products “certainly” formed at this reaction temperature and reaction conditions:

- Ethylene
- Propylene
- 1-Propene, 2-methyl-
- 1-Butene
- 2-Butene
- Isobutane
- Butane, 2-methyl-
- 1-Butene, 2-methyl-
- 2-Butene, 2-methyl-
- Cyclopropane, 1,2-dimethyl-, cis-
- Cyclopropane, 1,2-dimethyl-, trans-
- Pentane, 2-methyl-
- 1,4-Hexadiene

- Ethylbenzene
- p-Xylene
- 1,3-Dimethyl-1-cyclohexene
- 1,4-Pentadiene, 2,3,3-trimethyl-
- Benzene, 1-ethyl-2-methyl-
- Benzene, 1-ethyl-3-methyl-
- Mesitylene (or 1,3,5-trimethylbenzene)
- Benzene, 1,4-diethyl-
- Benzene, 1-methyl-3-(1-methylethyl)-
- 1,4-Pentadiene, 3-methyl-
- 1,4-Hexadiene, 2,3-dimethyl
- Benzene, 1,2,4-trimethyl-
- Benzene, 1,2,3-trimethyl-

Products identified at low temperature of 250 °C over tungsten-impregnated CBV50 include unreacted ethanol, ethylene resulting from intermolecular dehydration of ethanol, ethyl ether resulting from intermolecular dehydration of ethanol, 1-Propene-2-methyl and 2-butene. Thereby, the limit of olefins formed at this temperature is C^4. No propylene is detected at this level.

2.4. References

(n.d.). Retrieved from http://www.ifw-dresden.de/institutes/ikm/organisation/dep-31/methods/x-ray photoelctron-spectroscopy-xps

A. Le Bail, H. D. (1988). Ab-initio structure determination of LiSbWO6 by X-ray powder diffraction. *Mat. res. Bull.* , 447-452.

C.P. Stemmer, J. S. (xxxx). In-situ UV-Visible and Raman Spectroscopy for Gas-Liquid-Solid Systems. *Ind. Eng. Chem. Res.* , xxx-xxx.

Dumeignil, S. P. (2013). REALCAT-Driving Innovation in Catalysis. *Wiley-VCH Verlag GmbH & Co. KGaA, Weinheim* .

G. Scacchi, M. B. (2008). Livre Cinétique et catalyse. 401-402.

H. Xin, X. L. (2014). Catalytic dehydration of ethanol over post-treatedZSM-5 zeolites. *Journal of Catalysis* , 204-215.

K.K. Ramasamy, H. Z. (2014). Conversion of ethanol to hydrocarbons on hierarchical HZSM-5 zeolites. *Catalysis Today* , 103-110.

M. Colmont, G. B. (2015). Novel La3Fe(MoO4)6 phase: magnetic properties and ethanol selectivity. *Daton Transactions* , 14444-14452.

Masih, J. (2010). Hydroisomerization of a hydrocarbon feed containing n-hexane on Pt/H-Beta and Pt/H-Mordenite catalysts. *J. Chem. Pharm. Res.* , 546-553.

N. Nishiyama, M. K. (2009). Size control od SAPO-34 crystals and their catalyst lifetime in the methanol-to-olefin reaction. *Applied Catalysis A: General* , 193-199.

P. Amoros, D. B.-P. (1988). Crystal structure of A(VO~2~)(HPO~4~)(A=NH~4~^+^,K^+^, Rb^+^) solved from X-ray powder diffraction. *Eur. J. Solid. State. Inorg. Chem* , 599-607.

Rene, D. (2013, April 3). Analytics Department. *T1220 On-line GC analysis on FLOWRENCE® reactor system* . Amsterdam.

S. Brunauer, P. E. (1938). Adsorption of Gases in Multimolecular Layers. *J. Am. Chem. Soc* , 309.

Scherrer, P. (1918). Bestimmung der Grösse und der inneren Struktur von. Kolloidteilchen mittels Röntgenstrahlen. *Nachr. Ges. Wiss. Göttingen* , 98-100.

Tesquet, G. (2013, 10 25). PhD Thesis. *Etude de la reaction de Guerbet, à partir de boethanol, sur des oxydes mixtes de type pérovskite* .

Unnikrishnan, A. P. (1994). Synthesis of SAPO-34: high silicon incorporation in teh presence of morpholine as template. *Journal of the Chemical Society, Faraday Transactions* , 2291.

Valyon, F. L. (2001). On the interpretation of the NH3-TPD patterns of H-ZSM-5 and H-mordenite. *Microporous and Mesoporous Materials* , 293-301.

Y. Hirota, K. M. (2010). Dry gel conversion synthesis of SAPO-34 nanocrystals. *Materials Chemistry and Physics* , 507-509.

Y. Ma, N. L. (2006). Synthesis of SAPO-41 from a new reproducible route using H3po3 as the phosphorus source and its application in hydroisomerization of n-decane. *Journal of Molecular Catalysis A: Chemical* , 9-14.

Chapter 3: Prescreening – Results and Discussion

Chapter 3. Prescreening - Results and Discusion

Bare acid supports are not only active in ethanol dehydration to form ethylene and diethyl ether, but also in propylene formation (H. Oikawa, 2006). Different types of heterogeneous catalysts were dedicated in this study in order to find relations between properties (e.g. textural, acidity, etc...) and catalytic activity.

3.1. ZSM-5 zeolites

3.1.1. ZSM-5s with different SiO_2/Al_2O_3 mole ratios

Our first aim was to select the most adequate catalyst support, then to modify it with different metals (refined screening chapter). Our field of studies was focused on zeolites (ZSM-5s, SAPO-34s, etc.) and mesoporous catalysts (Sirals, MCM-41 etc.). In the ZSM-5 set, we performed characterizations and tests over supports with different SiO_2/Al_2O_3 ratios such as 23 (CBV 2314), 30 (CBV 3024E), 50 (CBV 5524G) and 280 (CBV 28014). We got these supports from Zeolyst International. To make things simpler, we will transform the labels into CBV23 for the ratio 23, CBV30 for the ratio 30, CBV50 for the ratio 50 and CBV280 for the ratio 280. Different catalysts not only have different pore dimensions, but also different acidities in terms of number, force and type. In order to study the influence of a calcination prior to the catalytic testing, CBV50 was chosen as a reference. The calcination temperature was 500 °C under static air, for two hours.

- N_2 porosimetry:

As one knows, zeolites are microporous materials. Hence the porosity was determined by nitrogen physisorption (Table 3.**5**). Raw CBV280 and CBV50 show similar BET surface areas (312-352 m^2/g) and pore volumes (around 0.1 cm^3/g). However, the raw CBV23 shows a lower BET surface area (163 m^2/g) and pore volume (0.06 cm^3/g). On the contrary, BJH pore distribution shows similar results for all samples with a mono modal distribution (Figure 3.**15**). The average pore sizes vary from 4 to 7 nm.

The effect of the calcination has been evaluated on the CBV50 sample. It leads to an increase of the specific surface to 418 m^2/g (Table 3.**5**). For calcined samples, calcinations was carried out at 500 °C for 2 hours. This can be explained by that CBV50 is highly amorphous, so calcination might have an effect on the morphology as we will see later in the XRD results section. We didn't calcine other supports nor performed nitrogen physisorption tests because the raw catalysts did not show interesting catalytic activity, as we will see later. BJH pore distribution of all raw CBV (s) shows a mono modal distribution (Figure 3.**15**).

Table 3.5. Textural parameters of the raw zeolites

Solid catalyst	S_{BET} (m^2/g)	pore volume (cm^3/g)	pore diameter (nm)
CBV23 (raw)	163	0.06	Mono-model 7
CBV280 (raw)	352	0.06	Mono-model 4
CBV50 (raw)	312	0.11	Mono-model 6
CBV50 (Cal 2 hrs)	418	0.12	Mono-model 5

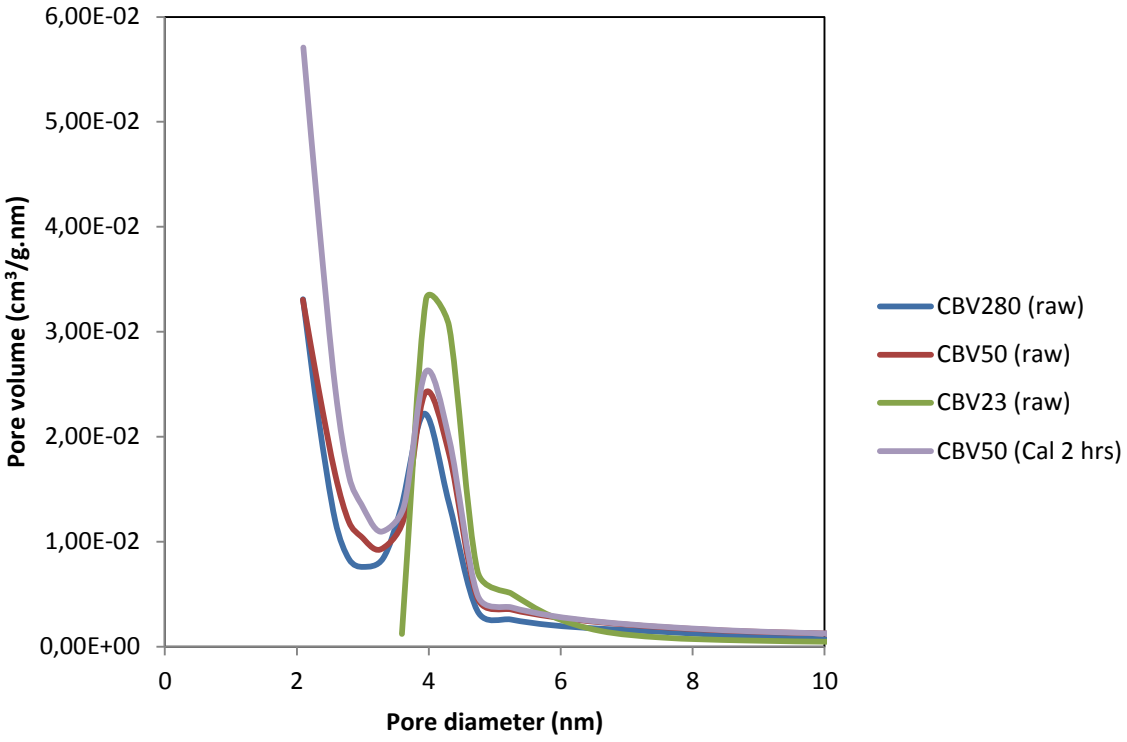

Figure 3.15. Pore distribution by BJH method for bare zeolites

- XRD:

In order to determine the crystallinity of the samples, the latter were analyzed by XRD. We see from the XRD results that all ZSM-5 catalysts show an orthorhombic SiO_2 crystal system, typical for H-ZSM-5 material (JCPDS 01-089-1421) (Figure 3.16).

The diffractogram of the calcined CBV23 did not change from that of the raw one, same for CBV50 (Figure 3.16). CBV23 and CBV50 show orthorhombic crystal structures, before and after calcination. This proves that the CBV series is robust against calcinations, even up to temperature of 500 °C.

If we compare the reference XRD to that of the raw CBV280, we realize that the intensity of the reflection planes (200) at 2θ: 8.83° and (020) at 2θ 8.93° had decreased (Figure 3.**17**). Peak intensities for the 2θ range 13.24-17.82° were conserved. Also, the reflection plane (332) at 23.07° decreased. On the other side and by comparing the reference spectrum to that of the calcined CBV280, we find that also the reflection plane (200) at 8.83° decreased. Same for the (131) plane at 15.55°. The reflection plane (332) at 2θ 23.07° increased, while on the contrary the (051) plane at 23.31° decreased.

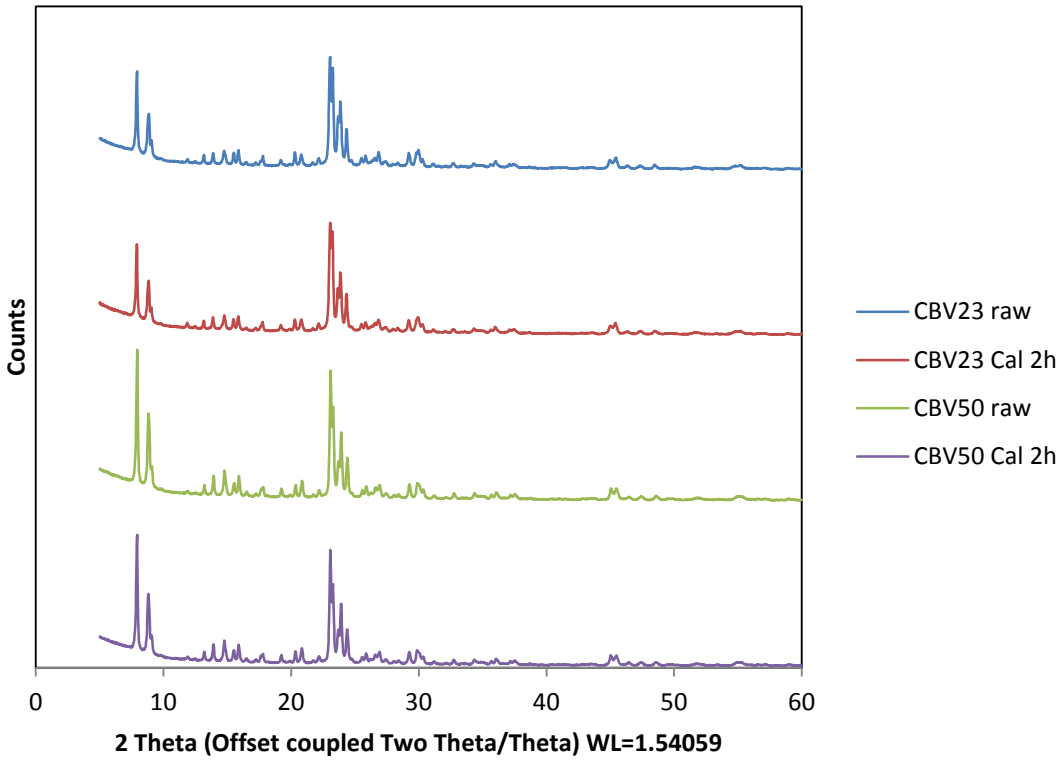

Figure 3.16. XRD patterns of raw and calcined CBV23 at 500 °C for 2 hrs, and raw and calcined CBV50 at 500 °C for 2 hrs

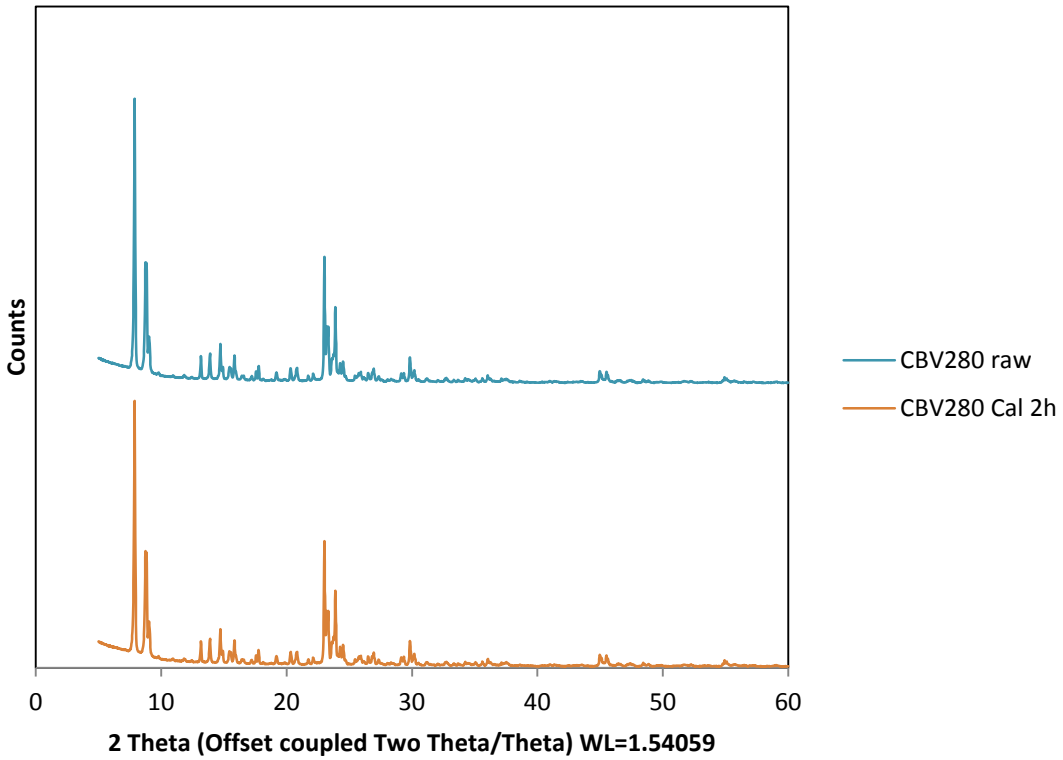

Figure 3.17. XRD patterns of raw and calcined CBV280 at 500 °C for 2 hrs

- Acidity measurement:

For a quantitative and qualitative evaluation of acid sites in the raw zeolites, NH_3 and pyridine were used as probe molecules.

Ammonia molecule is smaller and more basic than pyridine (kinetic diameter 3.75 vs. 5.33 Å, and proton affinity ca. 922.2 vs. 857.7 $kJ.mol^{-1}$, respectively). Concerning size, while ammonia can have access to almost all the acid sites in the microporous zeolites, pyridine may not approach to the acid sites situated in relatively small pores. The doses of probe molecules apply to the materials are also very different for the two techniques. So for all these reasons, we will use the two techniques in a different way and we will not compare the results in term of quantities. The NH_3 adsorption will be used to quantify the total number of acid sites and the pyridine FTIR will provide the nature of the site (i.e. Lewis or Brønsted).

- Pyridine FTIR experiment

The normalized spectrum of Figure 3.**18** belongs to raw CBV23 after pyridine desorption at 450 °C. The most important wavenumber range for us is 1400-1700 cm^{-1}.

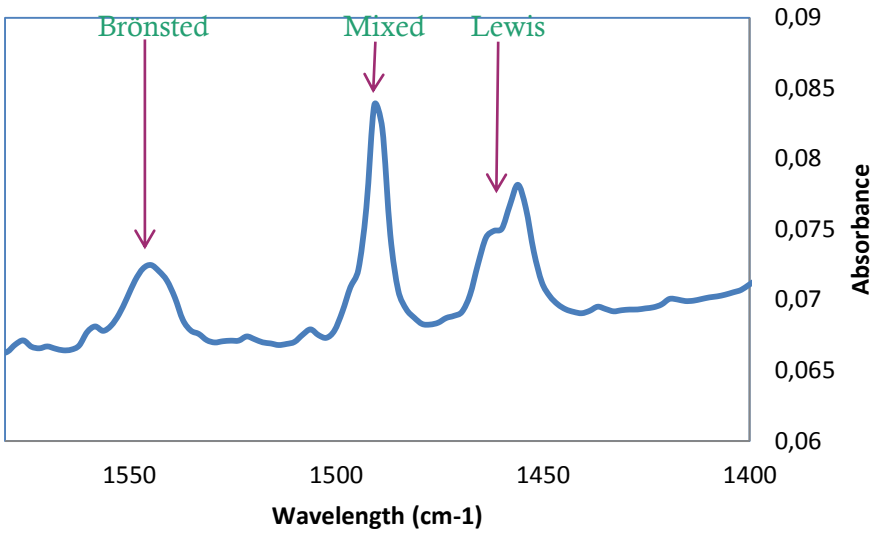

Figure 3.18. Spectrum of raw CBV 23 after pyridine desorption at 450 °C for 15 minutes minus spectrum of activated sample, in the range 1400-1700 cm^{-1} of wavenumber. band at 1454 cm^{-1} corresponding to Lewis acid site and band at 1545 cm^{-1} assigned to Brønsted acid sites

From integral intensities of individual bands [Figure 3.**19**; Figure 3.**20**] at 1454 cm^{-1} (resulting from the vibration of pyridine interacting with Lewis sites, PyL) and at 1545 cm^{-1} (resulting from the vibration of pyridinium, PyH^+) and using molar extinction coefficients of ε_L= 0.64 $cm.\mu mol^{-1}$ and ε_B= 0.73 $cm.\mu mol^{-1}$ respectively (M. Tamura, 2012), concentrations of both types of acid sites were calculated according to Beer-Lambert equation. Note that the activated sample spectrum is that of the sample after thermic treatment under vacuum. It is the reference spectrum before adsorption. It must be subtracted from the spectra obtained after pyridine adsorption. Further, there are four vibration modes for physical adsorption, hydrogen bonding, protonated pyridine Brønsted site and corrdinated pyridine Lewis site. We only consider the vibration mode 19b. The integration of individual bands in the corresponding region is only to calculate the overall area of each type of sites.

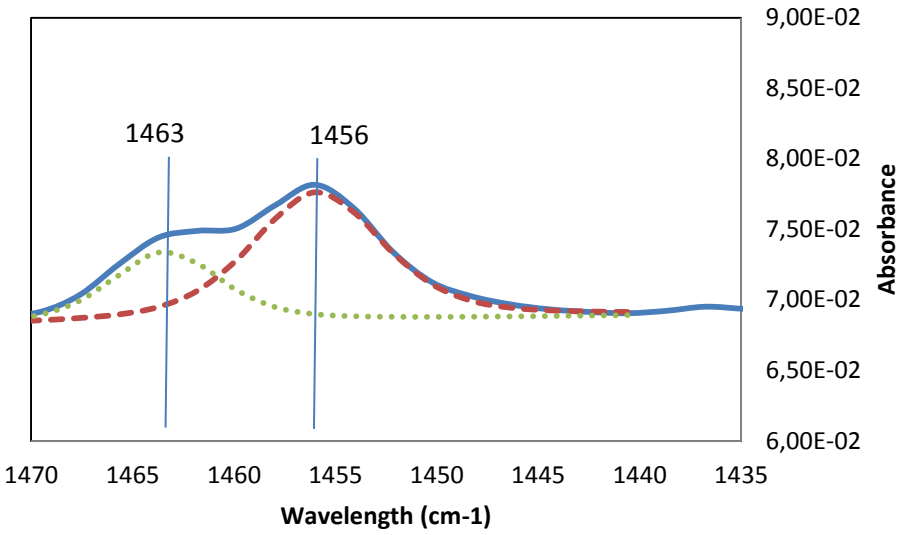

Figure 3.19. Lewis zone of the spectrum of raw CBV 23 after pyridine desorption at 450 °C, along with the spectral decomposition of the 1454 cm-1 band form

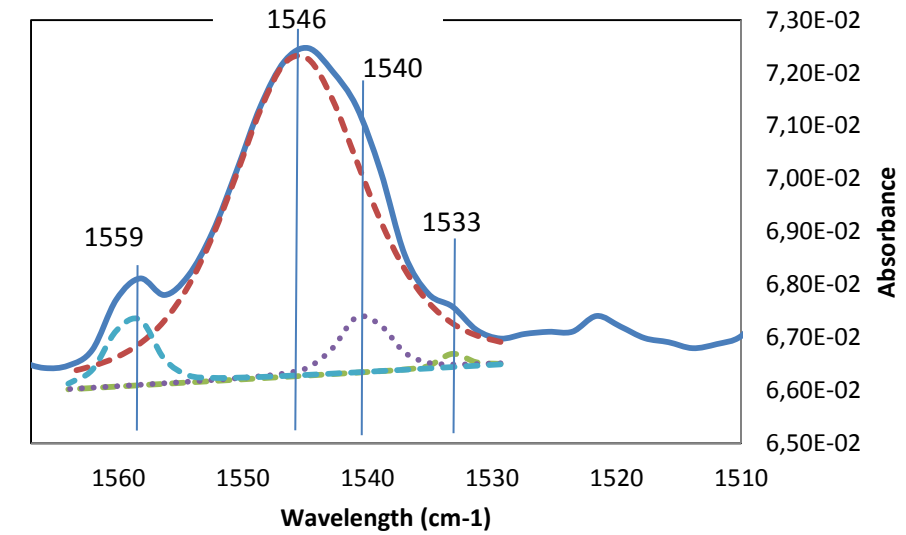

Figure 3.20. Brønsted zone of the spectrum of raw CBV 23 after pyridine desorption at 450 °C, along with the spectral decomposition of the 1545 cm^{-1} band form

- NH_3 TPD

In Figure 3.**21**, we see a NH_3 TPD graph for raw CBV23. The principle of the method is to adsorb a probe molecule, ammonia, selectively on acid sites then follows the desorption of the latter. The stronger the sites, the more energy should be provided to desorb the probe molecule. The total area was integrated by Origin software. The number of sites is obtained by integrating the response of the TCD signal and then applying to it the response factor determined by calibration. So, the NH_3 uptake in mmol/g represents the total acidity. Relative strengths are determined through relative integrated areas. Weak acid sites are those located

below 280 °C, medium acid sites between 280 and 480 °C and strong acid sites superior to 480 °C. The thermograms obtained are initially subtracted from a blank test in order to correct the drift of the baseline.

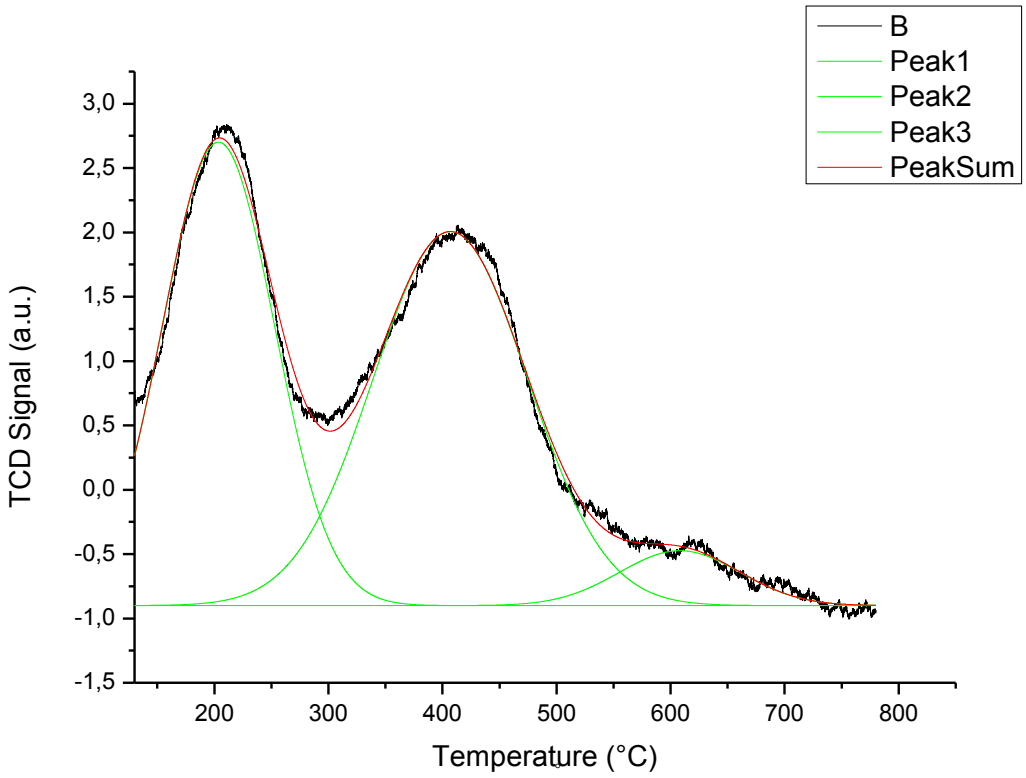

Figure 3.21. NH_3 TPD graph of raw CBV 23 showing acidity distribution. Temperature < 280 °C corresponds to weak acid sites, 280-480 °C to medium acid sites and that >480 °C to strong acid sites.

The results of NH_3 TPD for the CBV series are reported in the Table 3.**6**. As expected, the acid sites quantity depends of the Si/Al ratio. Less aluminum is present in the material, less acid site are present. We can see that CBV280 (raw) has low amount of acid sites (0.04 mmol/g), whereas CBV50 has moderate amount of acid sites (0.16mmol/g). CBV23 has the highest amount (0.24 mmol/g). The main acidity for each sample are medium ones.

We have evaluated the calcination effect on the acidity for one sample. From the NH_3 TPD results, we can see that CBV50 and CBV50 calcined for 2 hrs at 500 °C have similar moderate acidities (0.16 and 0.17 mmol/g) [Table 3.**6**]. Calcination had only an effect on increasing BET surface area (Table 3.**5**) which can be translated by better dispersion of the acid sites (i.e. when it is expressed in mmol of NH_3/m^2).

As raw CBV280 has a very low acidity, it is difficult to distinguish between Lewis and Brønsted for this one. CBV50 has more Brønsted acidity than Lewis, while it difficult to distinguish between the Brønsted and Lewis ratios for CBV23 as the pyridine FTIR tests cannot determine this (Table 3.**7**).

Table 3.6. Number of moles of acid sites of raw zeolites as determined by ammonia TPD measurements. Weak acid sites <280 °C, medium acid sites 280-480 °C and strong acid sites >480 °C.

Catalyst	Acidity (mmol/g)	Weak acidity (mmol/g)	Medium acidity (mmol/g)	Strong acidity (mmol/g)	S_{BET} (m^2/g)	Acidity (mmol/m^2)
CBV23 (raw)	0.24	0.099	0.134	0.006	163	1.48*10-3
CBV50 (raw)	0.16	0.022	0.084	0.053	312	5.13*10-4
CBV280 (raw)	0.04	0	0.027	0.012	352	1.14*10-4
CBV50 (Cal 2 hrs)	0.17	0.033	0.083	0.053	418	4.07*10-4

The pyridine FTIR experiments for the CBV50 before and after calcination are presented in the table 3. From FTIR results, calcined CBV50 shows higher Brønsted acidity than Lewis up to 10 times (Table 3.7). Catalytic tests results will provide us an insight of the influence of Brønsted acidity on propylene selectivity. After calcination, the measure number of acid site increase drastically. This fact has to be correlated with the destruction and rearrangement of the structure of the materials after FTIR treatment-as exhibited by XRD not shown here-which can be due to the appearance of extra frame work alumina as reported elsewhere ((Zhung W, 2003) (Kiwi-Minsker L, 2003) (Wichterlová B, 1998) (Borade R, 1990) (Dapaah JKA, 1997)).

Table 3.7. Relative percentages of number of moles of Brønsted and Lewis acid sites of raw zeolites as determined by pyridine FTIR spectroscopy. ƐB= 0.73, ƐL= 0.64 (according to recent references).

Catalyst	Temperature	n B (%)	n L (%)	Acidity (a.u.)
CBV23 (raw)	150 °C (Total acidity) 450 °C (Strong acidity) 150-450 °C (weak acidity)	Can't be determined		
CBV50 (raw)	150 °C (Total acidity) 450 °C (Strong acidity) 150-450 °C (weak acidity)	91 58 100	9 42 -	171 104 -
CBV280 (raw)	150 °C (Total acidity) 450 °C (Strong acidity) 150-450 °C (weak acidity)	0 0 0	0 0 0	0 0 0
CBV50 (Cal 2 hrs)	150 °C (Total acidity) 450 °C (Strong acidity) 150-450 °C (weak acidity)	84 75 91	16 25 9	1039 479 560

- Catalytic Tests Results:

Different ZSM-5 types with different SiO_2/Al_2O_3 ratios were tested at different amounts and different reaction temperatures, in order to select the best catalyst. Afterwards, the latter was tested at the most ideal conditions in order to verify its performance. Tests were

both performed at FLOWRENCE T1220 and the multi-valve reactor system. Same ethanol and inert gases flows were used between the two; i.e., 21 mL/min of inert gas and 0.0125 mL/min liquid ethanol flow per reactor.

In the first tests the best support amongst the following ZSM-5s was selected: CBV280, ZSM-5 (SiO_2/Al_2O_3 280), CBV23 and CBV50. For this, reactions were done with 300mg at 500 °C, except for CBV50 where only 100mg were used because the latter has low density and can overload the reactor. Conversion and selectivities of the two most desired products-propylene and ethylene-were plotted (Figure 3.22;Figure 3.23;Figure 3.24 respectively).

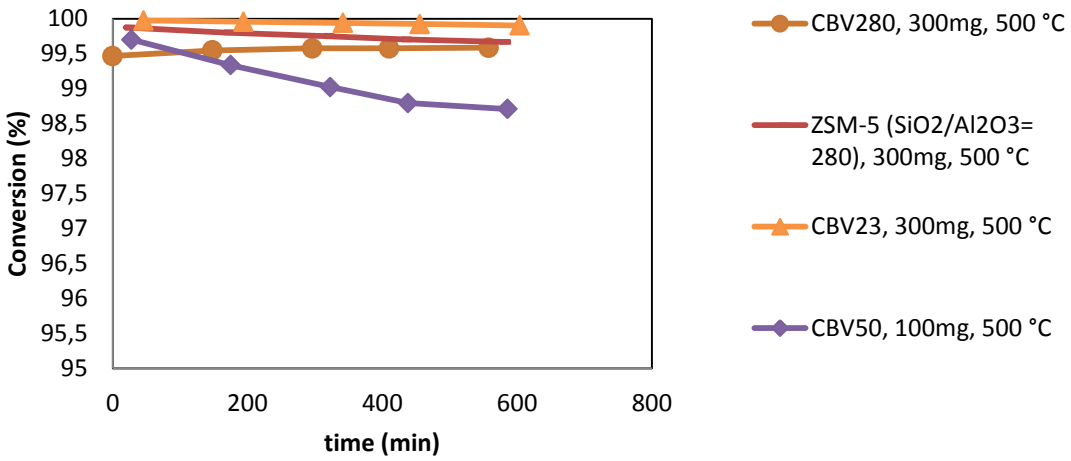

Figure 3.22. Graph showing the variation of conversion as a function of time (min) for raw ZSM-5s over "FLOWRENCE T1220". Reaction conditions: 1.05 mL/min He flow, 19.95 mL/min N_2 (Total of 21 mL/min of inert gas). Diluent flow (N_2) of 7.5 mL/min. 0.0125 mL/min as liquid ethanol flow (20% in gaseous phase). 300mg of the catalyst mass was used at different 500 °C reaction temperature, except for CBV 5524G (100mg). All conditions are per reactor. Supports are raw catalysts.

In our conditions, it's difficult, regarding the ethanol conversion, to select the best support among the four tested. We can note that the CBV50, (100 mg) seems to slightly deactivate with the time on stream while the other supports stay at 100% for the ethanol conversion during more than 10 hours.

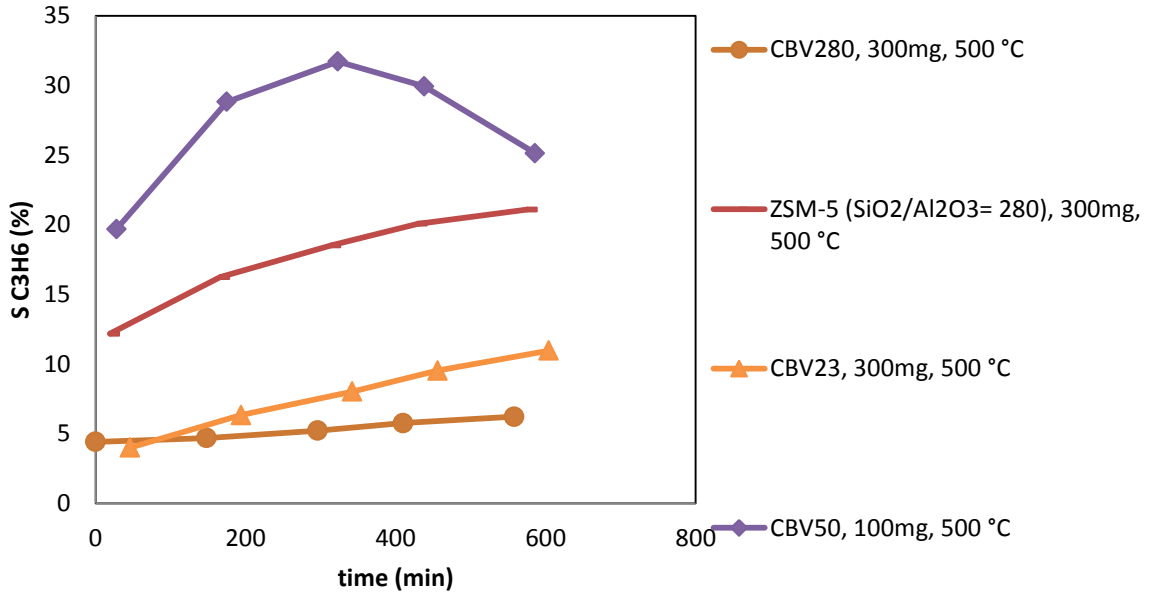

Figure 3.23. Graph showing the variation of propylene selectivity (%) as a function of time (min) for and raw ZSM-5s over "FLOWRENCE T1220". Reaction conditions: 1.05 mL/min He flow, 19.95 mL/min N_2 (Total of 21 mL/min of inert gas). Diluent flow (N_2) of 7.5 mL/min. 0.0125 mL/min as liquid ethanol flow (20% in gaseous phase). 300mg of the catalyst mass was used at 500 °C reaction temperature, except for CBV 55 (100mg). All conditions are per reactor. Supports are raw catalysts.

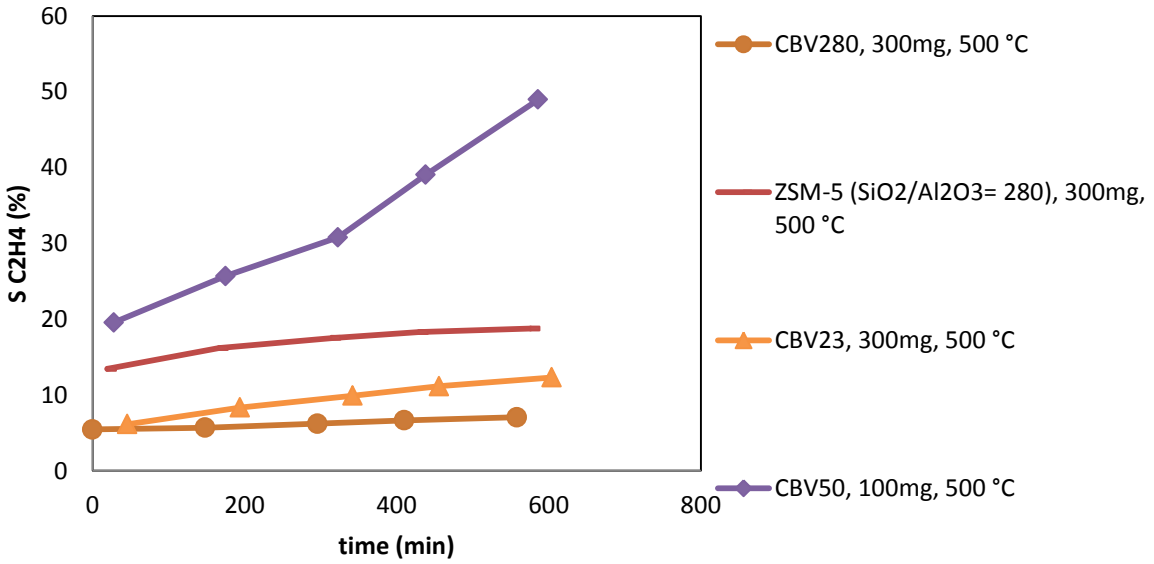

Figure 3.24. Graph showing the variation of ethylene selectivity (%) as a function of time (min) for raw ZSM-5s over "FLOWRENCE T1220". Reaction conditions: 1.05 mL/min He flow, 19.95 mL/min N_2 (Total of 21 mL/min of inert gas). Diluent flow (N_2) of 7.5 mL/min. 0.0125 mL/min as liquid ethanol flow (20% in gaseous phase). 300mg of the catalyst mass was used at different 500 °C reaction temperature, except for CBV 5524G (100mg). All conditions are per reactor. Supports are raw catalysts.

Regarding the selectivity of the target molecule, one can see that CBV50 showed to be the best support in the ZSM-5 series, because it showed the highest propylene selectivity in the set (32%) for the 100 mg mass at 500 °C (Figure 3.23) even if the ethanol conversion decreases slightly with time on stream. In Figure 3.24, we see that that ethylene selectivities for the catalysts was less than 15%, while that for CBV50 increased from 19 to 49%.

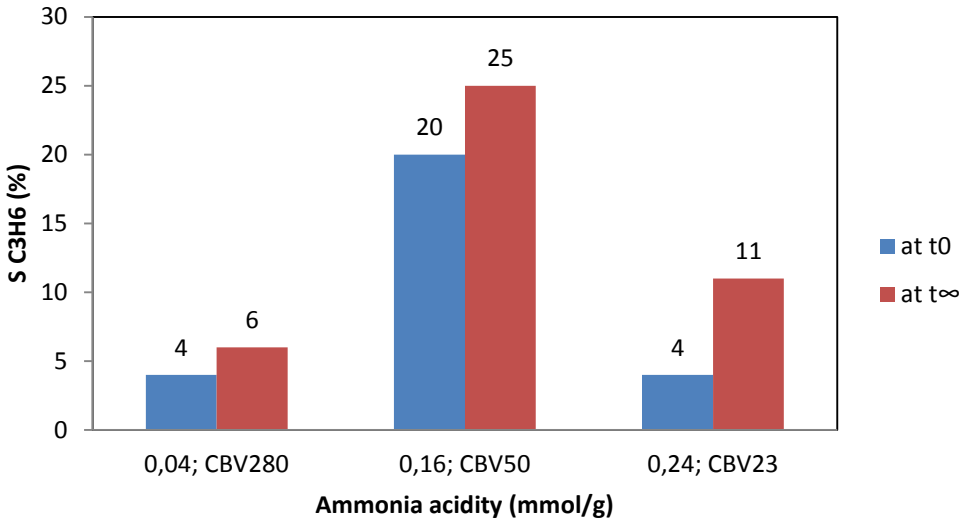

Figure 3.25. Graph showing the variation of propylene selectivity (%) as a function of ammonia TPD acidity (mmol/g) for raw ZSM-5s. Tests were performed over "FLOWRENCE T1220". Reaction conditions: 1.05 mL/min He flow, 19.95 mL/min N_2 (Total of 21 mL/min of inert gas). Diluent flow (N_2) of 7.5 mL/min. 0.0125 mL/min as liquid ethanol flow (20% in gaseous phase). 300mg of the catalyst mass was used at 500 °C reaction temperature, except for CBV 5524G (100mg). All conditions are per reactor.

We tried to correlate the catalytic activities with the acid/base properties of the support. Figure 3.25 presents the evolution of the propylene selectivity function of the number of acid site determined by NH_3 TPD. The poor performance for CBV280 can be directly related to the low acidity of this catalyst (0.04 mmol/g ammonia acidity) even if the acidity of this support is enough to transform all ethanol. On the other side, CBV50 tested showed an improved propylene selectivity (up to 32%) which correlates to the moderate amount of acid sites (0.16-0.17 mmol/g ammonia acidity) [Table 3.6], increasing the number of acid sites (i.e. CBV23) don't improve the propylene selectivity. In conclusion, the relation between propylene selectivity and acidity is not straightforward. At this stage, our support characterizations are not enough to explain the activity evolution of our materials even if it seems that the CBV50 seems to be the best support.

So, it was selected for further tests studying the influence of the reaction temperature (between 200 and 450 °C) and the amount of catalyst (from 25 to 100mg). The optimization of catalyst mass has been done (not displayed here) and show that the 50mg was the best catalyst mass leading to a GHSV equal to 2.21 h^{-1}.

After the selection of the best ZSM-5 support and mass, tests were done to determine the most convenient reaction temperature. Same tests at similar conditions were performed over the multi-valve reactor system, but with testing lower temperatures as well (Figure 3.26;Figure 3.27;Figure 3.28).

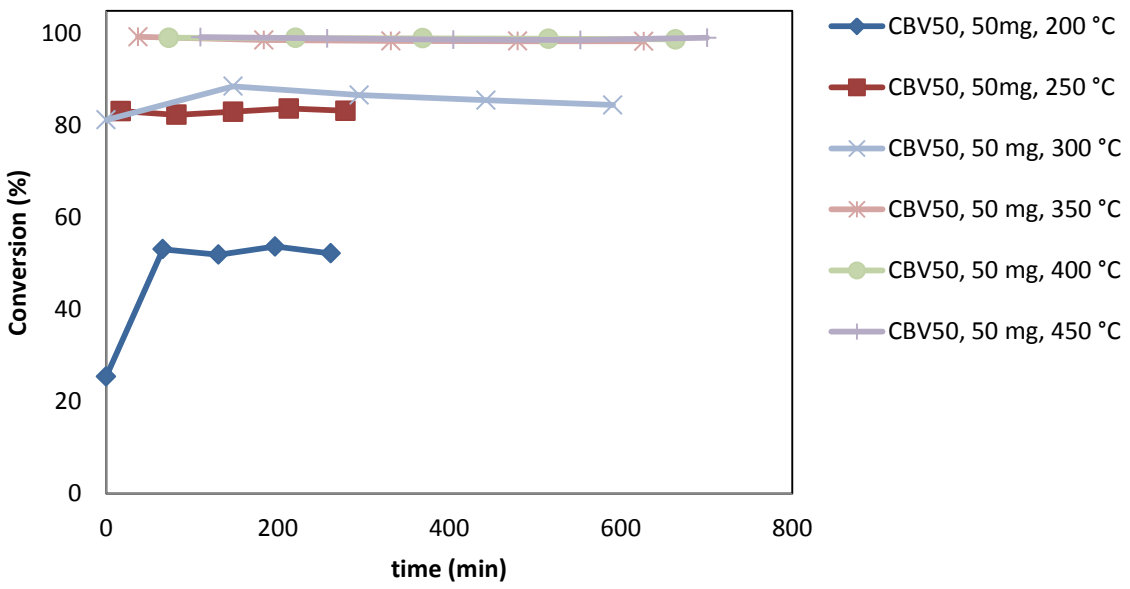

Figure 3.26. Graph showing the variation of conversion as a function of time (min) for raw CBV50s over "FLOWRENCE T1220" and multi-valve reactor system. Reaction conditions: 1.05 mL/min He flow, 19.95 mL/min N_2 (Total of 21 mL/min of inert gas). Diluent flow (N_2) of 7.5 mL/min. 0.0125 mL/min as liquid ethanol flow (20% in gaseous phase). 50mg of the catalyst mass was used at different temperatures (200, 250, 300, 350, 400 and 450°C). All conditions are per reactor. Supports are raw catalysts.

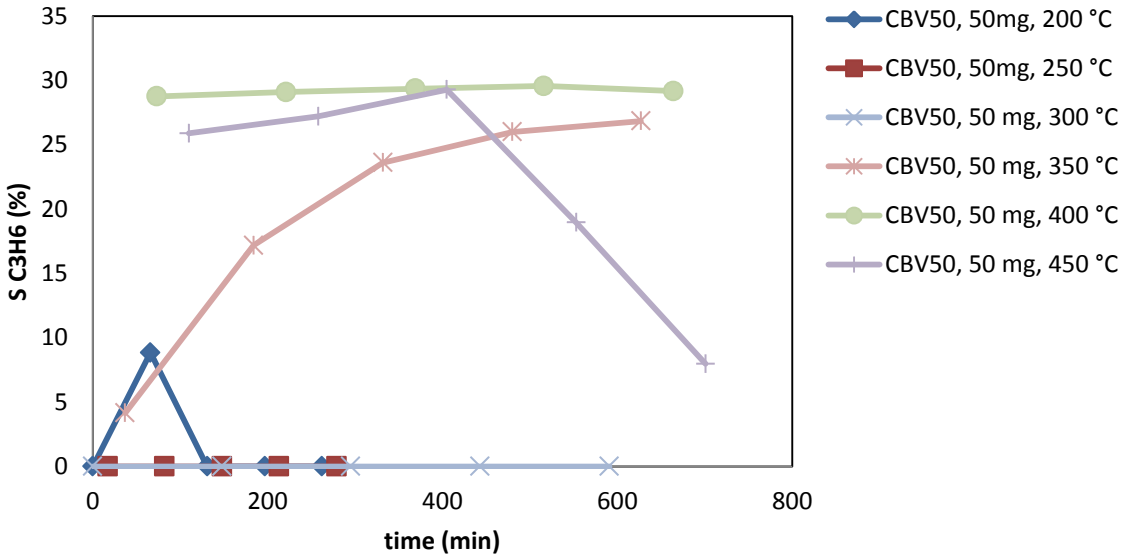

Figure 3.27. Graph showing the variation of propylene selectivity (%) as a function of time (min) for raw CBV50s over "FLOWRENCE T1220" and multi-valve reactor system. Reaction conditions: 1.05 mL/min He flow, 19.95 mL/min N_2 (Total of 21 mL/min of inert gas). Diluent flow (N_2) of 7.5 mL/min. 0.0125 mL/min as liquid ethanol flow (20% in gaseous phase). 50mg of the catalyst mass was used at different temperatures (200, 250, 300, 350, 400 and 450 °C). All conditions are per reactor. Supports are raw catalysts.

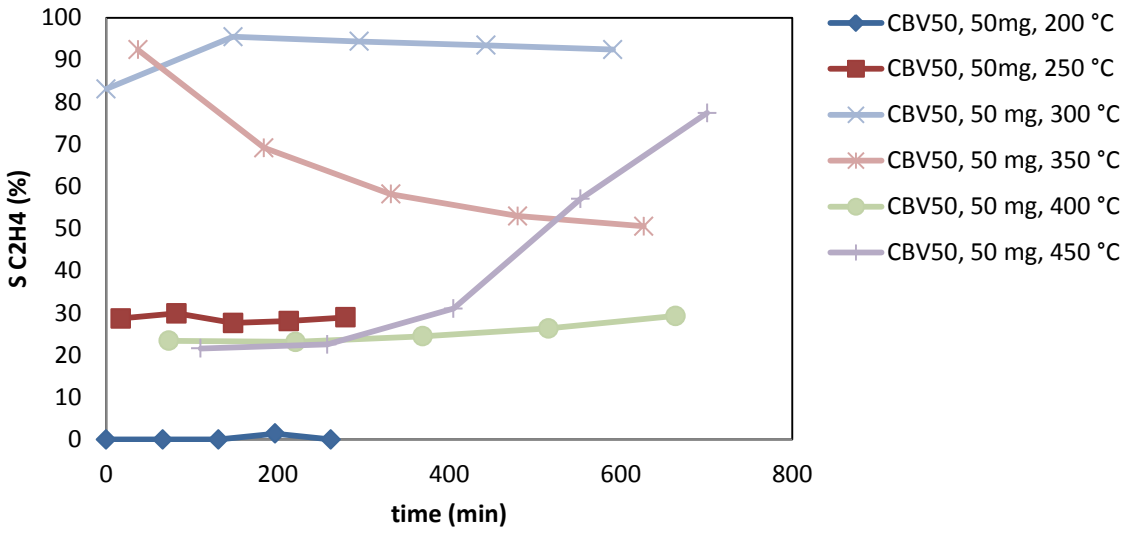

Figure 3.28. Graph showing the variation of ethylene selectivity (%) as a function of time (min) for raw CBV50s over "FLOWRENCE T1220" and multi-valve reactor system. Reaction conditions: 1.05 mL/min He flow, 19.95 mL/min N_2 (Total of 21 mL/min of inert gas). Diluent flow (N_2) of 7.5 mL/min. 0.0125 mL/min as liquid ethanol flow (20% in gaseous phase). 50mg of the catalyst mass was used at different temperatures (200, 250, 300, 350, 400 and 450 °C). All conditions are per reactor. Supports are raw catalysts.

We study the effect of reaction temperature on conversion and selectivities for the 50mg CBV50. From Figure 3.26, we see that for temperatures higher than 300 °C, conversion was full. While for 300 and 250 °C, conversion was roughly stable at 86%. For 200 °C, less than 60% of ethanol was converted. So, if we aim to study the products distribution at lower conversion, the 50mg/200 °C mass/temperature conjugate is a good choice.

In addition, for temperatures lower than 350 °C, propylene selectivities were inferior to 10% (Figure 3.27). At 350°C, the propylene selectivity increases with time on stream and reaches a plateau around 26% after 10 hours. Increasing the temperature up to 400°C leads to a stable propylene selectivity (~28%) and when the temperature reaches 450°C, the propylene selectivity is stable at 29% for 400 minutes and then decrease dramatically. This decrease of propylene selectivity corresponds to the increase of the ethylene one (Figure 3.28). This link between the two selectivities can be also observed when the reaction is carried out at 400°C.

As mentioned previously, no correlation has been evidence between total acidity and target molecule selectivity. In order to go deeper, we have chosen to study modified CBV series.

3.1.2. Na-exchanged CBV30

A way to modified the acidity of a materials is the partial substitution of proton by sodium atoms. Starting from a HZSM-5 with a Si/Al ratio equal to 30 (CBV30), we partially substituted the proton by Na and obtain five catalysts with different Na/Al ratios : Na0-ZSM-5, Na11-ZSM-5, Na17-ZSM-5, Na32-ZSM-5 and Na87-ZSM-5 (Table 3.8). The number after the Na correspond to the atomic percentage of substitution.

- Acidity and elemental composition:

I*n situ* FT-IR spectroscopy was used to monitor the evolution of polyalkyl benzene and polyaromatics within the different catalysts.

Brønsted acid sites dominate the H-ZSM-5 catalyst. To change the density of acid sites, NH_4^+ was exchanged by Na^+, as the latter does not undergo proton exchange at the conditions used (1 hour under He at 500 °C). The degree of ion exchange was determined by ICP-MS, providing the sodium weight percentage from which the Na/Al ratio was calculated (Table 3.8). On the other hand, with the peak area of both Lewis and Brønsted bands (at 1440 cm^{-1} and 1540 cm^{-1} respectively represented in Figure 3.29), it was possible to estimate the number of Lewis and Brønsted acid sites following Beer-Lambert law previously (Table 3.8).

Table 3.8. Calculated ion-exchange degree from ICP-MS and FT-IR acid site bands area

Name	Na (wt%)	Na (mmol/g)	Na/Al	L area/cm^{-1}	L mmol/g	B area/cm^{-1}	B mmol/g
HZSM5	0.00	0.0000	0.00	0.76	0.03	8.52	0.54
Na11ZSM5	0.26	0.1133	0.11	1.41	0.06	5.61	0.36
Na17ZSM5	0.40	0.1740	0.17	1.64	0.07	4.68	0.30
Na32ZSM5	0.76	0.3323	0.32	4.67	0.21	2.91	0.19
Na87ZSM5	2.09	0.9110	0.87	7.38	0.33	1.43	0.09

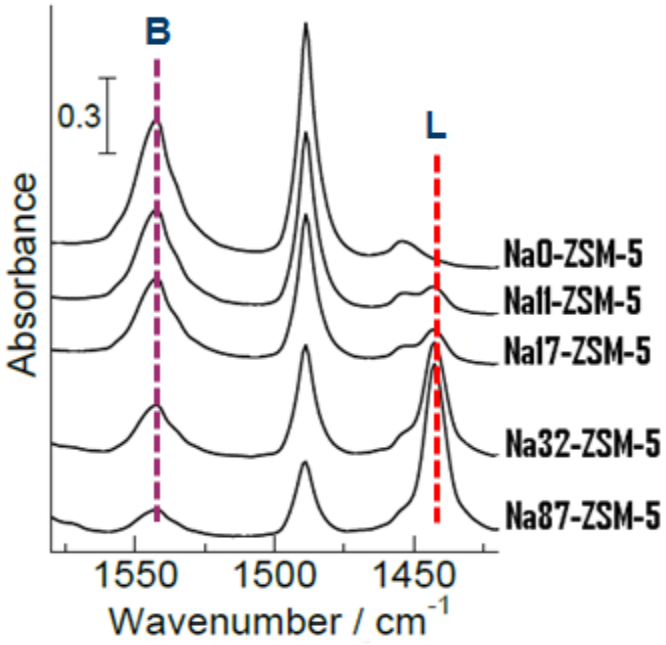

Figure 3.29. IR spectrum of pyridine adsorbed at 200 °C on Na-ZSM-5 samples

Pyridine FTIR spectroscopy measurements were done for the five catalysts (Figure 3.29). The signal at 1540 cm^{-1} refers to Brønsted acid sites, and results from the vibration of pyridine adsorbed on Brønsted OH groups (pyridinium). While the signal at 1440 cm^{-1} refers

to weak acid sites, and results from the vibration of pyridine adsorbed on sodium which acts as Lewis sites. From the above graph, one can see that when the sodium amount increases, the intensity of the signal at 1540 cm^{-1} decreases. On the other hand, as sodium amount increases, the intensity of the signal at 1440 cm^{-1} increases.

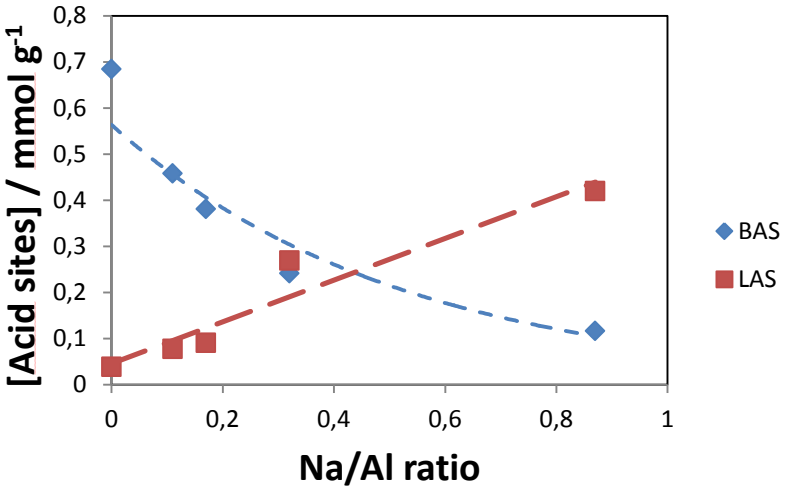

Figure 3.30. Amount of acid sites per weight of catalyst, calculated by Beer-Lambert law (BAS : Brønsted acid sites, LAS : Lewis acid sites)

By applying the Beer-Lambert law one can plot the variation of the concentration of acid sites versus Na/Al ratio as seen in Figure 3.30. The concentration of Lewis acid sites increases linearly, while that of Brønsted and Lewis acid sites correlate inversely.

- Catalytic Test Results:

ZSM-5s with different Na/Al ratios were tested for their activity and product distribution in ethanol conversion.

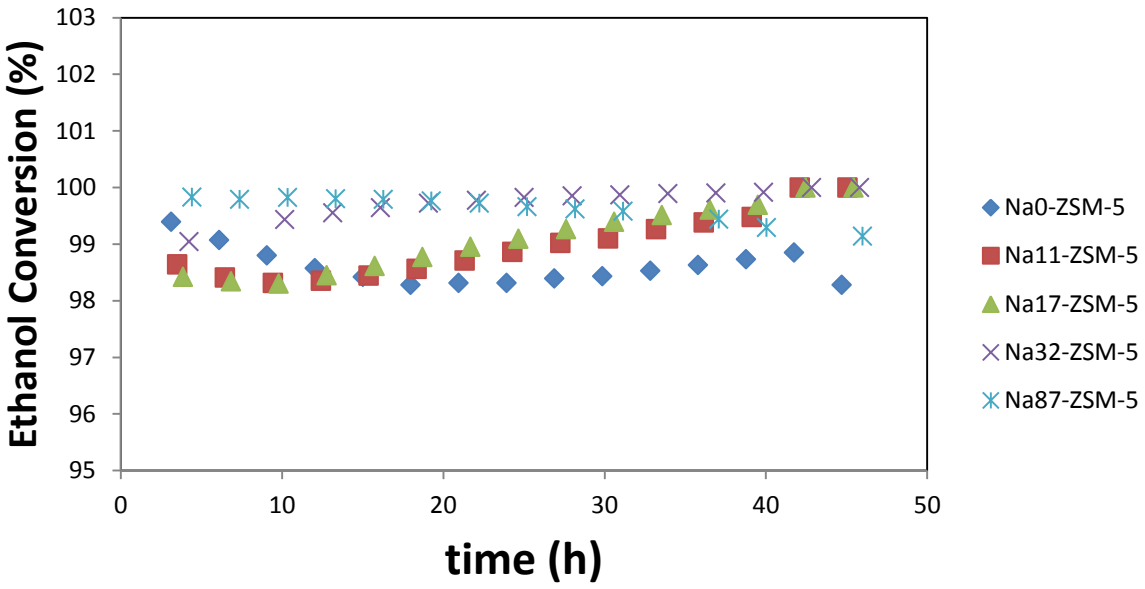

Figure 3.31. Graph showing the variation of ethanol conversion (%) as a function of time (h) for different Na-exchanged CBV 30 ZSM-5s. 1.05 mL/min He, 19.95 mL/min N_2 (Total of 21 mL/min of inert gas). Diluent flow (N_2) of 7.5 mL/min. 0.0125 mL/min as liquid ethanol flow (20% EtOH in gaseous phase). All conditions are per reactor. 50 mg of each catalyst was tested at 350 °C.

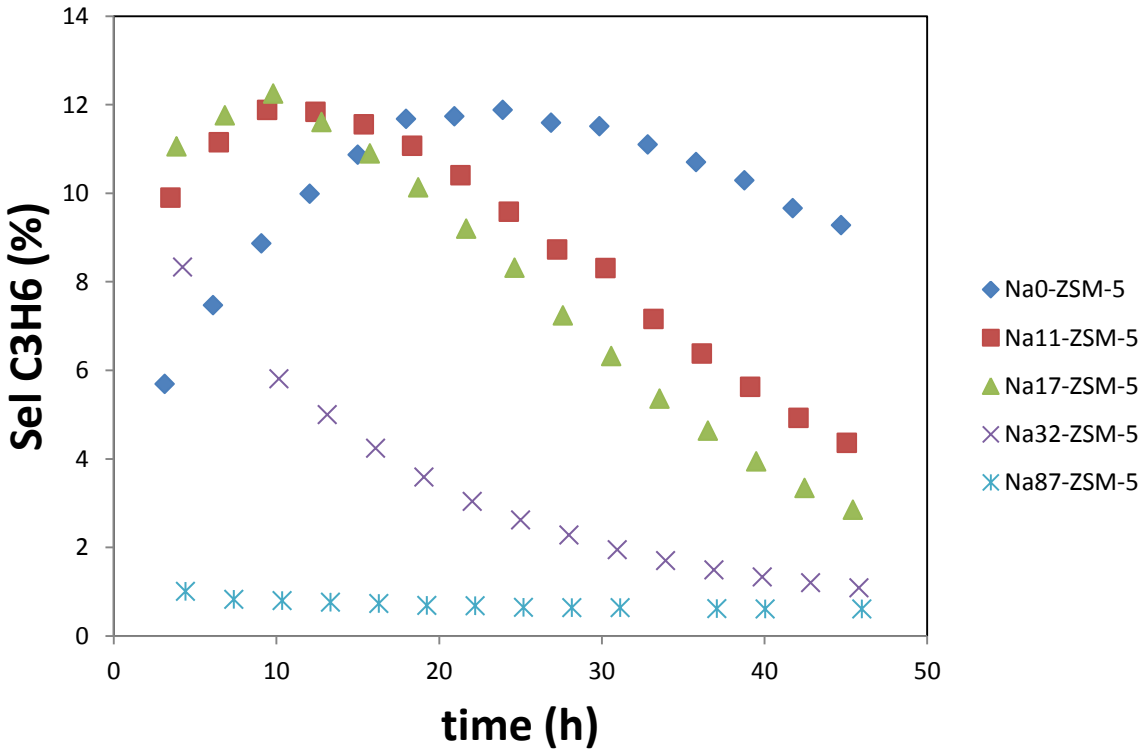

Figure 3.32. Graph showing the variation of propylene selectivity (%) as a function of time (h) for different Na-exchanged CBV 30 ZSM-5s. 1.05 mL/min He, 19.95 mL/min N_2 (Total of 21 mL/min of inert gas). Diluent flow (N_2) of 7.5 mL/min. 0.0125 mL/min as liquid ethanol flow (20% EtOH in gaseous phase). All conditions are per reactor. 50 mg of each catalyst was tested at 350 °C.

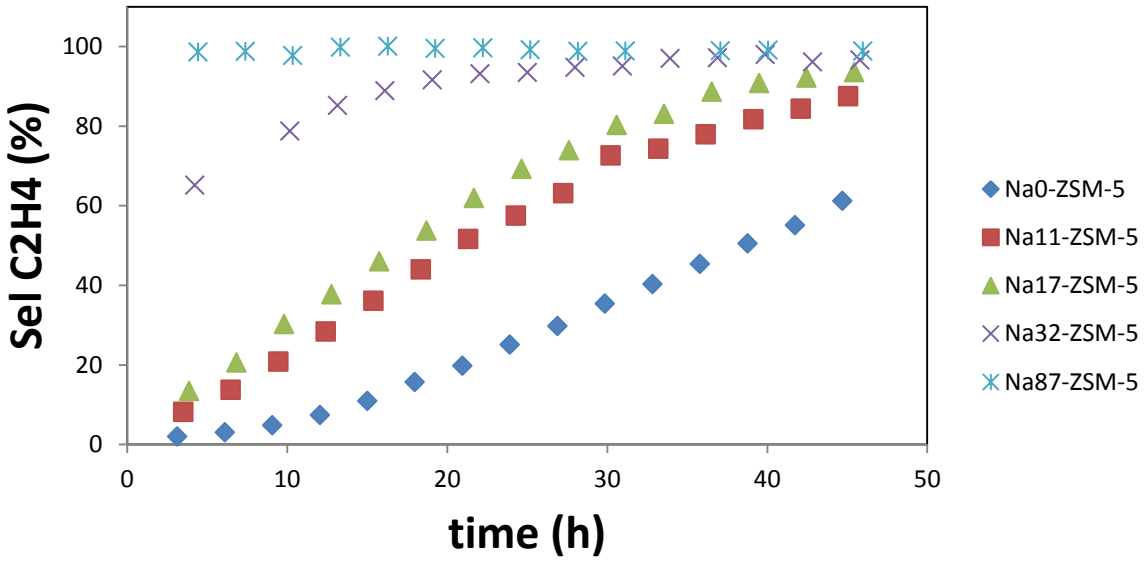

Figure 3.33. Graph showing the variation of ethylene selectivity (%) as a function of time (h) for different Na-exchanged CBV 30 ZSM-5s. 1.05 mL/min He, 19.95 mL/min N_2 (Total of 21 mL/min of inert gas). Diluent flow (N_2) of 7.5 mL/min. 0.0125 mL/min as liquid ethanol flow (20% EtOH in gaseous phase). All conditions are per reactor. 50 mg of each catalyst was tested at 350 °C.

The catalytic performance of Na11, 17, 32 and 87-ZSM-5 shows almost full conversion no matter the reaction time (Figure 3.31). Concerning the product selectivity, low Na/Al ratio (0, 11 and 17) showed a low initial ethylene selectivity (2-13%), increasing with time-on-stream to reach up to 90%. The higher is the Na/Al ratio, the higher and more stable was the ethylene selectivity with time-on-steam (Figure 3.33).

Concerning propylene selectivity, the higher the Na/Al ratio, the lower and more stable was the propylene selectivity with time-on-steam, contrary to the ethylene selectivity (Figure 3.32). In addition to the major products ethylene and propylene, various aromatics products like BTXs, etc. were detected. The decrease in propylene at low Na-content catalyst can be justified by two different theories: either decrease in acid sites amounts, or to the condensation of active radical aromatics. On the other hand, ethylene selectivity continues to form for low Na-content catalysts, despite the fact that ethanol dehydration requires strong acidity.

The aim of this ethanol-to-hydrocarbon study was the following: setting up a method to study the ETH reaction mechanism by focusing of the retained precursors, plus evaluating the properties of the catalysts (such as amount of acid sites). It was also to see the relevance of all these with propylene production.

- In situ UV/Vis Spectroscopy:

The complexity of the hydrocarbon pool mechanism concerns the intermediate species involved in it. To study what goes on inside the framework of the catalyst, non-destructive

and *in situ* techniques are required. Both of these techniques provide complementary information.

Ultraviolet-visible (UV/Vis) spectroscopy is another powerful tool to be used in the study of the ethanol-to-hydrocarbons reaction, as both the olefin-based and aromatic-based hydrocarbon pool cycles involve molecules possessing optically active C=C bonds. Most notably, its ability to identify the nature of hydrocarbon species (e.g. carbocation or neutral) can provide significant insight on the way the hydrocarbon pool behaves as the reaction progresses and beyond.

In order to further proof the reaction pathway via radical species, *in situ* UV/Vis spectroscopy was employed over the sodium-exchanged CBV30 ZSM-5 samples during the ETO reaction which was performed for 100 minutes at 450 °C with 12% EtOH/N_2 feed.

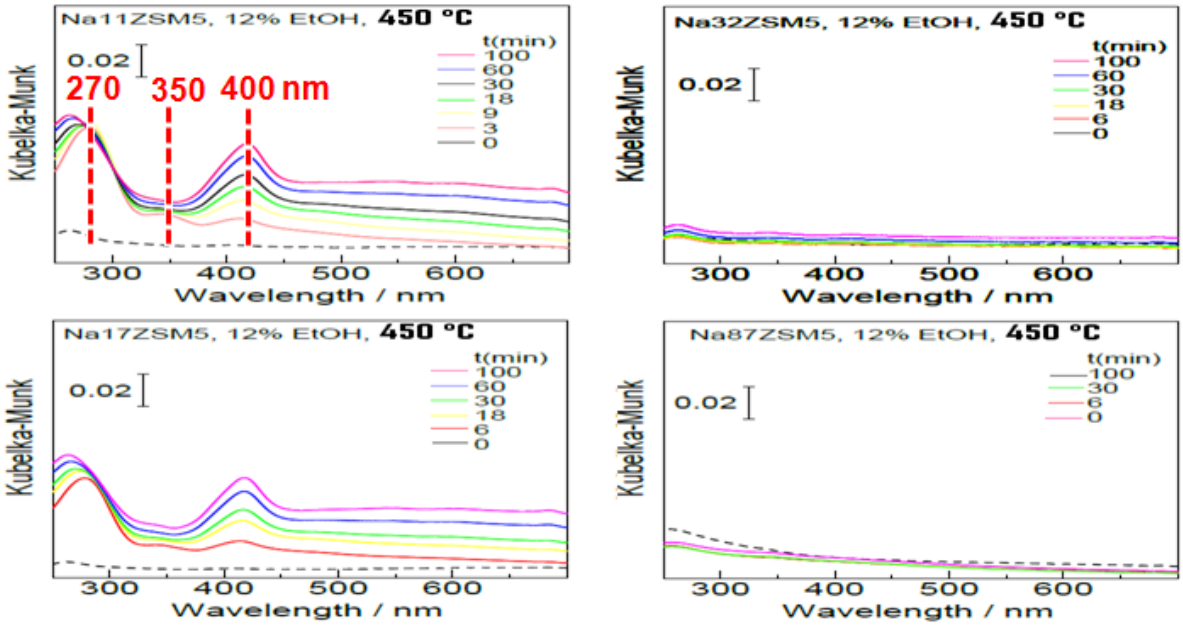

Figure 3.34. UV/Vis spectra recorded during the ETO reaction over the different ion-exchanged ZSM5 catalysts at 450 °C and a concentration of 12% EtOH

We validated through earlier FTIR measurements that as sodium amount increases, the amount of Brønsted acid sites decreases (see FTIR results section). Peaks in the UV/Vis spectrum at 270, 350 and 400 nm refer to aromatic and polyaromatic species. From Figure 3.34, we observe that as the sodium amount increases, the peak intensities of these products decreases. So, we deduce that the decreasing amount of acid sites manifests itself by the reduction of carbonaceous species formation. In conclusion, Brønsted acidity is essential to the formation of aromatics.

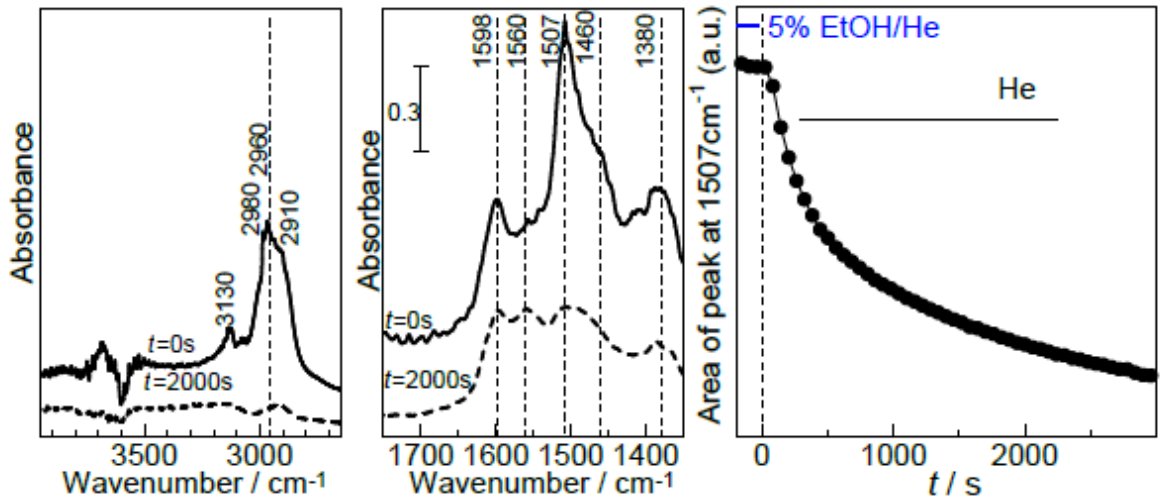

Figure 3.35. (Left to right) O-H stretching and C-H stretching regions of IR spectra ; C=C stretching and C-H bending regions of IR spectrum ; Area under peak at 1507 cm^{-1} ; For all figures : HZSM5, 5% EtOH, 300 °C, after switch to pure He ; full line : t= 0 seconds ; Dotted line : t= 2000 seconds.

Additionally to UV-Vis, *in situ* FTIR was performed. The assignment of peaks belonging to hydrocarbon species is as follows: 2800-3100 cm^{-1} (C-H) and 1350-1650 cm^{-1} (C=C and C-H deformation). The signal at 3600 cm^{-1} belongs to the OH stretching. As one can see from the left of Figure 3.35, the full line represents time zero of the ETH reaction while the dotted one represents the FTIR peaks after 2000 seconds of the reaction. The peak located at 1507 cm^{-1} has been suggested to belong to alkylated aromatics, the species believed to be the intermediate in the HCP mechanism. After 2000 seconds, almost all peaks at lower wave numbers have been eroded. This erosion can be attributed to the conversion of alkylated aromatics into condensed aromatic species, which in turn cause pore blockage.

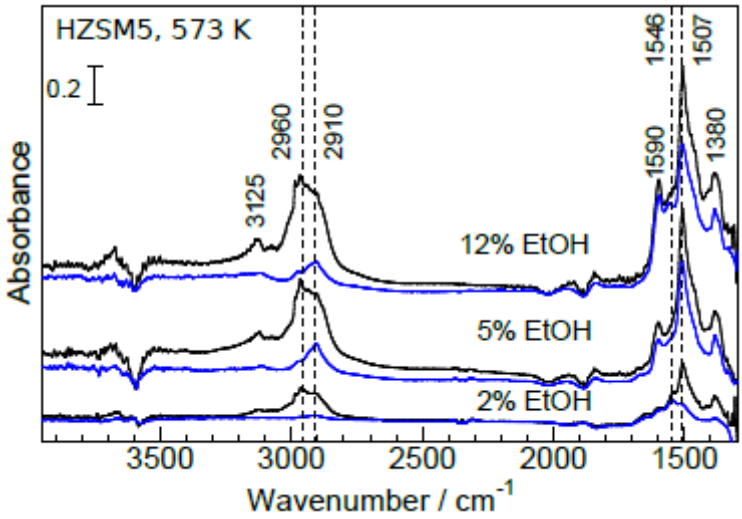

Figure 3.36. IR spectra post-ETH reaction at different EtOH concentrations ; Black line : t= 0 seconds ; Blue line : t= 100 seconds.

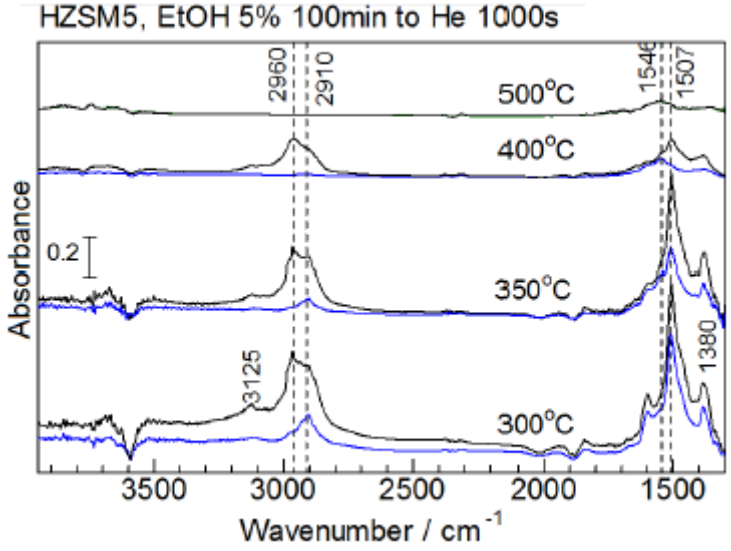

Figure 3.37. IR spectra in pure He post-ETH reaction over HZSM5, 5% EtOH for 100 minutes ; Black line : t= 0 seconds ; Blue line : t= 100 seconds.

By examining the spectra showing the effect of the ethanol concentration (from 2 to 5 to 12% - (Figure 3.36)), one can see an increase of the carbon species adsorbed with increasing ethanol concentration. On the other hand, high reaction temperature (Figure 3.37) leads to a fast desorption of light hydrocarbons. The last observable signal at 500 °C is located at 1546 cm^{-1} and is assigned to polyaromatic species.

- TPR-MS:

TPR-MS was performed on a CBV30 after test in order to validate the hydrocarbon pool mechanism. The goal of this work is to focus on the formation and behavior of the aromatic intermediates and polyaromatic coke. Most publications on the ethanol-to-hydrocarbons reaction focus exclusively on the catalytic activity as well as the nature and yield of the products, providing little information on what occurs inside the catalyst.

Attention is focused on polyalkyl benzenes and polyaromatics. To do so, experiments were conducted on the behavior of these species after the reaction is over and in absence of ethanol feed. According to the hydrocarbon pool mechanism mentioned in literature, some activity should persist, with different species interacting with each other in the case of the olefin-based cycle and with polyalkyl benzyl cations being able to continue on forming olefins from their remaining alkyl groups.

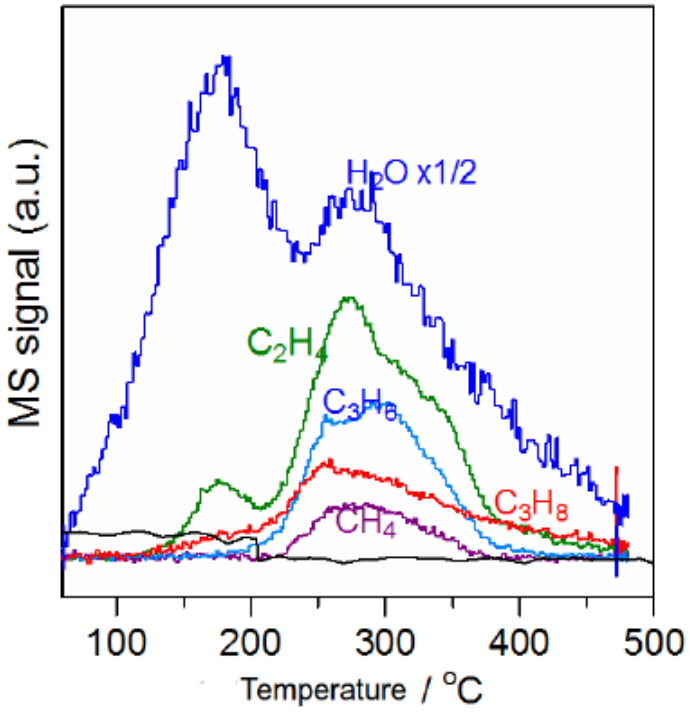

Figure 3.38. MS signal of the retained hydrocarbon species during the TPR experiment conducted from a HZSM5 sample quenched after 10 minutes of ethanol-to-hydrocarbons reaction with the temperature increased to 500 °C.

The TPR-MS experiment was conducted in an IR system connected with a capillary line to a mass spectrometer. The ZSM-5 zeolite was first preheated at 500 °C under helium flow to protonate the catalyst by gassing out the ammonia, after which the ethanol-to-hydrocarbons reaction was conducted for 10 minutes at 250 °C with a feed of 12% EtOH/He. Following this, the catalyst was quickly cooled down. The temperature was then increased to 475 °C under helium to expel lighter hydrocarbons into the MS spectrometer.

The MS signal observed for water (Figure 3.38) refers to water produced during the ETH reaction. Ethylene at low temperature results from olefin desorption. Olefins and paraffins culminate near 300 °C, which corresponds to the reaction temperature, and continue to form up to 400-450°C. The absence of diethyl ether in the zone inferior to 300 °C indicates that the dehydration of ethanol didn't occur, thus the ethanol trapped inside the catalyst didn't undergo the ETH reaction mechanism. The presence of light olefins and alkanes suggests the continuation of the ETH's hydrocarbon mechanism even in the absence of ethanol under reductive conditions (hydrogen). Their formation occurs through the dealkylation of polyalkyl benzene species trapped inside the catalyst to generate olefins (propene and butene). The corresponding results strongly support the hydrocarbon pool mechanism suggested by L. Pinard *et al.* [(L. Pinard K. B., 2013);(S. Hamieh, 2015)].

From catalytic test results for modified ZSM-5 (s), we found that the higher is the Na/Al ratio, the higher and more stable is the ethylene selectivity with time-on-stream. This was the opposite for propylene selectivity. The decrease in the selectivity in propylene peak intensity of high Na-content is due to the decrease in acid sites amounts (pyridine FT-IR

results) or to the condensation of active radical aromatics. From UV/Vis spectroscopy results, we found that the decreasing amount of acid sites manifests itself by the reduction of carbonaceous species formation. We also found from such results that Brønsted acidity is essential to the formation of aromatics. From the TPR-MS study, we concluded that polyalkyl benzene species undergo dealkylation to generate olefins before being dehydrogenated by the polyalkyl benzene. This proves the occurrence of the so-called modified hydrocarbon pool mechanism involving radicals. It was validated both by characterizations and catalytic tests through the absence of diethyl ether intermediate as extra evidence. Overall, we conclude that the formation of propylene is related to the presence of active radical aromatics contrary to the formation of ethylene which results directly from the dehydration of ethanol.

3.2. SAPO Zeotypes

SAPO-34 is a micro pore zeolite whose structure is similar to one met in chabazite structure (ACS Material Molecular Sieve SAPO-34-MSDS). It has a special water absorbing capacity and Brønsted acidity. It can be used as catalyst and support in different applications, including ethanol-to-olefins reaction. We wanted to test different zeolites in this reaction, not only ZSM-5 ones. In the following, we have prepared SAPO-34 by two different preparation routes: the hydrothermal synthesis (consequently the catalyst is denoted by HT-SAPO-34) and the dry-gel conversion (the catalyst herein is denoted by DGC-SAPO-34). The catalyst was recuperated at different stages of the preparation methods, characterized and tested. HT-SAPO-34-BC, HT-SAPO-34-AC, DGC-SAPO-34-BC and DGC-SAPO-34-AC denote HT-SAPO-34 before calcination, HT-SAPO-34 after calcination, DGC-SAPO-34 before calcination and DGC-SAPO-34 after calcination, respectively. The final HT-SAPO-34-AC is microcrystalline (10 μm as size of microcrystals), while the final DGC-SAPO-34-AC is nanocrystalline (80 nm as size of nanocrystals). The preparation method of these materials is described in the experimental part chapter.

- N_2 porosimetry:

Textural parameters and pore distribution were determined for the raw and the as-synthesized SAPO-34 (s) at different stages of the synthesis procedure.

Table 3.9. Textural parameters of the raw and prepared SAPO-34

Catalyst	S_{BET} (m^2/g)	Pore volume (cm^3/g)
SAPO-34 (raw)	445	0.02
SAPO-34 (Cal 2 hrs)	494	0.03
SAPO-34 (Cal 10 hrs)	388	0.02
SAPO-34-HT, before calcination	109	-
SAPO-34-HT, after calcination	655	-
SAPO-34-DGC, before calcination	115	-
SAPO-34-DGC, after calcination	570	-

First, the influence of the calcination was studied showing that all commercial samples (supplier, ACS Material) exhibited similar BET surface areas (388-495m²/g) and pore volumes (0.02-0.03 cm^3/g) [Table 3.9], but without any pore distribution. With respect to these results, the calcination was limited to 2h.

In the following, SAPO-34 was as-synthesized by hydrothermal treatment and dry gel conversion. From BET monopoint results (Table 3.9), we can see that the highest surface area was obtained for the HT-SAPO-34–AC (655 m^2/g), which is also close to that of DGC-SAPO-34-AC (570 m^2/g).

We can also see that the calcination steps have a tremendous effect on the surface area of the catalyst for both preparation procedures with an increase of 5-6 times (calcinations, 115-570 m^2/g and 109-655 m^2/g for DGC and HT respectively) [Table 3.9]. It is normal that the surface area of catalysts before calcination is lower than calcined ones. Calcination is necessary to decompose the structure directing agent used during the synthesis.

- XRD:

Only one study concerning the effect of crystal size for the ethanol-to-hydrocarbons reaction with SAPO-34 can be found in literature (I.M. Dahl, 1999). Using the newest dry-gel synthesis method, efforts were dedicated to produce SAPO-34 crystals twice-as-small to be compared with their micro-sized equivalent. Also, XRD patterns were plotted for both catalysts, HT-SAPO-34 and DGC-SAPO-34, each before and after calcination (denoted by BC and AC, respectively).

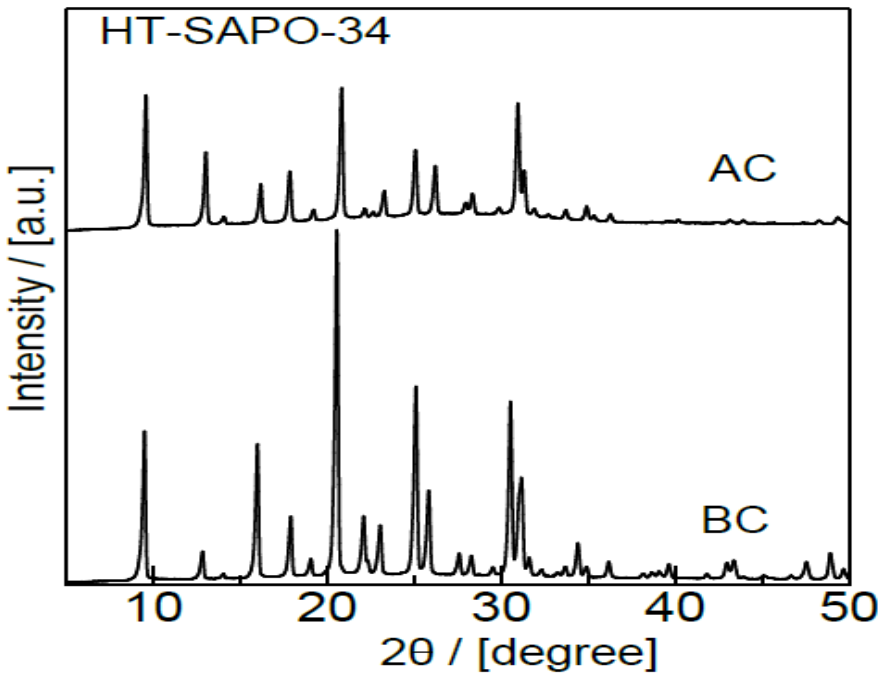

Figure 3.39. XRD patterns for HT-SAPO-34, pre- and post-calcination

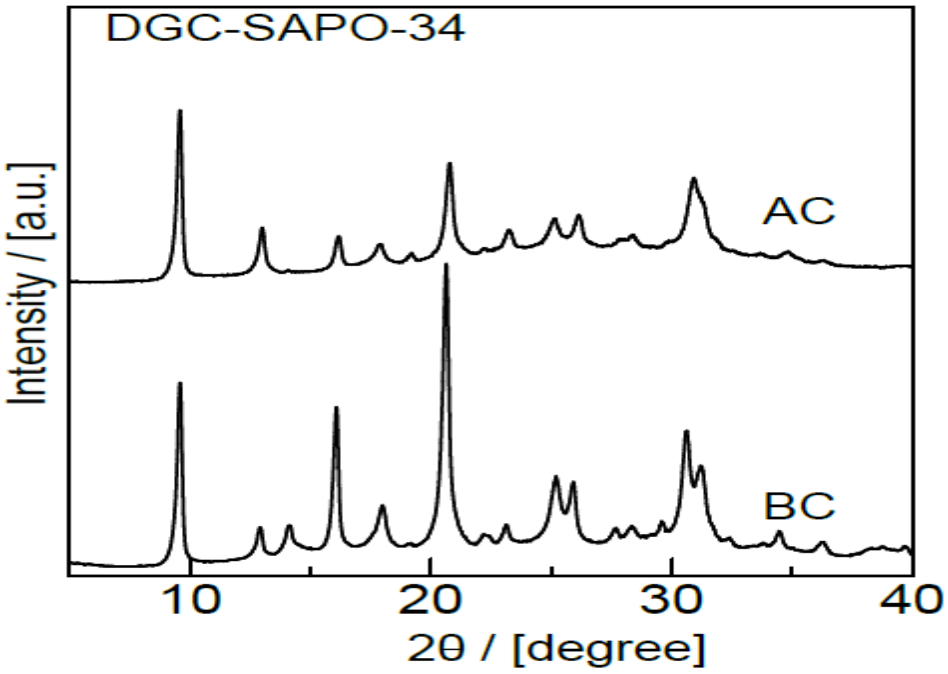

Figure 3.40. XRD patterns for DGC-SAPO-34, pre- and post-calcination

Table 3.10. Crystallinity parameters of prepared SAPO-34s

Catalyst	L (Crystallites size in nm)
HT-SAPO-34 (AC)	33
HT-SAPO-34 (BC)	24
DGC-SAPO-34 (AC)	31
DGC-SAPO-34 (BC)	24

HT-SAPO-34 and DGC-SAPO-34 show a slight decrease in peak intensity after calcinations (Figure 3.39,Figure 3.40). Provided that the used wavelength was Cu 1.5480 Å and by using Scherrer equation, one is able to estimate the mean size of the ordered (crystalline) domains [Table 3.10]. As one can see, the prepared catalysts have bigger crystallites sizes after calcinations, which refers to the sintering of the crystals. HT and DGC-SAPO-34 (s) show similar crystallites sizes after calcination, also before calcination. On the other hand, by examining the BET surface area of each catalyst before and after calcination, we observed a drastic increase in S_{BET} after calcination (X6 times for HT while X 5 times for DGC), due to the destruction of the structure directing agent.

- Investigation of the reaction mechanism:

Recent publications by Qian *et al.* have met great success in analyzing the emergence of intermediate and coke species during the ethanol-to-hydrocarbons reaction over SAPO-34 using inseparable *in situ* UV Vis and IR microscopy (Q. Qian J. R.-M.-T., 2013) (Q. Qian J. R.-M.-T., 2014) (Q. Qian J. R.-M.-T., 2014). Inspired by these results, this work aims to go beyond by combining a similar mix of *in situ* spectroscopy techniques in correlation with

catalytic testing to further understand the relation between the role of intermediate species, the nature of the products and their influence on coke production. This will be done to obtain new insight on the reaction with the ultimate goal to maximize propylene production.

UV/Vis spectroscopy was employed in order to evaluate any improvement in the reduction of carbonaceous species for the dry-gel conversion preparation method (for SAPO-34) in comparison with the classical hydrothermal synthesis method and thus the deactivation behavior of the catalysts.

The ETH reaction was conducted for 100 minutes at 350 °C over DGC-SAPO-34-AC and HT-SAPO-34-AC while being monitored by UV/Vis spectroscopy at repeated intervals with a feed of 12% EtOH/N_2. The bands at 280-330, 345-380, 400-420, around 500, around 600 and 662-737 designate monoenylic carbenium ions (or light aromatics), dienylic carbenium ions (or polycyclic aromatics), polyalkylbenzene, polyaromatics, larger polyaromatics and graphite-like polyaromatics, respectively [(W. Dai X. S., Verifying the mechanism of the ethene-to-propene conversion on zeolite H-SSZ-13, 2014) ; (Ahmad, 2003) ; (Q. Qian, 2014) ; (D. Mors, 2011)].

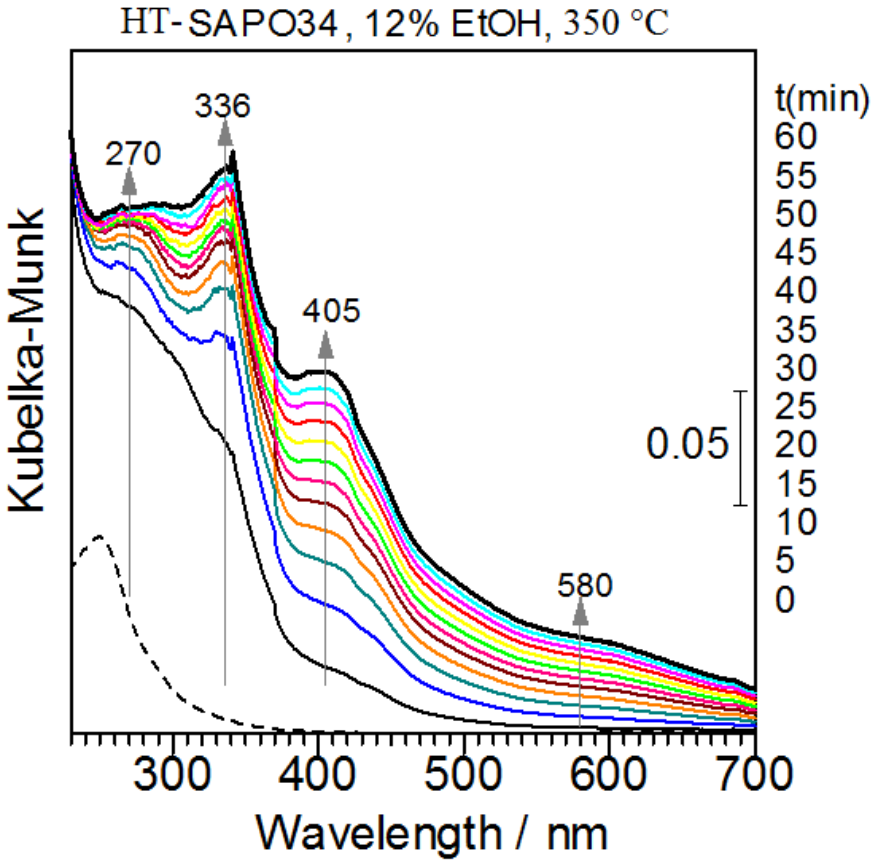

Figure 3.41. UV/Vis spectrum recorded during the ETO reaction for 100 minutes at 350 °C and a concentration of 12% EtOH using HT-SAPO34-10 to measure the effect of crystal size

UV/Vis spectroscopy measurements were done over the as-synthesized SAPO-34s to evaluate the effect of crystal size on the reaction mechanism (Figure 3.41). For microcrystalline

HT-SAPO34 during the ETO reaction at 350 °C (12% EtOH for 1 h), all bands at 270 nm, 336 nm, 405 nm and between 450-700 nm increase at an astounding rate, which underlines the rapid formation of carbonaceous species.

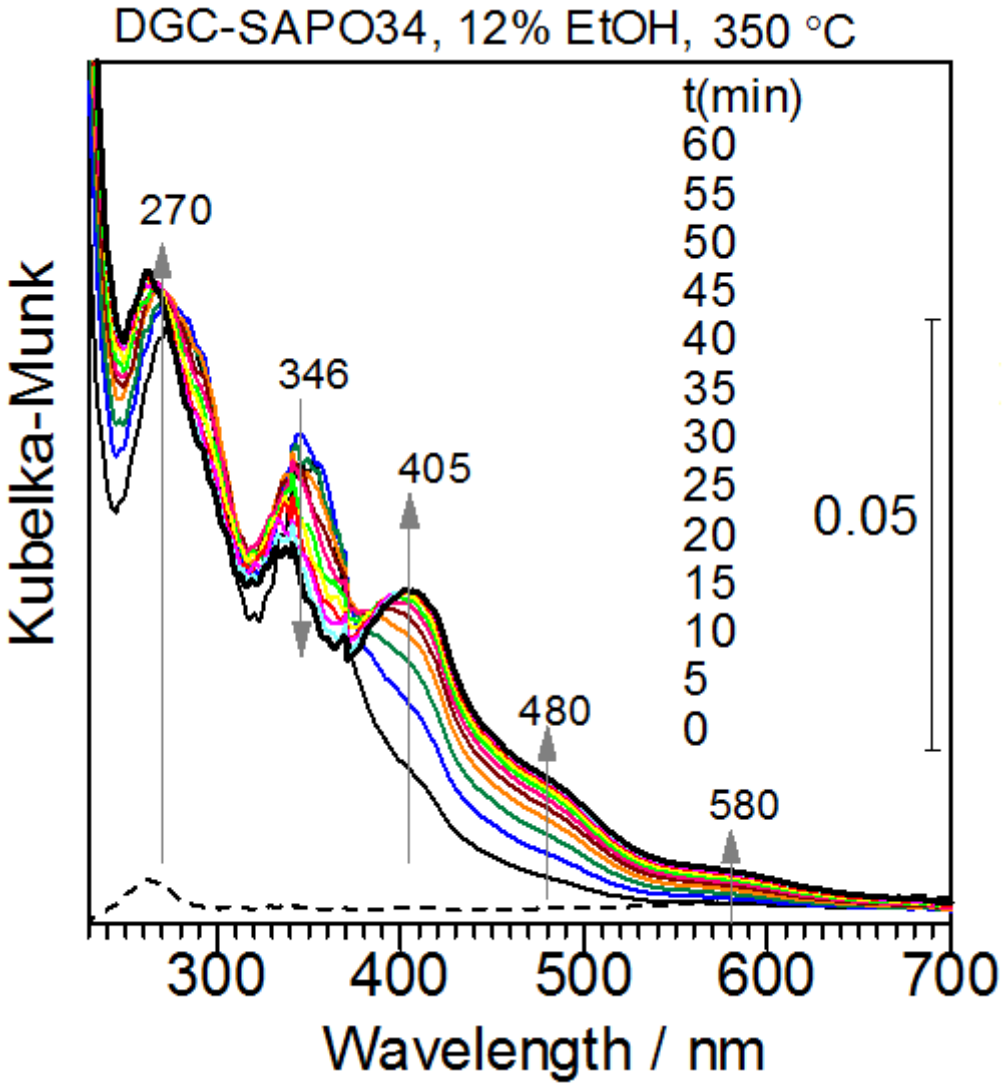

Figure 3.42. UV/Vis spectrum recorded during the ETO reaction for 100 minutes at 350 °C and a concentration of 12% EtOH using DGC-SAPO34-80 to measure the effect of crystal size

For the DGC-SAPO-34 (Figure 3.42), the 270 nm band increases till it gets stable, while the 346 nm band also grows before being eroded back. This suggests that the specie at the 346 nm band is being consumed likely to form species at the 405 nm and 480 nm bands respectively. If we consider that the direction of the carbonaceous species formation is in increasing wavelength order, the cycle is running well to yield carbonaceous species.

All peak intensities for the HT-SAPO-34 are higher than those for the DGC-SAPO-34 (> 3 times) suggesting that there are more carbonaceous species and that their formation rate is much larger. The formation of carbonaceous species is significantly reduced when using DGC-SAPO-34 compared to HT-SAPO-34. This is due to the limitation of the channel size

of the nanocrystalline catalyst whereby the low-molecular polyaromatics precursors are expelled out of the catalyst pores before accumulating into carbonaceous species (Figure 3.41;Figure 3.42).

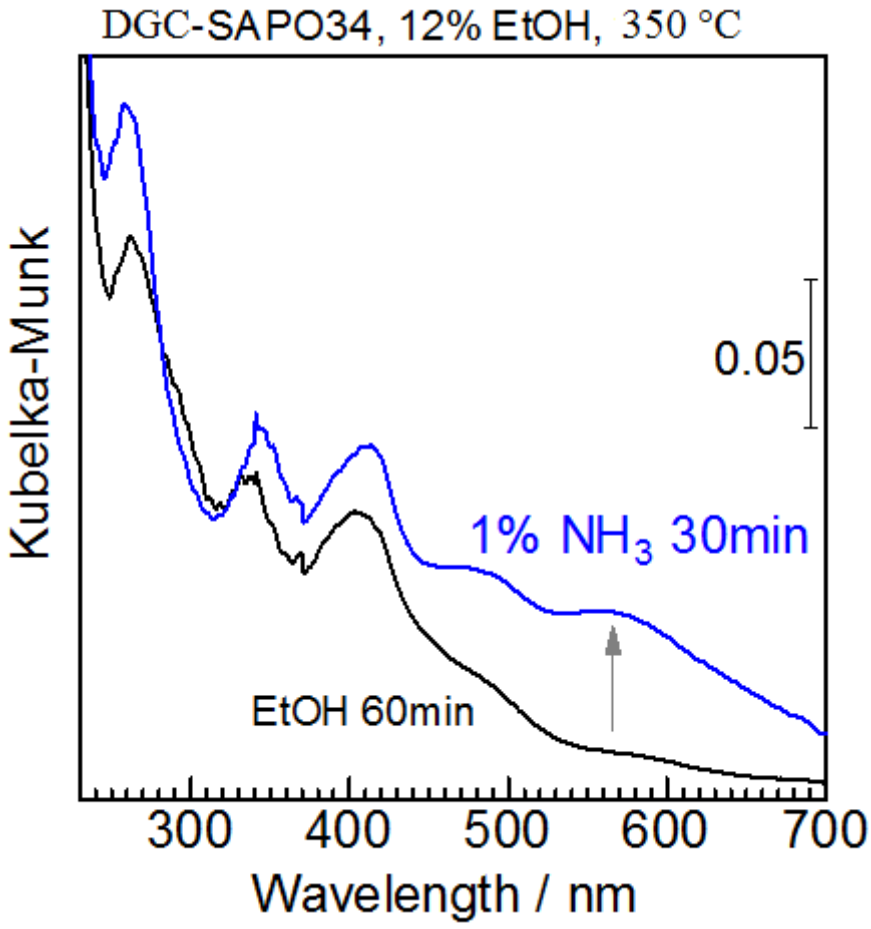

Figure 3.43. UV/Vis experiments with DGC-SAPO34 first during the ETO reaction for 1 h at 350 °C for a feed of 12% EtOH, then using a feed of 1% ammonia

After an ETH reaction of one hour over DGC-SAPO34 at 350 °C with a feed of 12% $EtOH/N_2$, the feed was switched to 1% NH_3/N_2. The spectrum in Figure 3.43 shows that none of the bands were eroded by ammonia, meaning that none of the species observable in DGC-SAPO34 is cationic in nature but rather neutral. So, one can conclude that early-formed carbenium ions over DGC-SAPO34 rapidly diminish.

- Catalytic Test Results:

Combining the observations made *in situ* within the catalyst and the effect it has on product distribution of the ethanol-to-hydrocarbons reaction will require actual catalytic testing to link the nature of trapped species to that of the products. This can be achieved with

a fixed-bed catalytic reactor and on-line chromatograph. Conditions should be standardized for all experiments in order to match between *in situ* results and product distribution.

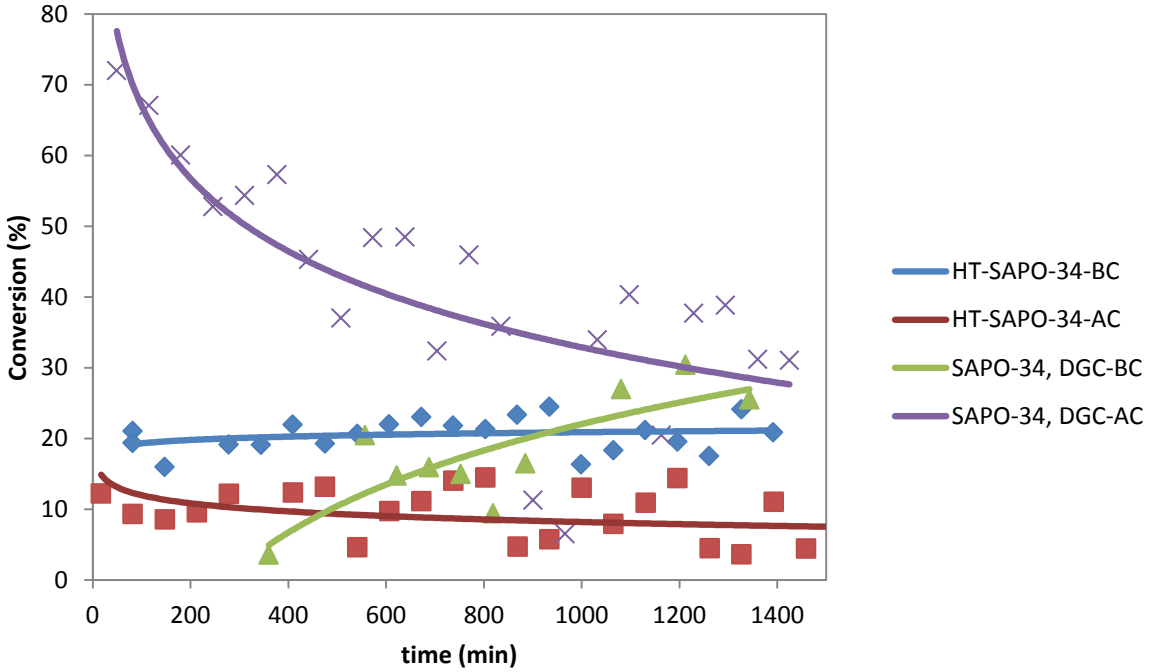

Figure 3.44. Graph showing the variation of conversion (%) as a function of time (min) for 10mg HT-SAPO-34 and DGC-SAPO-34 at different stages of the preparation procedure. Conditions: 0.0501 mL/min EtOH (50% EtOH flow in gaseous phase), 21 mL/min inert gas (He+N_2) and 350 °C reaction temperature. All conditions are per reactor.

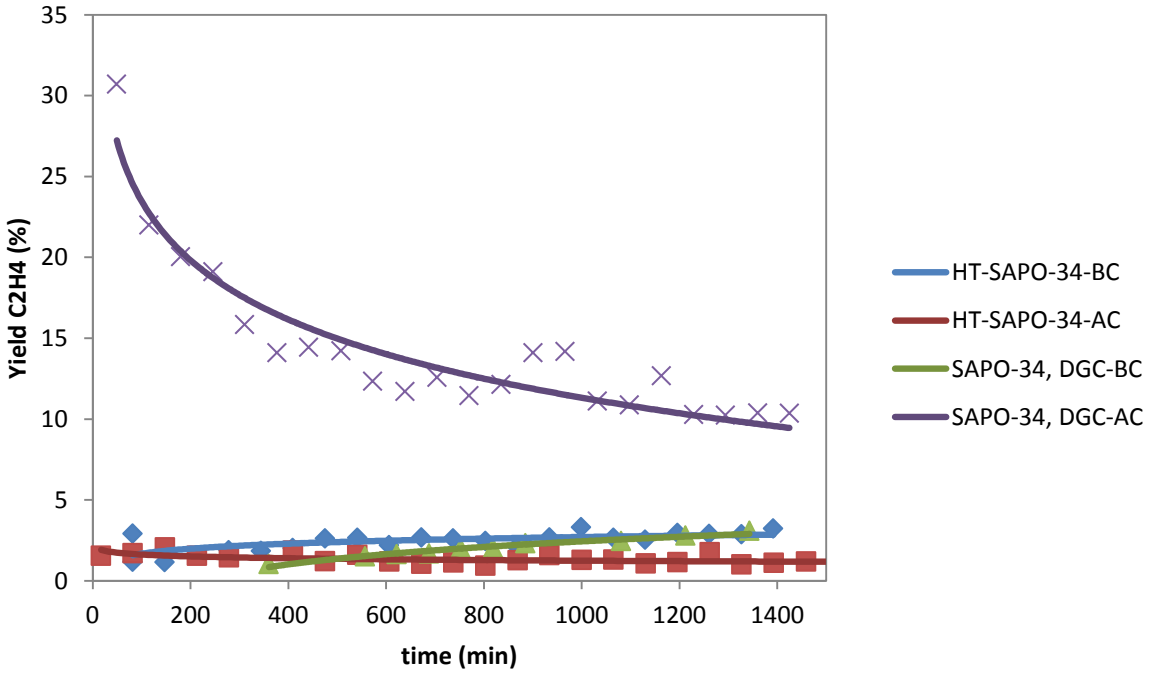

Figure 3.45. Graph showing the variation of ethylene yield (%) as a function of time (min) for 10mg HT-SAPO-34 and DGC-SAPO-34 at different stages of the preparation procedure. Conditions: 0.0501 mL/min EtOH (50% EtOH flow in gaseous phase), 21 mL/min inert gas ($He+N_2$) and 350 °C reaction temperature. All conditions are per reactor.

SAPO-34 zeotypes are known to catalyze various reactions including the ethanol-to-olefins reaction. Its channel structure is composed of large cavities interconnected through small pores. Their pore size is comparable to the kinetic diameter of propylene (4.5 Å), thus they selectively tune propylene. However, these catalysts are readily deactivated by carbon deposition. To avoid the flaw of "cage effect", we synthesized nano-size SAPO-34 particles for the purpose of: faster removal of products, shorter diffusion path lengths.

Ethanol conversion was higher and more stable before calcination than after calcination for HT-SAPO-34 (at 21%). The same trend is also observed for the DGC-SAPO-34, the most ideal conversion was for DGC-SAPO-34-AC. It started at 78% at t_0, despite that it dropped to 29% at t_∞ (Figure 3.44).With regards to the products distribution, the ethylene yield was too low for HT-SAPO-34 with a maximum of 3% (Figure 3.45). It was also too low for DGC-SAPO-34, but it increased suddenly for DGC-SAPO-34-AC (28-11%). For all catalysts, negligible propylene yields were obtained.

To interpret the absence of propylene, it is important to refer back to the ethanol-to-olefins reaction mechanism proposed by Pinard *et al.* [(L. Pinard K. B., 2013);(S. Hamieh, 2015)]. They argument that the nature of active species in the hydrocarbon pool mechanism is believed to be cationic and radical at the same time. According to them, propylene and butylene are believed to be produced through a pairing mechanism on cationic free radical aromatics, subsequently transformed into the remaining products observed through conjunct polymerization (Figure 3.46).

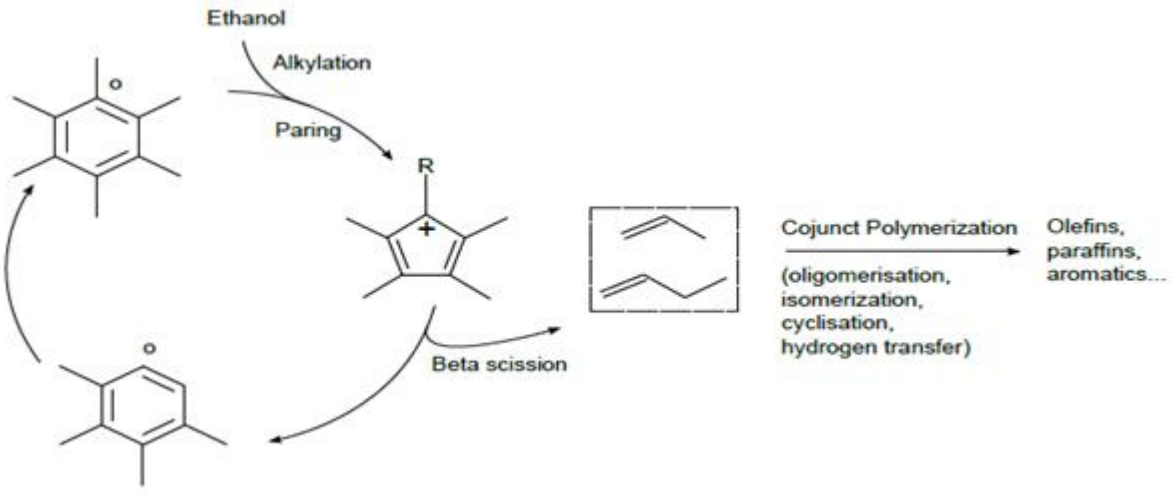

Figure 3.46. Hydrocarbon pool mechanism involving radicals as proposed by Pinard *et al.* [(L. Pinard K. B., 2013); (S. Hamieh, 2015)]

This is a so-called "modified" hydrocarbon pool mechanism. It meets with the original hydrocarbon pool mechanism in the point that the initial stage of olefins formation is the oligomerization of ethylene. 1-hexene is an example of such heavy oligomer capable of

cyclisation into aromatized products in the course of carbonaceous species formation cycle. These aromatized products are at a certain stage of the cycle, the active radical polyalkyl aromatics. By having a look 1-hexene trends, we observe that the highest yield was recorded for DGC-SAPO-34-AC (19-13%, Figure 3.47). This was followed by HT-SAPO-34-BC (constant at 9-8%, Figure 3.47). If propylene would form from the oligomerization of ethylene then cracking, we should have observed higher yields for propylene. This can be interpreted by the fact that decreasing crystal size decreased the channel length as well, thus aromatized products (including 1-hexene) were expelled rapidly whereby the formation of propylene was hindered.

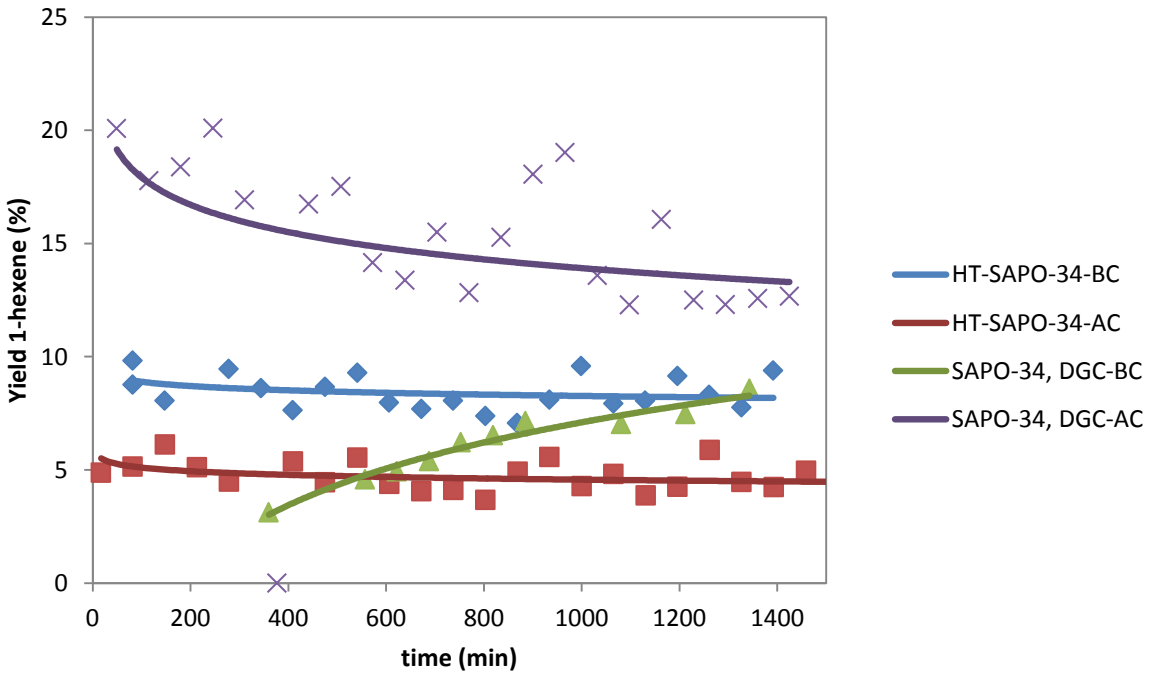

Figure 3.47. Graph showing the variation of 1-hexene yield (%) as a function of time (min) for 10mg HT-SAPO-34 and DGC-SAPO-34 at different stages of the preparation procedure. Conditions: 0.0501 mL/min EtOH (50% EtOH flow in gaseous phase), 21 mL/min inert gas (He+N_2) and 350 °C reaction temperature. All conditions are per reactor.

So, calcination had a bad effect on HT-SAPO-34; It seems that this treatment completely decrease the activity of the support. The products form with these materials are mainly ethylene and 1-hexene yields. The formation of the aforementioned product can be explained by the so-called "modified" hydrocarbon pool mechanism. However, no trace of propylene have been observed. Therefore, the prepared nanoparticles failed to produce propylene.

3.3. Mesoporous Catalysts

Not only ZSM-5s were characterized and tested to choose convenient supports for the ethanol-to-olefins reactions, but also a mesoporous silica-alumina from Sasol. Siral-1 and Siral-40 are both silica alumina provided by Sasol®. Siral-1 has an Al_2O_3:SiO_2 mole ratio of

99:1, while that of Siral-40 is 60:40. In the datasheet supplied by the company, both supports have the same particle size (d_{50}) of 50 µm.

- N_2 porosimetry:

Raw supports were characterized for their textural parameters using nitrogen adsorption.

Table 3.11. Textural parameters of the mesoporous catalysts

Solid catalyst	S_{BET} (m^2/g)	pore volume (cm^3/g)	pore diameter (nm)
Siral-1 (raw)	305	0.64	7
Siral-40 (raw)	446	0.99	8

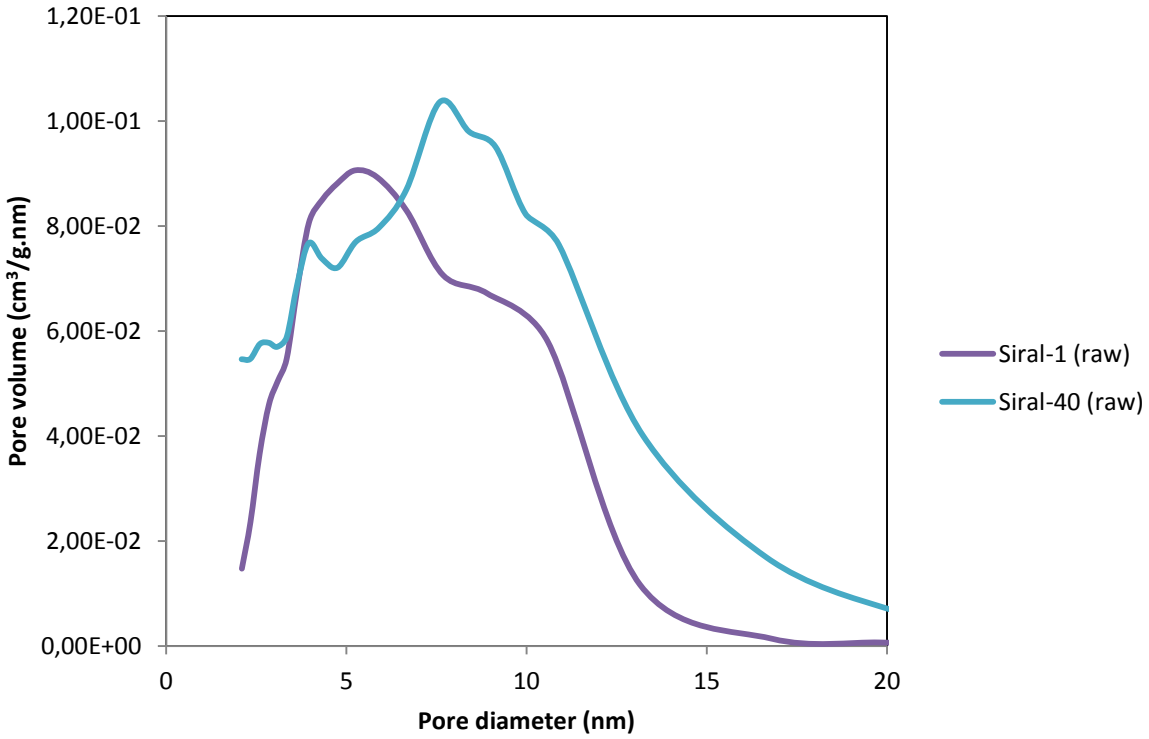

Figure 3.48. Pore distribution by BJH method for the mesoporous catalysts

Siral-40 and Siral-1 show high specific surface areas of 440 and 300 m²/g, respectively (Table 3.11). The pore volume is 50% higher for the Siral-40 and pore diameters are quite similar for both sample with a distribution centered around 7-8 nm (Figure 3.48).

- Acidity Measurement:

Mesoporous catalysts are known for their big pores, so it is expected that pyridine adsorption-desorption will not destroy their structure. Hence, acidity would be determined properly. As we can see from Table 3.12, both catalysts show dominant Lewis acidity. ZSM-5s and Siral-s

show good examples of dissimilar Brønsted and Lewis acidities. Siral-40 exhibits higher acidity than Siral-1, but for each material, the weak Lewis sites predominate.

Table 3.12. Relative percentages of number of moles of Brønsted and Lewis acid sites of raw mesoporous catalysts as determined by pyridine FTIR spectroscopy. Ɛ B= 0.73, Ɛ L= 0.64 (according to recent references).

Catalyst	Temperature	n B (%)	n L (%)	Acidity (a.u.)
Siral-1 (raw)	150 °C (Total acidity)	0	100	31
	450 °C (Strong acidity)	0	100	9
	150-450 °C (weak acidity)	0	100	22
Siral-40 (raw)	150 °C (Total acidity)	4	96	499
	450 °C (Strong acidity)	0	100	90
	150-450 °C (weak acidity)	5	95	409

- NH_3 TPD:

As ammonia is a small molecule and can penetrate into zeolitic pores as well, so it is also suitable to measure the acidity (amount and strength) of mesoporous supports using ammonia TPD.

Table 3.13. Number of moles of acid sites of raw mesoporous catalysts as determined by ammonia TPD measurements. Weak acid sites <280 °C, medium acid sites 280-480 °C and strong acid sites >480 °C.

Catalyst	Acidity (mmol/g)	Weak acidity (mmol/g)	Medium acidity (mmol/g)	Strong acidity (mmol/g)	Acidity (mmol/m^2)
Siral-1 (raw)	0.69	0	0.627	0	2.26*10-3
Siral-40 (raw)	0.56	0.019	0.457	0.082	1.26*10-3

Raw Siral-1 and Siral-40 showed very high acidity (0.69 versus 0.56 mmol/g in NH_3 TPD) which was found to be exclusively to originate from Lewis sites (Table 3.12). Raw Siral-40 also shows high ammonia acidity as the raw Siral-1; however, for the former the acidity distribution is not limited to medium strength as for the latter (0.02 mmol/g weak, 0.46 mmol/g medium and 0.08 strong acidity) [Table 3.13].

- Catalytic Tests Results:

Comparing previously discussed zeolite type supports with Siral, one can see that CBV50 and Siral-1 have similar BET surface areas (418 m^2/g), pore volume (0.12 cm^3/g), moderate acidities (0.17 and 0.20 mmol/g respectively) and acidity distributions (0.03-0.02 mmol/g respective weak acidities, 0.08-0.05 respective medium acidities and 0.05-0.13 mmol/g respective strong acidities) [Table 3.5;Table 3.11;Table 3.6;Table 3.13]. The only, but

important difference between the CBV50 and the Siral-1 is that the acidity for the first one is mostly Brønsted, while that of the latter is strictly Lewis (Table 3.7;Table 3.12). Hence, by testing the bare Siral-1, it will be possible to determine again the role of the Brønsted acidity for the ethanol-to-propylene reaction, but also the influence of the porosity, remembering that Siral is a mesoporous support.

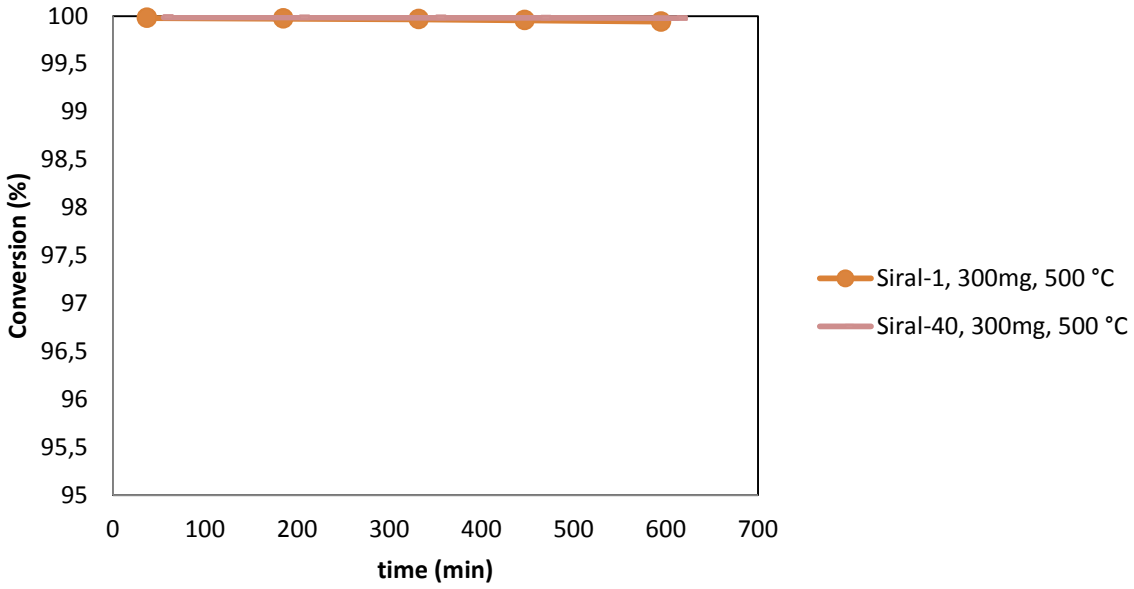

Figure 3.49. Graph showing the variation of conversion as a function of time (min) for raw Siral (s) over "FLOWRENCE T1220". Reaction conditions: 1.05 mL/min He flow, 19.95 mL/min N_2 (Total of 21 mL/min of inert gas). Diluent flow (N_2) of 7.5 mL/min. 0.0125 mL/min as liquid ethanol flow (20% in gaseous phase). 300mg of the catalyst was used at 500 °C temperature. All conditions are per reactor. Supports are raw catalysts.

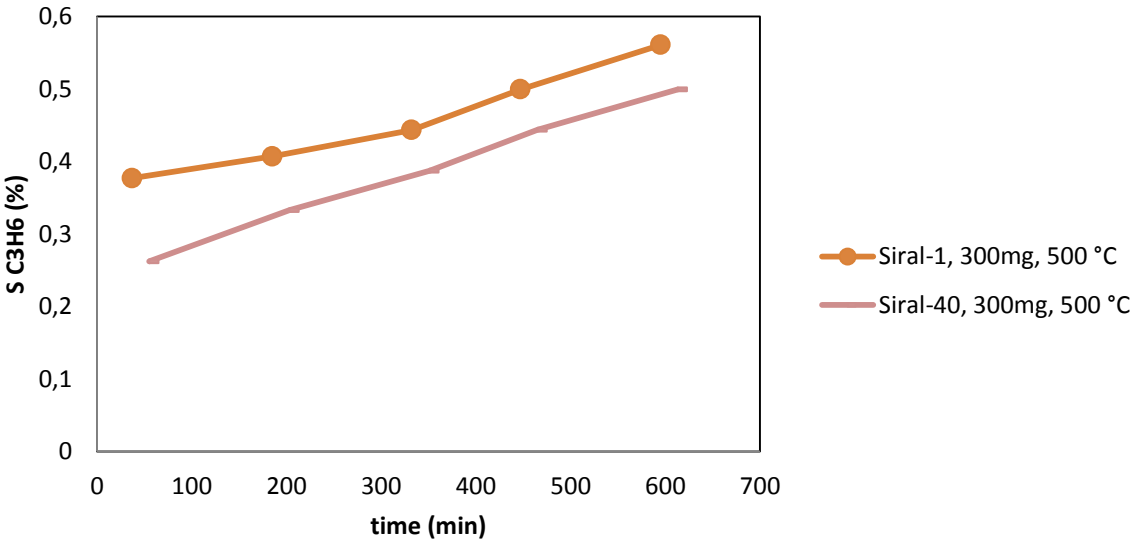

Figure 3.50. Graph showing the variation of propylene selectivity (%) as a function of time (min) for raw Siral (s) over "FLOWRENCE T1220". Reaction conditions: 1.05 mL/min He flow, 19.95 mL/min N_2 (Total of 21 mL/min of inert gas). Diluent flow (N_2) of 7.5 mL/min. 0.0125 mL/min as liquid ethanol flow (20% in gaseous phase). 300mg of the catalyst was used at 500 °C temperature. All conditions are per reactor. Supports are raw catalysts.

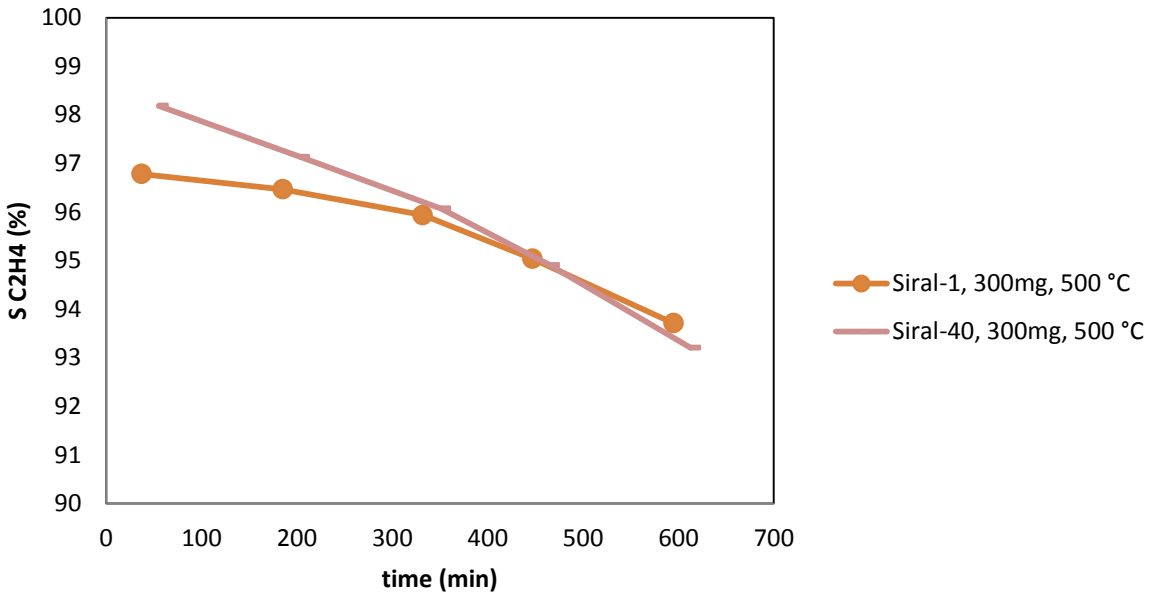

Figure 3.51. Graph showing the variation of ethylene selectivity (%) as a function of time (min) for raw Siral (s) over "FLOWRENCE T1220". Reaction conditions: 1.05 mL/min He flow, 19.95 mL/min N_2 (Total of 21 mL/min of inert gas). Diluent flow (N_2) of 7.5 mL/min. 0.0125 mL/min as liquid ethanol flow (20% in gaseous phase). 300mg of the catalyst was used at 500 °C temperature. All conditions are per reactor. Supports are raw catalysts.

Siral-1 and 40 showed similar performances at 500 °C (nearly 100% conversion and ethylene selectivity which decreases slightly from ~99 to 94% after 10 hours of reaction); however, propylene selectivity for both bare supports is zero (Figure 3.49;Figure 3.51;Figure 3.50 respectively).

In order to study the influence of the reaction temperature more in details, 50mg of Siral-1 catalyst was tested at different temperatures: 300-450 °C over Flowrence T1220 and 200-350 °C over the multi-valve reactor system. Siral-1 at 400 and 450 °C both show 100% ethanol conversion, 0% propylene selectivity and 97% ethylene selectivity meaning that these conditions are suitable for the dehydration of ethanol. 50mg Siral-1 at 350 °C shows 78% conversion, a sudden drop of initial propylene selectivity from 13 to 0%, and a sharp increase of ethylene selectivity from 44 to 56% at 185 min followed by smooth increase from 56 to 61% at 628 min. So, this catalyst is not suitable to form propylene as the latter is not stable throughout the reaction. The conversion at 300 °C temperature is very low (23-31%), while propylene selectivity is null, so too is ethylene selectivity (8%). This is normal as less ethanol is converted. For the 250 °C temperature, conversion varied at around 40%, whereas ethylene selectivity was nearly negligible (3%). For the 200 °C, conversion was lower than 10% and ethylene selectivity was zero (Figure 3.52;Figure 3.53;Figure 3.54).

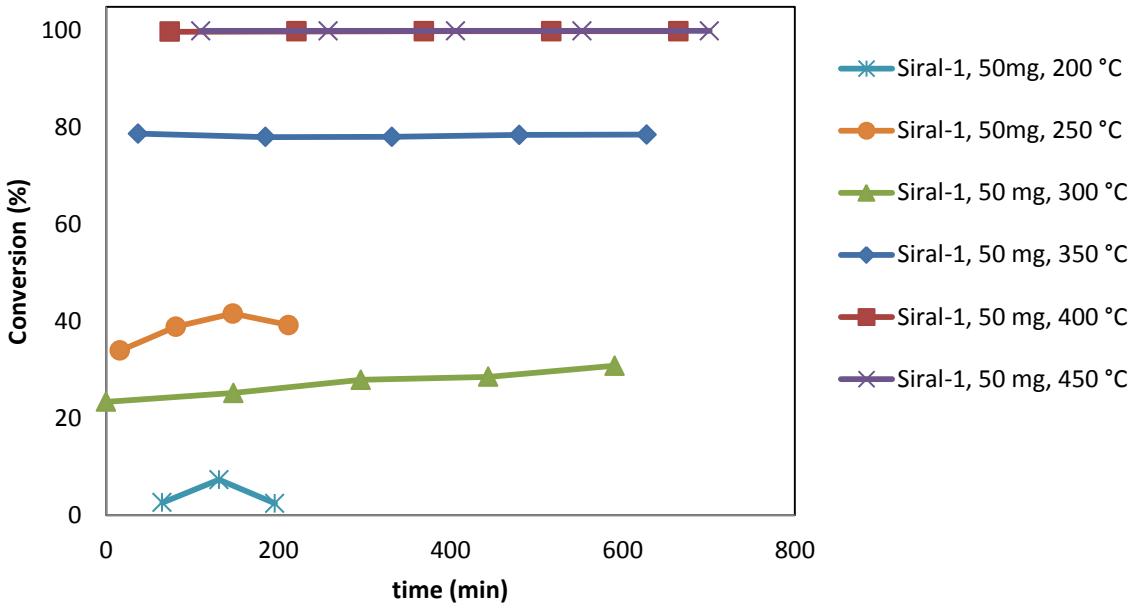

Figure 3.52. Graph showing the variation of conversion (%) as a function of time (min) for raw Siral-1s over "FLOWRENCE T1220" and multi-valve reactor system. Reaction conditions: 1.05 mL/min He flow, 19.95 mL/min N_2 (Total of 21 mL/min of inert gas). Diluent flow (N_2) of 7.5 mL/min. 0.0125 mL/min as liquid ethanol flow (20% in gaseous phase). 50mg of the catalyst mass was used at different temperatures (200, 250, 300, 350, 400 and 450 °C). All conditions are per reactor. Supports are raw catalysts.

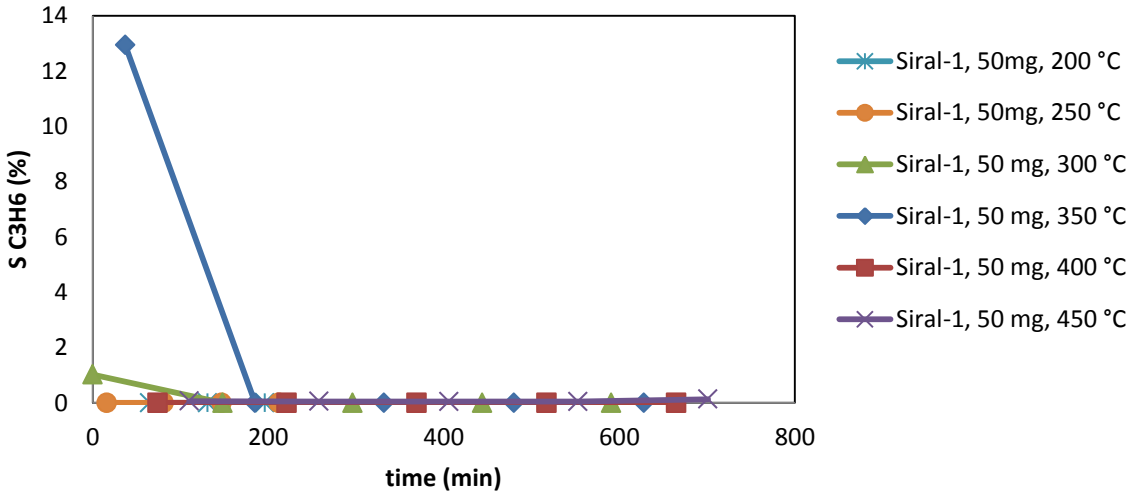

Figure 3.53. Graph showing the variation of propylene (%) as a function of time (min) for raw Siral-1s over "FLOWRENCE T1220" and multi-valve reactor system. Reaction conditions: 1.05 mL/min He flow, 19.95 mL/min N_2 (Total of 21 mL/min of inert gas). Diluent flow (N_2) of 7.5 mL/min. 0.0125 mL/min as liquid ethanol flow (20% in gaseous phase). 50mg of the catalyst mass was used at different temperatures (200, 250, 300, 350, 400 and 450 °C). All conditions are per reactor. Supports are raw catalysts.

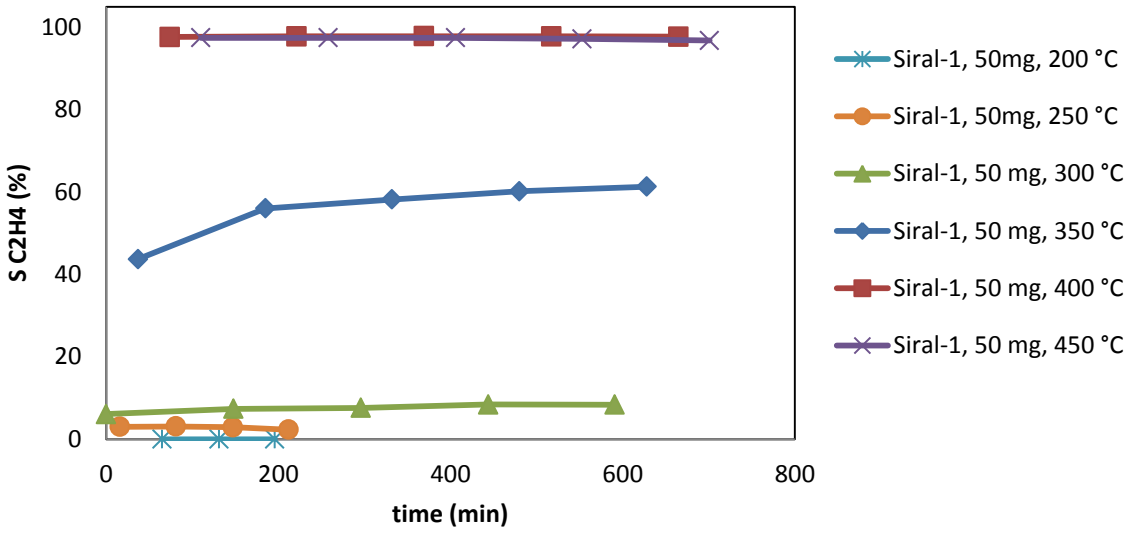

Figure 3.54. Graph showing the variation of ethylene selectivity (%) as a function of time (min) for raw Siral-1s over "FLOWRENCE T1220" and multi-valve reactor system. Reaction conditions: 1.05 mL/min He flow, 19.95 mL/min N_2 (Total of 21 mL/min of inert gas). Diluent flow (N_2) of 7.5 mL/min. 0.0125 mL/min as liquid ethanol flow (20% in gaseous phase). 50mg of the catalyst mass was used at different temperatures (200, 250, 300, 350, 400 and 450 °C). All conditions are per reactor. Supports are raw catalysts.

From the results one can see that the conversion remains complete until a reaction temperature of 350°C (Figure 3.52). In terms of the selectivity, ethylene was always the main product up to 250°C (Figure 3.54), whereas at lower temperature other products formed – supposedly diethylether. Propylene selectivity was null with time-on steam for all catalysts (Figure 3.53). If we take a look back to zeolites, CBV50 exhibited at 500 °C full conversion and propylene selectivity up to 32% [ethylene selectivity <50% (Figure 3.23;Figure 3.24)], while Siral-1 at the same conditions had full conversion but zero propylene selectivity while ethylene selectivity is nearly full (Figure 3.50;Figure 3.51).

This means that either Lewis acidity or mesoporosity are not favorable to form propylene. In order to discriminate between the influence of each parameter, our effort has been devoted to control the acidity of Siral-1 by manipulating it with a variety of metals including tungsten, silver and aluminum etc. We thought that decreasing its acidity might have a direct effect on propylene formation. The moderate range acidities with efficient propylene selectivities were recorded for ZSM-5s only.

3.4. Conclusion

After all, among the raw supports, it was found that the raw CBV50 shows high propylene selectivity even before metal-modification. On the other hand, Siral-1 shows in specific reaction conditions excellent ethylene selectivity which seems to be promising to produce propylene if we modify it with metals. The best performance was observed for moderate levels of acidity, with the major actor being Brønsted acidity. The next step will be the modification of the surface of supports with metals, covering different groups of the periodic table. In our assumptions, this should have a dual effect: first, the fixation of new

elements on the surface of the catalyst definitively has an effect in changing pore dimensions and so forth. Second, this will have a direct effect on the acidity of the catalyst as the metal will coordinate with the acid sites. Some authors suggest that H-ZSM-5 is the active component, while added P and Fe, for example, act as modifiers (M. Inaba K. M., 2011). We will see the resultant consequences on the propylene production in the next chapter. Hence, we will present in chapter four which metals were impregnated, textural and chemical modifications, and their relevance with the catalytic activity.

3.5. References

ACS Material Molecular Sieve SAPO-34-MSDS. (s.d.). Récupéré sur ACS Material: http://www.acsmaterial.com/sapo-240.html

Ahmad, R. (2003). Isomerization of n-butane and of n-pentane in the presence of sulfated zirconia: formation of surface deposits investigated by in situ diffuse reflectance spectroscopy. *Journal of Catalysis* , 365-374.

Borade R, S. A. (1990). Characterization of acidity in ZSM-5 zeolites: an x-ray photoelectron and IR spectroscopy study. *The Journal of Physical Chemistry* , 5989-5994.

D. Mors, J. K. (2011). Coke Formation during the Methanol-to-Olefin Conversion: In Situ Microscopy on Individual H-ZSM-5 Crystals with Different Brønsted Acidity. *Chemsitry A European Journal* , 2874-2884.

Dapaah JKA, A. L. (1997). Enhancement of Catalytic Activity of Natural Zeolites by Surface Modification for 1-Butene Isomerization. *Muroran Institute of Technology* , 89-95.

E. Selli, L. F. (1999). Comparison between the surface acidity of solid catalysts determined by TPD and FTIR analysis of pre-adsorbed pyridine. *Microporous and Mesoporous Materials* , 129-140.

H. Oikawa, Y. S. (2006). Highly selective conversion of ethene to propene over SAPO-34 as a solid acid catalyst. *Applied Catalysis A: general* , 181-185.

I.M. Dahl, R. W. (1999). The effect of crystallite size on the activity and selectivity of the reaction of ethanol and 2-propanol over SAPO-34. *Microporous and mesoporous materials* , 159-171.

Kiwi-Minsker L, B. D. (2003). Active sites in HZSM-5 with low Fe content for the formation of surface oxygen by decomposing N2O: is every deposited oxygen active? *Journal of Catalysis* , 273-285.

L. Pinard, K. B. (2013). On the involvement of radical "coke" in ethanol conversion to hydrocarbons over HZSM-5 zeolite. *Catalysis Today* , 218-219.

M. Inaba, K. M. (2011). Production of olefins from ethanol by Fe and/or P-modified H-ZSM-5 zeolite catalysts. *J Chem Technol Biotechnol* , 95-104.

M. Tamura, K. S. (2012). Comprehensive IR study on acid/base properties of metal oxides. *Appl. Catal, A* , 135-145.

Masih, J. (2010). Hydroisomerization of a hydrocarbon feed containing n-hexane on Pt/H-Beta and Pt/H-Mordenite catalysts. *J. Chem. Pharm. Res.* , 546-553.

Q. Qian, J. R.-M.-T. (2014). Single-catalyst particle spectroscopy of alcohol-to-olefins conversions: Comparison between SAPO-34 and SSZ-13. *Catalysis Today* , 14-24.

Q. Qian, J. R.-M.-T. (2014). Single-Particle Spectroscopy of Alcohol-to-Olefins over SAPO-34 at Different Reaction Stages: Crystal Accessibility and Hydrocarbons Reactivity. *Chem - CatChem* , 772-783.

Q. Qian, J. R.-M.-T. (2013). Single-Particle Spectroscopy on Large SAPO-34 Crystals at Work: Methanol-to-Olefin versus Ethanol-to-Olefin Processes. *Chemistry - A European Journal* , 11204-11215.

S. Hamieh, C. C. (2015). Methanol and ethanol conversion into hydrocarbons over H-ZSM-5 catalyst. *The European Physical Journal Special Topics* , 1817-1830.

W. Dai, X. S. (2014). Verifying the mechanism of the ethene-to-propene conversion on zeolite H-SSZ-13. *Journal of Catalysis* , 10-20.

Wichterlová B, T. Z. (1998). Determination and properties of acid sites in H-ferrierite: A comparison of ferrierite and MFI structures. *Microporous and Mesoporous Materials* , 223-233.

Zhung W, H. X. (2003). Characterization of teh acid sites in dealuminated nanosized HZSM-5 zeolite with probe molecule trimethylphosphine. *Journal of Molecular Catalysis. A: Chemical* , 107-113.

Chapter 4: Refined Screening – Results and Discussion

Chapter 4. Refined Screening – Results and Discussion

Porous materials (zeolites, mesoporous silicas and periodic mesoporous organosilica) have been largely studied because of their interesting physico-chemical properties in terms of high internal and external specific surface area, presence of ordered uniform pores, and easy surface functionalization, rendering these solids suitable for various applications, such as catalysts (F. Carniato, 2010). After the selection of the proper supports (CBV 55 from the zeolites series and Siral-1 from the mesoporous catalysts series), it was time to impregnate them with metals covering different groups of the periodic table, and to treat them with acids or bases etc. All that is in order to improve the selectivity to propylene.

4.1. CBV50 and Siral-1

4.1.1. Metal-modified catalysts

We found from the prescreening results, both at the level of characterizations and catalytic tests, that acidity and channel structure significantly affect the catalyst performances. For this, it is necessary to play on these two factors in order to ameliorate the propylene selectivity. Impregnating the surface of the catalyst with metals changes its acidity and – to less extend – the porous dimensions at the same time.

The distribution of products obtained in ethanol conversion using zeolitic material is strongly dependent on the acidity as well as the channel structure of the zeolites. For us, we tried modifiers covering all groups of the periodic table. This was specifically that we were interested in finding metals which are less precious than noble metals (e.g. Re) but also showing at the same time high propylene selectivity.

- Preliminary Analyses:

We doped CBV50 and Siral-1 with metals covering different groups of the periodic table. Below we show the selectivity to propylene (%) versus the conversion at t_0 (beginning of the reaction in the presence of ethanol), and $t\infty$ (at the end of the reaction). The top 5 catalysts giving the highest selectivity at a near full conversion and one catalyst giving low selectivity at high conversion, were selected for further catalytic tests investigations. After all tests are presented, characterizations will be discussed for these catalysts in order to link structural and chemical properties to the activity.

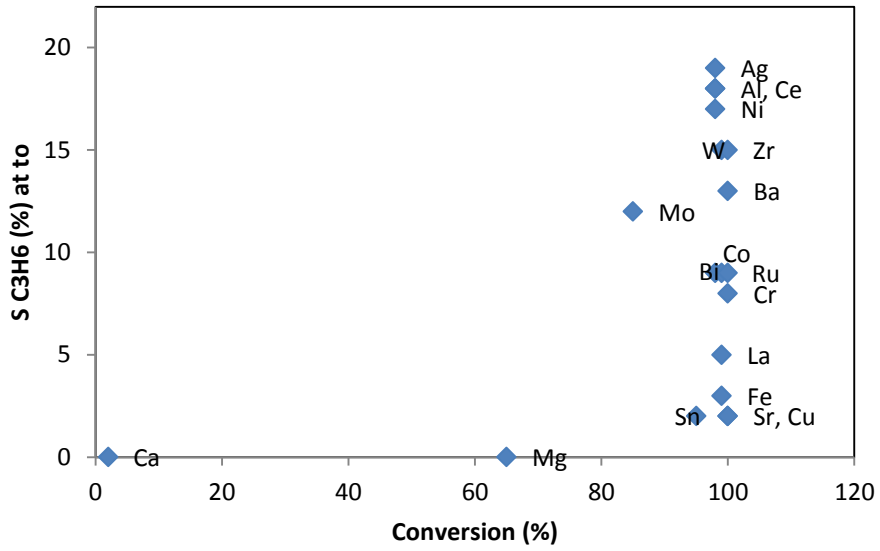

Figure 4.55. Propylene selectivity (%) versus conversion (%) at t0 for various metal-modified CBV50 (s) over "FLOWRENCE T1220" and multi-valve reactor system. Reaction conditions : 0.0125 mL/min liquid ethanol flow (20% EtOH in gaseous phase), 1.05 mL/min inert gas flow He, 19.95 mL/min N_2 (Total of 21 mL/min of inert gas), diluent flow (N_2) of 7.5 mL/min, 350 °C reaction temperature, and 50 mg catalyst mass. All conditions are per reactor.

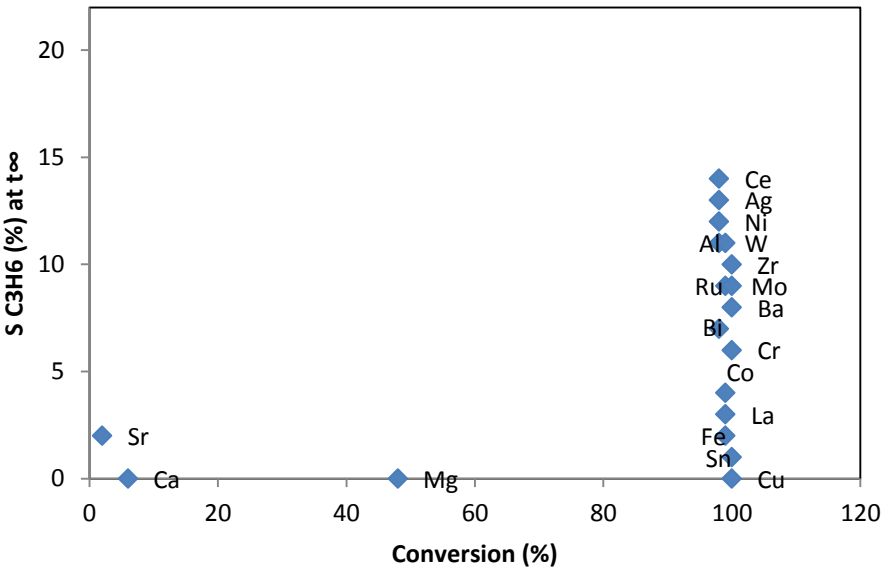

Figure 4.56. Propylene selectivity (%) versus conversion (%) at t∞ for various metal-modified CBV50 (s) over "FLOWRENCE T1220" and multi-valve reactor system. Reaction conditions : 0.0125 mL/min liquid ethanol flow (20% EtOH in gaseous phase), 1.05 mL/min inert gas flow He, 19.95 mL/min N_2 (Total of 21 mL/min of inert gas), diluent flow (N_2) of 7.5 mL/min, 350 °C reaction temperature, and 50 mg catalyst mass. All conditions are per reactor.

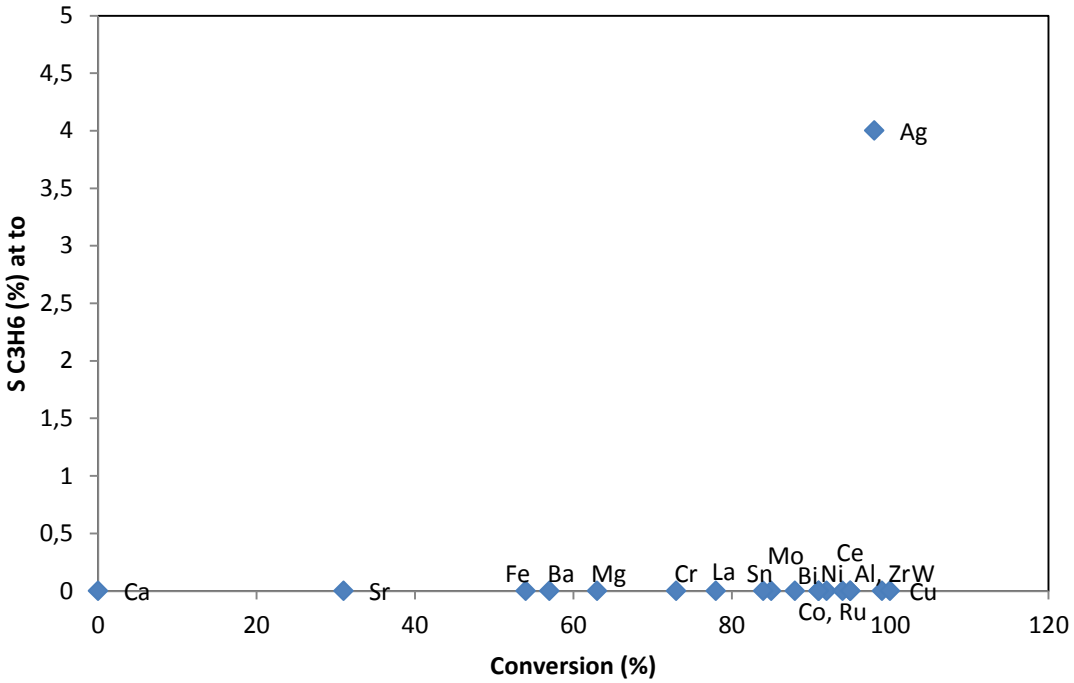

Figure 4.57. Propylene selectivity (%) versus conversion (%) at t0 for various metal-modified Siral-1 (s) over "FLOWRENCE T1220" and multi-valve reactor system. Reaction conditions : 0.0125 mL/min liquid ethanol flow (20% EtOH in gaseous phase), 1.05 mL/min inert gas flow He, 19.95 mL/min N_2 (Total of 21 mL/min of inert gas), diluent flow (N_2) of 7.5 mL/min, 350 °C reaction temperature, and 50 mg catalyst mass. All conditions are per reactor.

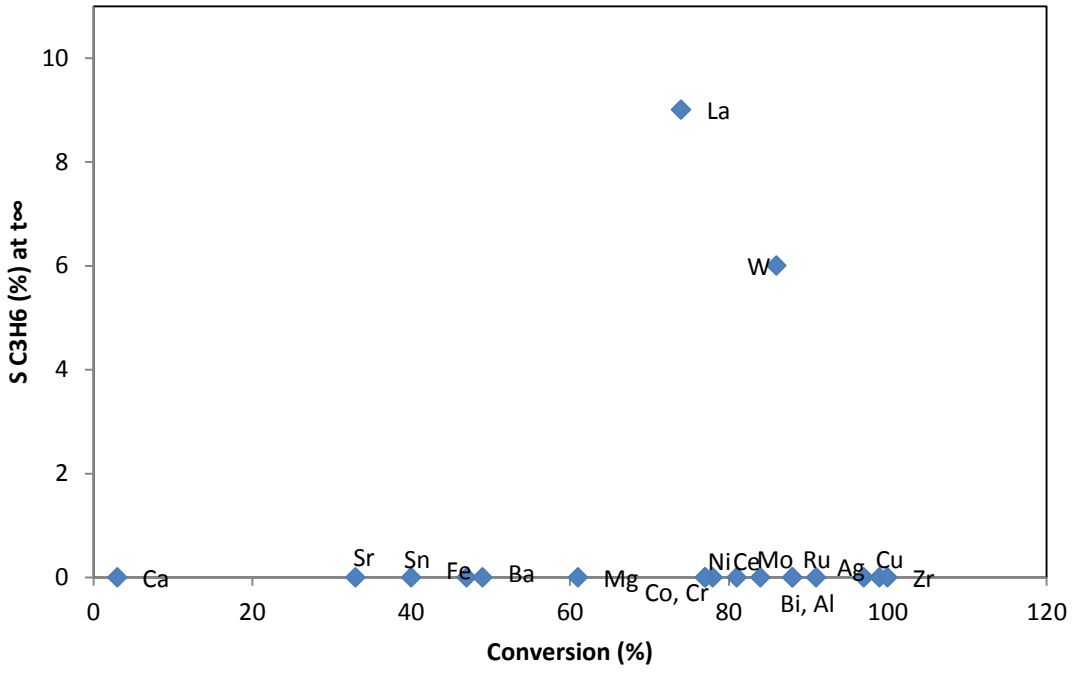

Figure 4.58. Propylene selectivity (%) versus conversion (%) at t∞ for various metal-modified Siral-1 (s) over "FLOWRENCE T1220" and multi-valve reactor system. Reaction conditions : 0.0125 mL/min liquid ethanol flow (20% EtOH in gaseous phase), 1.05 mL/min inert gas flow He, 19.95 mL/min N_2 (Total of 21 mL/min of inert gas), diluent flow (N_2) of 7.5 mL/min, 350 °C reaction temperature, and 50 mg catalyst mass. All conditions are per reactor.

We have selected to impregnate the raw supports CBV50 and Siral-1 with 19 different metals from all over the periodic table. Since our target product is propylene, the criteria for the selection of the top 3 metals is based on this along with full conversions of ethanol. We plotted propylene selectivities versus conversions So, the interesting region for us in the graphs is the top-right corner. We plotted the selectivities at t_0 (*i.e.* the beginning of the reaction in the presence of ethanol) and at t_∞ (*i.e.* at the end of the reaction). As we can see from the graphs of S C_3H_6 at t_0 and S C_3H_6 at t_∞, the three best showing doped metals are: silver, aluminum and tungsten. In Figure 4.55, both tungsten and zirconium are nearly equivalent; however, in Figure 4.56 – after 15h of reaction – tungsten is better than zirconium. All 3 metals show high conversions (98-100%).

In the Siral-1 impregnated set, the results are very disappointing. Silver showed the highest selectivity at t_0 with 4% at 98% conversion (Figure 4.57), while we recorded 9% for lanthanum at 74% conversion at t_∞ and 6% for tungsten at 88% conversion at t_∞ (Figure 4.58). This directly proves that Lewis acidity and mesoporosity dominant in Siral-1s cannot be useful to produce propylene. Also, even if we modify the surface acidity and pore dimensions with metal-doping, this is not much efficient. Note that the tests shown from Figure 4.55 to Figure 4.58 were realized at 350 °C and 50mg catalyst mass.

For these three selected metals *i.e.* silver, aluminum and tungsten, we choose to make further tests at different reaction conditions, and investigate the selectivity in ethylene as well. From the previous results, we show that the mesoporous materials, even modified, don't provide expected improvement to propylene selectivity. For this reason, we will focus to the zeolites type support (*i.e.* CBV).

- Catalytic Tests Results:

With respect to the promising results, further tests were performed over CBV on the selected set of catalysts to investigate in details their performance at different conditions (temperature, catalyst mass, etc.).

- Influence of metals:

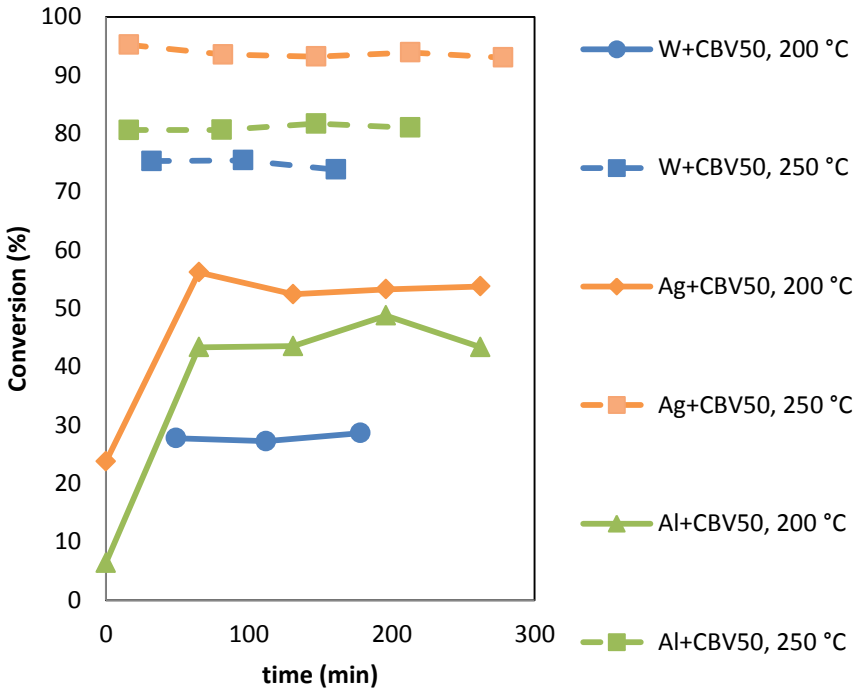

Figure 4.59. Conversion (%) versus time (min) for metal-modified CBV50 (s) over "Multi-Valve Reactor System". Reaction conditions: 21 mL/min He/Kr flow, 0.0125 mL/min as liquid ethanol flow (20% EtOH in gaseous phase). 50mg of the catalyst was used at reaction temperature of 200 and 250 °C. All conditions are per reactor.

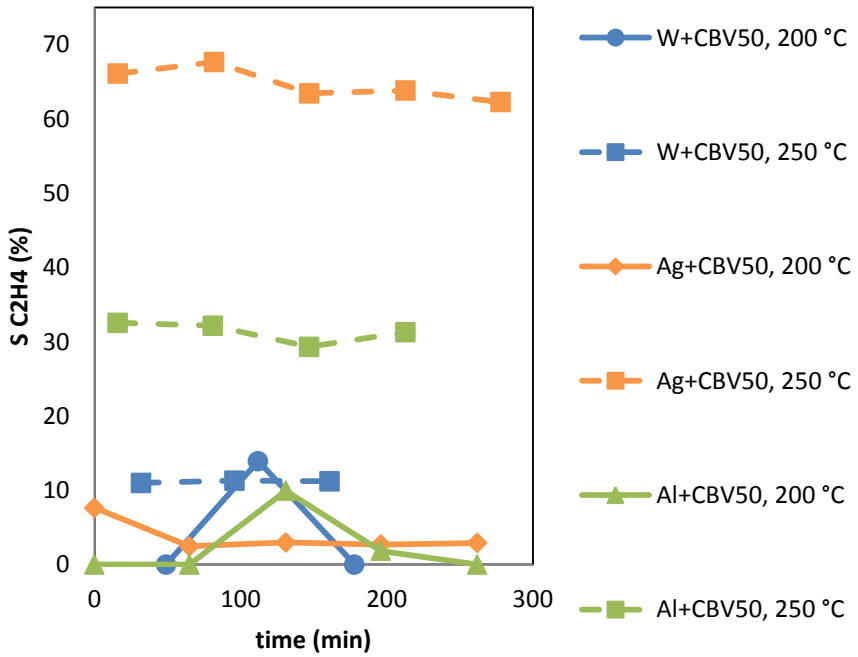

Figure 4.60. Ethylene selectivity (%) versus time (min) for metal-modified CBV50 (s) over "Multi-Valve Reactor System". Reaction conditions: 21 mL/min He/Kr flow, 0.0125 mL/min as liquid ethanol flow (20% EtOH in gaseous phase). 50mg of the catalyst was used at reaction temperature of 200 and 250 °C. All conditions are per reactor.

The temperature effect is, as expected: the ethanol conversion increases with the temperature. It varied at the equilibrium between 30 and 50% at 200°C and between 75 and 95% at 250° function of the tested material (Figure 4.59). The Ag-CBV50 shows the best ethanol conversion and the W-CBV50 the worst between the three materials. The ranking is the same for both temperatures. At these low temperatures, the quantities of propylene are close to zero. With regards to ethylene selectivity (Figure 4.60), 250 °C reaction temperature showed higher and more stable ethylene selectivities than at 200 °C. The highest selectivity was recorded for Ag-CBV50 (250 °C) slowly decreasing from 66 to 62%. This was followed by Al-CBV50 at 250 °C with a stable selectivity at about 30%, after is W-CBV50 at 250 °C at 12%.

W-CBV50 and Al-CBV50 both at 200 °C, show zero selectivities in ethylene with two peaks at 14% at 112 min and 10% at 131 min, respectively (Figure 4.60). If these sudden increases in selectivities were observed at the beginning of the reaction, we can either say that ethanol dehydration occurred very fast. But as long as this change happened in the middle of the reaction, we can predict that the mobility of resulting reaction products had changed during the reaction. As if some ethanol was trapped inside the catalyst pores, or ethylene is generated by products other than ethanol. Other products formed in this case are C5 alkanes and alkenes, which are formed up to 100% selectivity. This is interesting for future work if we want to invest these catalysts for the production of light hydrocarbons at the mentioned conditions.

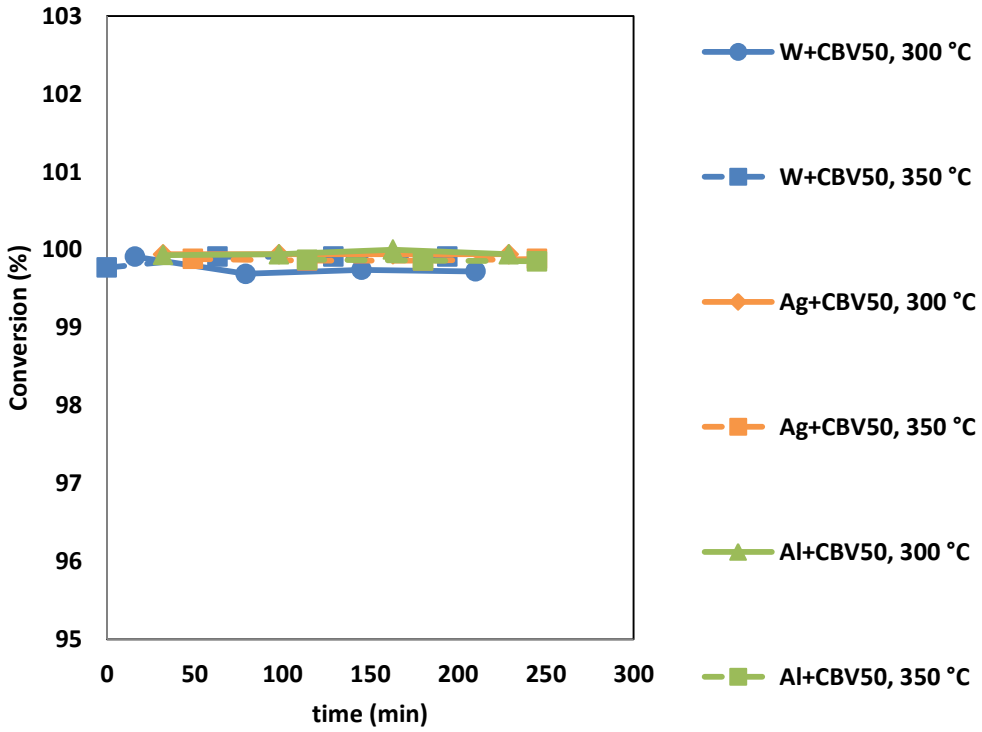

Figure 4.61. Conversion (%) versus time (min) for metal-modified CBV50 (s) over "Multi-Valve Reactor System". Reaction conditions: 21 mL/min He/Kr flow, 0.0125 mL/min as liquid ethanol flow (20% EtOH in gaseous phase). 50mg of the catalyst was used at reaction temperature of 300 and 350 °C. All conditions are per reactor.

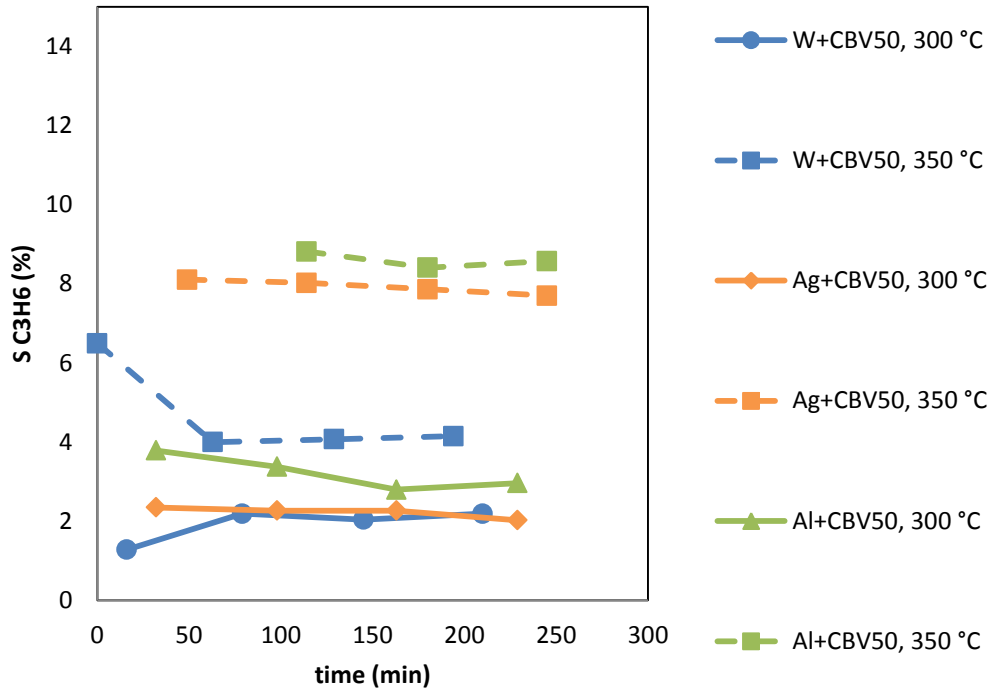

Figure 4.62. Propylene selectivity (%) versus time (min) for metal-modified CBV50 (s) over "Multi-Valve Reactor System". Reaction conditions: 21 mL/min He/Kr flow, 0.0125 mL/min as liquid ethanol flow (20% EtOH in gaseous phase). 50mg of the catalyst was used at reaction temperature of 300 and 350 °C. All conditions are per reactor.

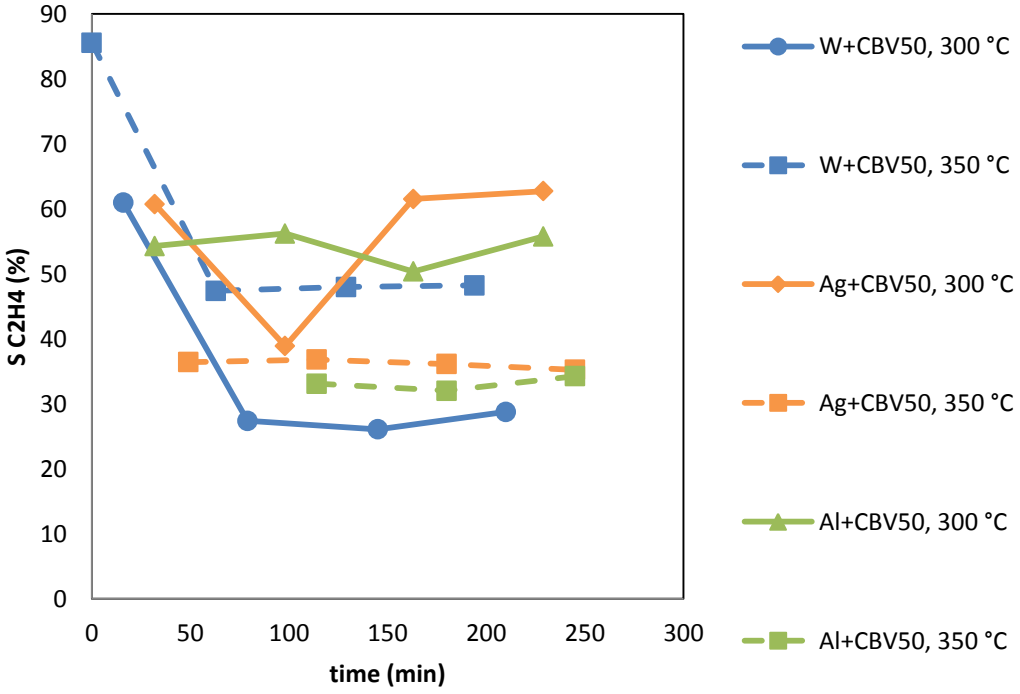

Figure 4.63. Ethylene selectivity (%) versus time (min) for metal-modified CBV50 (s) over "Multi-Valve Reactor System". Reaction conditions: 21 mL/min He/Kr flow, 0.0125 mL/min as liquid ethanol flow (20% EtOH in gaseous phase). 50mg of the catalyst was used at reaction temperature of 300 and 350 °C. All conditions are per reactor.

Increasing temperature up to 350°C, the ethanol conversions reach 100% (Figure 4.61). The propylene selectivity appears as soon as the temperature reach 300°C for each catalysts, increasing the temperature leads to an increase of the propylene selectivity. The The best one (i.e. 9%) was obtained for the Al-CBV. It has to be noted, whatever the value obtained for the different catalysts, it stays stable with the time on stream (Figure 4.62). As shown in Figure 4.63, W-CBV50 and Ag-CBV50 both at 300 °C, started to have similar ethylene selectivities at t_0 (around 60%). For the primer it dropped severely then it got stable at 26%. For the latter, it dropped then retrieved back the original value. For Al-CBV50 at 300 °C, ethylene selectivity fluctuated at around 56%.

- Influence of GHSV:

Conversion of ethanol was performed using a fixed bed reactor (Figure 4.61). Before the experiment, 50mg of the sample was inserted between two layers of SiC in order to create an isothermal zone. The lower layer of SiC is about 5.8 cm, while the upper layer of SiC fills the the reactor of up to around 10.5cm. The catalytic tests were carried out in a stainless steel reactor of 3mm internal diameter. The gas composition was kept at 20 vol% ethanol and 80 vol% helium/krypton as a carrier gas. Since different catalysts had different volumes even for the same mass, this had an influence of the height of the catalytic bed inside the reactor and consequently different GHSVs were obtained for different catalysts. The total gas flow rate (GHSV) for every reactor was maintained throughout the reaction. Under these conditions, the 50mg W+CBV50 and the 50mg Ag+CBV50 both showed nearly the same GHSV (5.96 and 6.28 h^{-1}, respectively). The 50mg Al+CBV50 also showed a very low GHSV of 9 h^{-1}. So, the GHSV did not have any effect here.

We conclude that 350 °C temperature is more effective for the formation of propylene than the 300 °C for the 50mg mass. Also, Ag+CBV50 was more effective than the W+CBV50 in terms of propylene selectivity because propylene was accompanied with more aromatic products, which will be validated later on in this chapter.

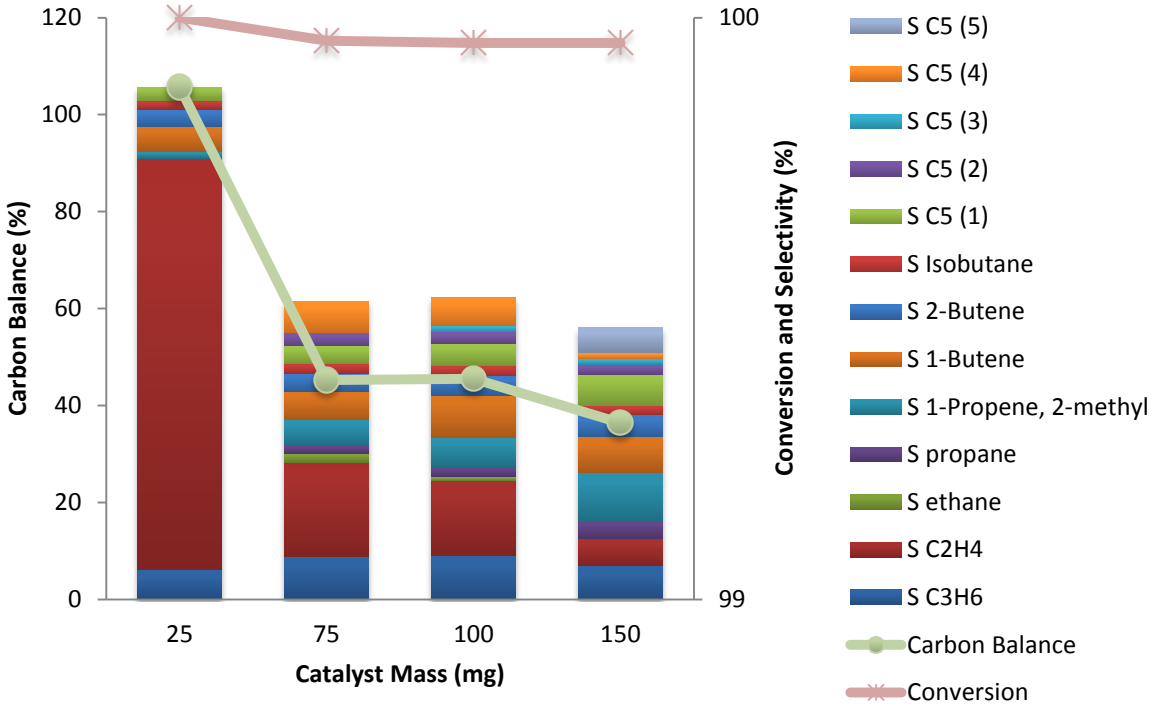

Figure 4.64. Conversion, carbon balance and selectivities of different products (%) for Ag-modified CBV50 catalyst over "Multi-Valve Reactor System". Reaction conditions: 21 mL/min He/Kr flow, 0.0125 mL/min as liquid ethanol flow (20% EtOH in gaseous phase). 25, 75, 100 and 150mg of the catalyst were used at reaction temperature of 350 °C. All conditions are per reactor.

In order to check the influence of GHSV, we have chosen the Ag-CBV50 catalyst (Figure 4.64). It exists two ways to vary the GHSV: modify the total gas flow or play on the mass of catalysts. It is this second way that we have chosen. The respective GHSVs for 25, 75, 100 and 150mg masses of Ag+CBV50 are: 13, 4, 3 and 2 h^{-1}. It was as mentioned before for the 50mg of Ag+CBV50, almost 6 h^{-1}. Thus, as mass increases, GHSV increases too, with a sharp decrease (nearly to the half) between the 25 and 50mg masses.

As one can see, whatever the mass of catalyst, the ethanol conversions always reach 100% at 350°C. The biggest difference is the carbon balance. With 25 mg, the carbon balance is equal to 100% (all products have been identified and quantified). The main product is ethylene, with more than 70% of selectivity, other products are propene, butenes and C5+ products. Increasing the catalyst mass, we also decrease the carbon balance and numerous new products appear. The increase of catalyst mass and the increase the contact time between gas and catalysts, lead to reactions implying the first form product (*i.e.* ethylene) to produce higher molecular weight compounds as C5 alkanes and alkenes (see the figure). Increasing the contact time, the carbon balances decrease drastically due to the presence of non-quantified compounds as BTX (s) and other sorts of heavy aromatics. These are formed by chain growth and cyclization. The formation of aromatics was realized for the first glimpse, as the color of the catalyst turned balck after the end of the reaction.

The influence of temperature on the different products formed has been also checked (Figure 4.65). As usual for this reaction, we can first see that the ethanol conversion increase with the temperature to reach 100% as soon as the temperature reaches 250-300°C.

Surprisingly, the main product at low temperature is a C5 one. These C5 (s) are alkanes and alkenes. From GC-MS results, products as Butane, 2-methyl and 1-Butene, 2-methyl… were identified to be formed. At higher temperature, the main product is always ethylene even if its selectivity decreases with the increase of temperature while the ones of propylene and butenes increase. In the same time, carbon balance decreases down to 66% due to the presence of non-quantified products as aromatics and/or carbon deposited on the catalysts. Note that trans-2-pentene was calibrated here as a representative of the C5 set of products, but it is difficult to say that this product is exactly formed in the reaction, for this we see high selectivity value for C5 at about 98% (Figure 4.65).

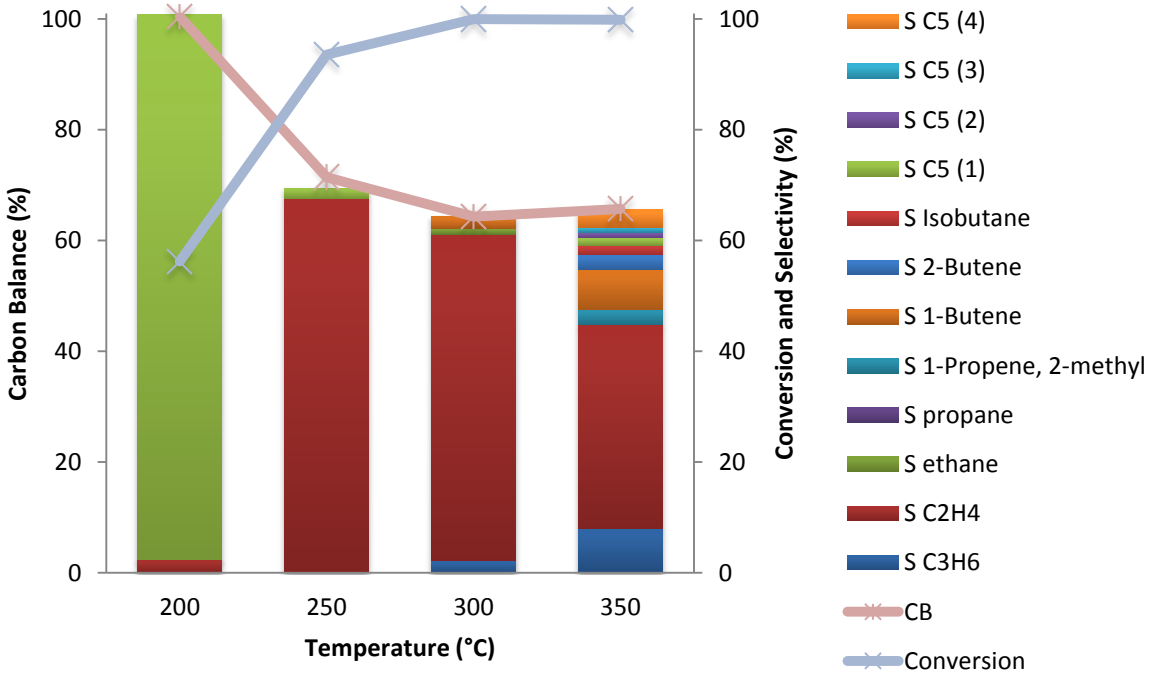

Figure 4.65. Conversion, carbon balance and selectivities of different products (%) for Ag-modified CBV50 catalyst over "Multi-Valve Reactor System". Reaction conditions: 21 mL/min He/Kr flow, 0.0125 mL/min as liquid ethanol flow (20% EtOH in gaseous phase). 50mg of the st were used at reaction temperatures of 200, 250, 300 and 350 °C. All conditions are per reactor.

In order to check this point, we have performed a TGA analysis coupled with a mass spectrometer on the spent sample. The results are depicted in Figure 4.66.

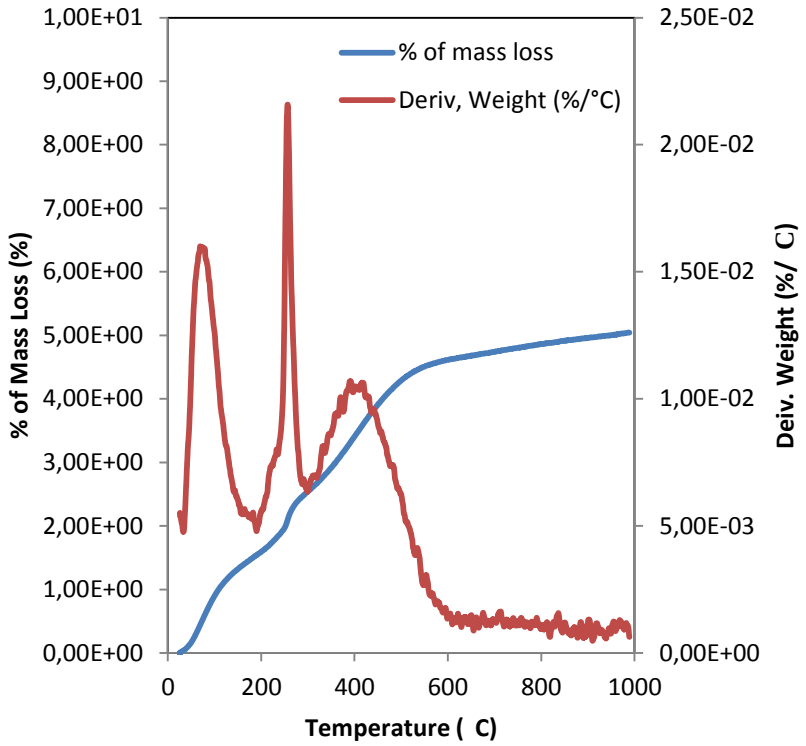

Figure 4.66. DSC-TGA of 16.5529 mg of Ag+CBV50 (after reaction at 350 °C) upon heating up to 1000 °C (10 °C/min) under 20% O_2/He and using Ramp method

Accordingly, the first weight loss at 100°C relates to the elimination of physisorbed water, while the other two weight losses belong to the oxidative elimination of carbonaceous species. The percentage of coke was 3.1% which is rather low.

- Characterizations

In order to understand the differences obtained in the catalytic tests, many characterizations have been done.

- N_2 porosimetry results:

N_2 physisorption was performed in order to determine if changes occurs in the texturale properties of our materials after impregnation.

Table 4.14. Textural Parameters of the selected metal-modified CBV50 (s)

Solid catalyst	S_{BET} (m^2/g)	pore volume (cm^3/g)	pore diameter (nm)
CBV50 (Cal 2 hrs)	418	0.12	Mono-model 5
Ag + CBV50	272	0.10	Mono-model 6
Al + CBV50	289	0.14	Mono-model 8
W + CBV50	298	0.10	Mono-model 6

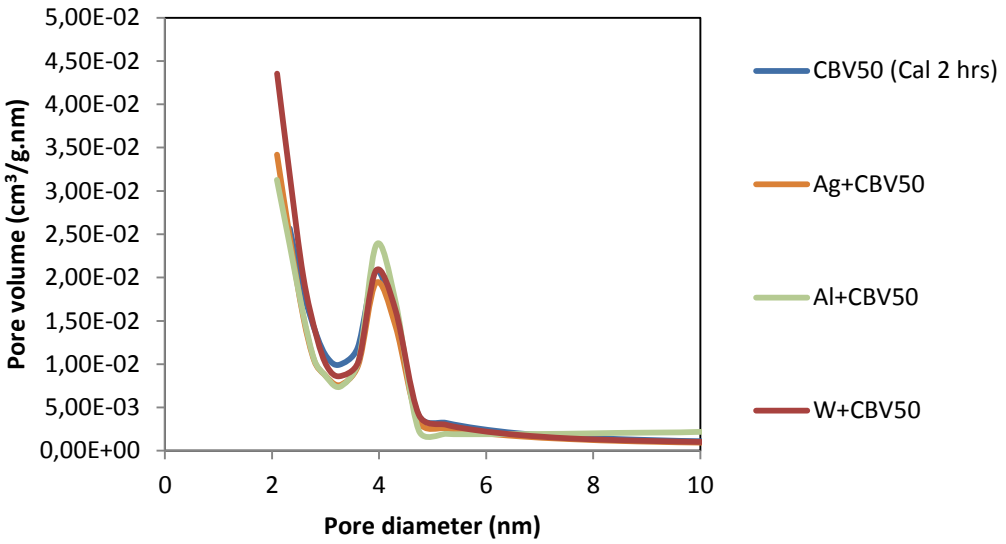

Figure 4.67. Pore distribution by BJH method for the raw CBV50 and the selected metal-modified CBV50 (s)

The metal-modified CBV50 samples all show similar BET surface areas (Table 4.14). All CBV50 based samples have mono-model pore diameter (Figure 4.67), with a BET surface area in the range of 250-300 m^2/g and a pore volume of 0.1 cm^3/g. One can see from Table 4.14 that the modification of the CBV resulted in a decreasing BET surface area of the raw catalyst (up to 25% less than the initial precursor). Regarding this effect over pore volume, it was conserved for CBV50. The pore diameter was conserved for both supports.

- Acidity Measurement:

Pyridine probe molecule was adsorbed on the surface of selected metal-impregnated catalysts, followed by desorption at different temperatures 150-450 °C. This technique is used to identify the Brønsted-to-Lewis acidity ratio, as well as to determine the total, weak and strong acidities.

Table 4.15. Relative percentages of number of moles of Brønsted and Lewis acid sites of metal-impregnated CBV50 (s) as determined by pyridine FTIR spectroscopy. Ɛ B= 0.73, Ɛ L= 0.64 (M. Tamura, 2012).

Catalyst	Temperature	n B (%)	n L (%)	Acidity (a.u.)
CBV50 (Cal 2h)	150 °C (Total acidity) 450 °C (Strong acidity) 150-450 °C (weak acidity)	84 75 91	16 25 9	1039 479 560
W+CBV50	150 °C (Total acidity) 450 °C (Strong acidity) 150-450 °C (weak acidity)	66 52 75	34 48 25	591 222 369
Ag+CBV50	150 °C (Total acidity) 450 °C (Strong acidity) 150-450 °C (weak acidity)	42 0 46	58 100 54	45 4 41

Pyridine has been used as a probe molecule for the quantitative analysis of surface acidity of some solid catalysts by FTIR spectroscopy. For pyridine, an evaluation of the relative acid strength at different temperatures (150-450 °C) was obtained for both Brønsted- and Lewis-acid sites. Correlation was later verified between the concentration of Brønsted sites and the catalytic activity of the catalysts examined for the conversion of ethanol.

In Table 4.15 we see total, strong and weak acidities for both Brønsted and Lewis sites. Catalysts tested were W- and Ag-modified CBV50, along with the raw support after calcination. This is because the calcined supports were impregnated and not the raw ones. W-modified catalyst was selected because this metal doped showed high propylene selectivity and ethanol conversion, along with reduced coke formation. In contrast, Ag-modified catalyst was also selected to perform an FTIR study because also this catalyst was effective for propylene formation, but aromatics formation as well (carbon balance 43%). Ag+CBV50 shows very weak general acidity. W+CBV50 conserved the same Lewis acidity as the raw one, while Brønsted acidity decreased nearly to the half in terms of number of moles.

- XPS:

XPS analyses served to determine the chemical composition of the surface of our materials, the oxidation degrees in which the elements are found, and the percentage of incorporation of the impregnated metal on the surface. We were interested specifically in the W-CBV50 catalyst because it was an active catalyst with low aromatics formation, in contrast to Ag-CBV50. This one was also active, but with high aromatics formation.

Table 4.16. XPS peak positions and atomic percentages for the elemental composition of raw and metal-impregnated CBV50 (s)

Catalyst	O 1s Peak Position; At%; Wt%	Si 2p Peak Position; At%; Wt%	Al 2p Peak Position; At%; Wt%	C 1s Peak Position; At%; Wt%	W 4f Peak Position; At%; Wt%	Ag 3f Peak Position; At%; Wt%
CBV50 (Cal 2 hrs)	532.80; 47.238; 44.25	103.40; 18.717; 30.78	74.80; 0.966; 1.69	285.00; 33.079; 23.26	-	-
W+CBV50	533.10; 51.096; 45.27	103.60; 21.082; 32.79	75.10; 0.921; 1.37	285.00; 26.622; 17.71	36.20; 0.279; 2.84	-
Ag+CBV50	532.80; 49.705; 42.65	103.50; 19.886; 29.95	74.30; 0.908; 1.31	285.00; 28.126; 18.11	-	369.10; 1.376; 7.96

Zeolyst corporation datasheet show that CBV50 is a classical aluminosilicate zeolite with a silica/alumina ratio of 50. While 10 wt% of the metal were impregnated on the bare

CBV50 support, only 3% wt% of tungsten was detected at the surface by XPS analysis (Table 4.16). Only one oxidation state of W exists; i.e., 4f orbitals being filled with electrons. Concerning the Ag-containing CBV50 catalyst, about 8% wt% of silver was impregnated on the surface CBV. It seems that the migration of W inside the support is favored compare to Ag.

- XRF:

Here we present the elemental and oxides composition of the 5 best-performing catalysts, along with their Siral-1 impregnated conjugates. The aim behind this study is to verify the exact weight percentage of the elements as the XPS study cannot be as precise as the X-ray fluorescence.

Table 4.17. Elemental composition study by X-ray fluourescence for the top five best performing impregnated CBV50 (s)

	Catalyst	Oxide (wt%)						
		Al_2O_3	SiO_2	WO_3	Ag_2O	Ce_2O_3	NiO	Fe
1	W+CBV50	1.11	52.82	46.05	-	-	-	-
2	Ag+CBV50	4.58	92.95	-	2.45	-	-	-
3	Al+CBV50	11.84	88.15	-	-	-	-	-

The respective oxides of Al, Si, W, Ag, Ce and Ni are Al_2O_3, SiO_2, WO_3, Ag_2O, Ce_2O_3 and NiO after the decomposition of the metal precursor on the support. Table 4.17 shows that tungsten was successfully impregnated over CBV50 (in a percentage higher than 10% as previously calculated). This relates to the high propylene selectively and ethanol conversion linked to this catalyst.

- NH_3 TPD:

Ammonia TPD tests were performed for the bare catalysts and also for the tungsten- and silver-modified CBV50, to study their acidities (amount and distribution).

Table 4.18. Number of moles of acid sites of metal-modified CBV50 (s) as determined by ammonia TPD measurements. Weak acid sites <280 °C, medium acid sites 280-480 °C and strong acid sites >480 °C.

Catalyst	Acidity (mmol/g)	Weak acidity (mmol/g)	Medium acidity (mmol/g)	Strong acidity (mmol/g)	S_{BET} (m^2/g)	Acidity (mmol/m^2)
CBV50 (Cal 2hrs)	0.17	0.033	0.083	0.053	418	4.07*10-4
W+CBV50	0.21	0.053	0.092	0.063	298	7.04*10-4
Ag+CBV50	0.11	0.030	0.058	0.020	272	4.04*10-4

In the prescreening chapter, we saw that for the calcined CBV50, acidity is moderate 0.17 mmol/g, and it is distributed over weak (0.03 mmol/g), medium (0.08 mmol/g) and strong (0.05 mmol/g). W and Ag-modified CBV50 show moderate total acidity of 0.17-0.21 mmol/g determined by NH_3 TPD (Table 4.18). Upon impregnation with tungsten the acidity slightly increases (0.21 mmol/g), while it decreased when impregnating Ag (0.11 mmol/g).

W- and Ag-modified CBV50s have mostly medium acidities. We refer back to pyridine FTIR results shown in Table 4.15. We have seen that calcined CBV50 shows a mixture of Brønsted and Lewis acidities with a majority of Brønsted ones. Adding W leads to a decrease in the amount of Brønsted acid sites even if they still are dominant. Ag-modified CBV50 showed an enormous drop in the amounts of both Brønsted and Lewis amounts. This attributed to the catalytic performance observed.

- Relevance between Catalysts Activity and their Chemical Properties:

For 50mg of W+CBV50 at 350 °C, the propylene selectivity was nearly stable at 11% and ethylene selectivity at 83% with full conversion (Figure 4.62, Figure 4.63 and Figure 4.61, respectively). From XPS results, we know that only 0.2 at% of tungsten is present on the catalyst surface (Table 4.16). Under the same conditions for raw CBV50, propylene selectivity got stable at 27%, and ethylene selectivity decreased from 92% to 51% with time-on-stream (See prescreening chapter). Conversion in the latter case was also full. Both acidities of CBV50 before and after calcination are nearly similar (0.16 vs. 0.17 mmol/g). So, modifying the CBV50 support with tungsten increased the acidity (to 0.21 mmol/g) [Table 4.18], thus it increased ethylene selectivity and decreased the propylene selectivity to the half.

On the other hand, Ag-modification resulted in a decrease in propylene selectivity from 19 to 13% for the 50mg catalyst at 350 °C when comparing nearly the same reaction time as for the raw CBV50 (682 vs. 627 min) [Figure 4.62]. Remember that from XPS results, only 1 at% of silver is present on the surface of the catalyst (Table 4.16), and the ammonia acidity of Ag-modified CBV50 is 0.11 mmol/g (as compared to 0.17 for bare CBV50) [Table 4.18]. Ethylene selectivity increased from 55 to 72% (Figure 4.63), and conversion is full (Figure 4.61). So, decreasing the acidity of raw CBV50 by silver-modification did not affect the propylene selectivity but decreased ethylene selectivity.

Therefore modifying CBV50 with W and Ag leads us to say that CBV50 has a moderate acidity (0.17 mmol/g) which should not be neither decreased (by silver modification to 0.11 mmol/g) nor increased (by tungsten modification to 0.21 mmol/g), in order to yield the highest propylene selectivity possible. Of course other factors than acidity interfere here (as channel structure, degree of impregnation, metal distribution…).

After all, we deduce that Lewis acidity-which is characteristic for raw and impregnated Siral-1 (s)-is ineffective to produce propylene. Only Brønsted acidity is capable to produce propylene, as for CBV50 catalysts. So, the simple impregnation by metals which show to be effective in other systems don't work with CBV zeolites. In order to try to

improve our goal, we decided to modify the raw material by applying different treatments described here after.

4.1.2. Hydrothermally treated catalysts

The following studies characterization and catalytic activity of the nano-size hierarchical H-ZSM-5 zeolite with high mesoporosity produced *via* a solvent evaporation procedure. This procedure not only induces mesoporosity within the framework of the zeolite, but also generates nano-size zeolite crystals. Further, this study compares hierarchical zeolites with conventional HZSM-5 zeolite with similar Si/Al ratios for the ethanol-to-hydrocarbon conversion process. Correlation was observed between catalyst life time, porosity and crystal size of the zeolite.

- Nitrogen physisorption:

Table 4.19. Textural parameters of the hydrothermally treated CBV50 (s)

Catalyst	BET Surface Area (m^2/g)	t-Plot Micropore Area (m^2/g)	Pore Volume (cm^3/g)	t-Plot Micopore Volume (cm^3/g)	Pore Size (Å)	Nanoparticle Size (Å)
CBV50 (raw)	328	255	0.06	0.13	75.85	183
CBV50 (autoclave + 110 °C)	318	245	0.06	0.13	87.71	188
CBV50 (autoclave + 110 °C + Cal)	360	227	0.06	0.12	79.61	166

From nitrogen physisorption, we see that the hydrothermal treatment did not affect the BET surface area of raw CBV50 (328-318 m^2/g) [Table 4.19]. Calcining the hydrothermally-treated catalysts did not change much the BET surface area (360 m^2/g for the calcined CBV50). In all cases, the pore volume remained constant (0.06 cm^3/g) for the CBV50 series and the pore distribution stays mono model.

- XRD:

XRD tests were performed to study the variation of the crystal system of each catalyst type in each step of the preparation procedure and compared with the reference ICDD cards which belong to commercial CBV50.

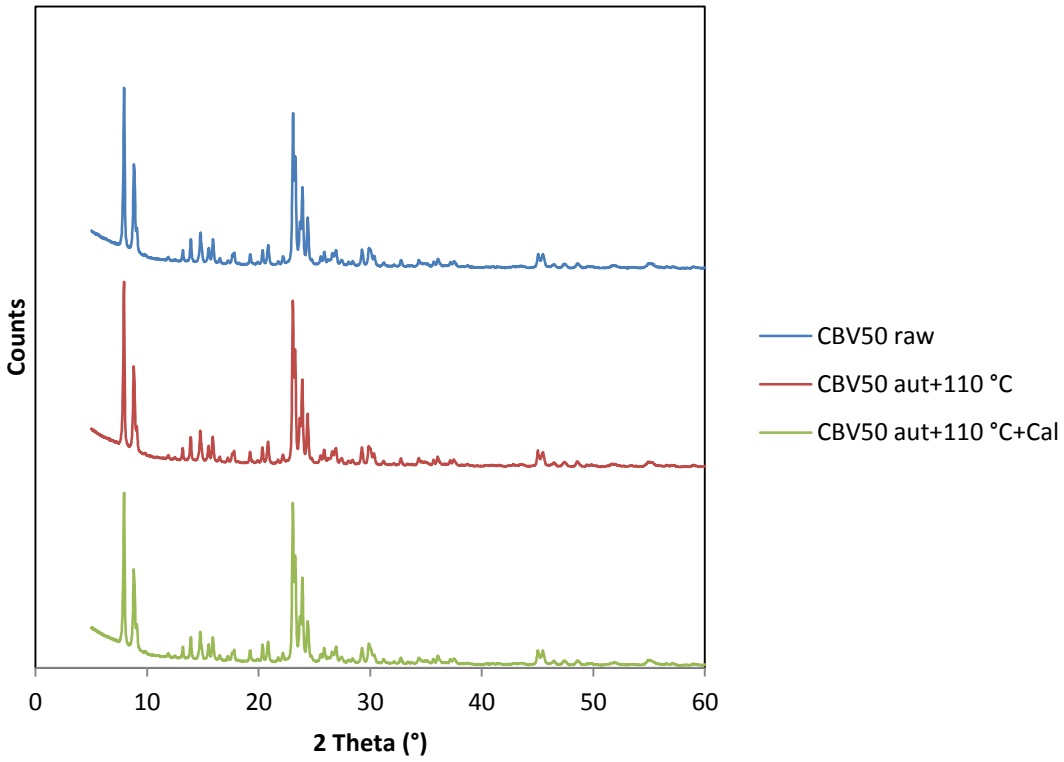

Figure 4.68. XRD patterns of raw CBV50, hydrothermally treated CBV50 and hydrothermally treated CBV50 followed by calcination

XRD of Figure 4.68 suggests that the pattern most matching to CBV50 is for the compound silica. Also, we can see that CBV50 preserved the orthorhombic crystallinity after hydrothermal treatment, even after hydrothermal treatment followed by calcinations. If we refer back to XRD results of "Prescreening Chapter", we see that even after calcining the CBV50 at 500 °C for 2 hrs the orthorhombic structure is also conserved. This implies that this structure is stable for CBV50 ZSM-5 zeolite.

By observing patterns of CBV50, we see that it is the same between the raw, hydrothermally-treated and calcined hydrothermally-treated CBV50. By applying Scherrer equation, we see that the crystallites sizes of the CBV50 set decreased to the half after its hydrothermal-treatment (1.13-0.76 nm), then the original crystallites size was retrieved back after calcinations (1.14 nm).

- TGA:

TGA can provide information about physical phenomena, in which changes in physical and chemical properties of materials are measured as a function of increasing temperature. In the following we will track the loss in water for the hydrothermally-treated samples.

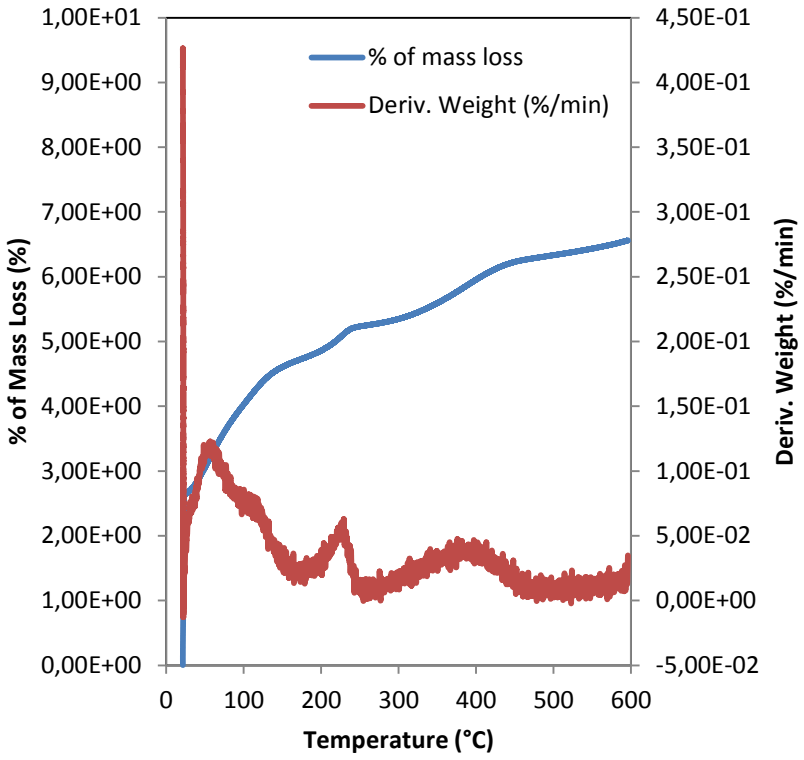

Figure 4.69. DSC-TGA spectrum of 10.8390 mg of CBV50 (autoclave+110 °C) upon heating up to 600 °C (5 °C/min) under air and using DSC Heatflow method

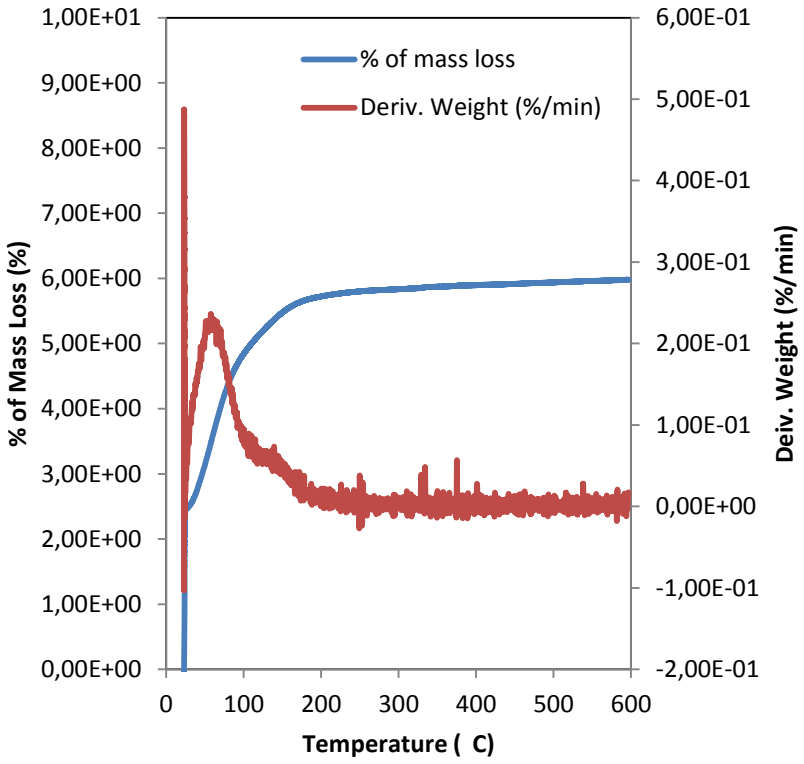

Figure 4.70. DSC-TGA spectrum of 8.2370mg of CBV50 (autoclave+110 °C+Cal) upon heating up to 600 °C (5 °C/min) under air and using DSC Heatflow method

The objective of the TGA study done on the two catalysts (*i.e.* hydrothermally treated CBV50, hydrothermally treated CBV50 followed by calcination), was to study the content in water of each catalyst and the temperature of water loss. For hydrothermally treated CBV50 [CBV50 (autoclave plus 110 °C drying)], the first weight loss relates to the elimination and vaporization of water of crystallization (Figure 4.69). Since the maximum heating temperature reached here is 600 °C, so all weight losses relate to water.

The percentage in water loss of the hydrothermally treated CBV50 is 6.3%, which is nearly similar to that of hydrothermally treated CBV50 followed by calcination (Figure 4.70). The only explanation is that water comes from the moisture in the air.

- Catalytic Tests Results:

The most important thing in the prepared catalysts is their activity in propylene production. Mesoporosity did not change, so we will see the effect of acidity change.

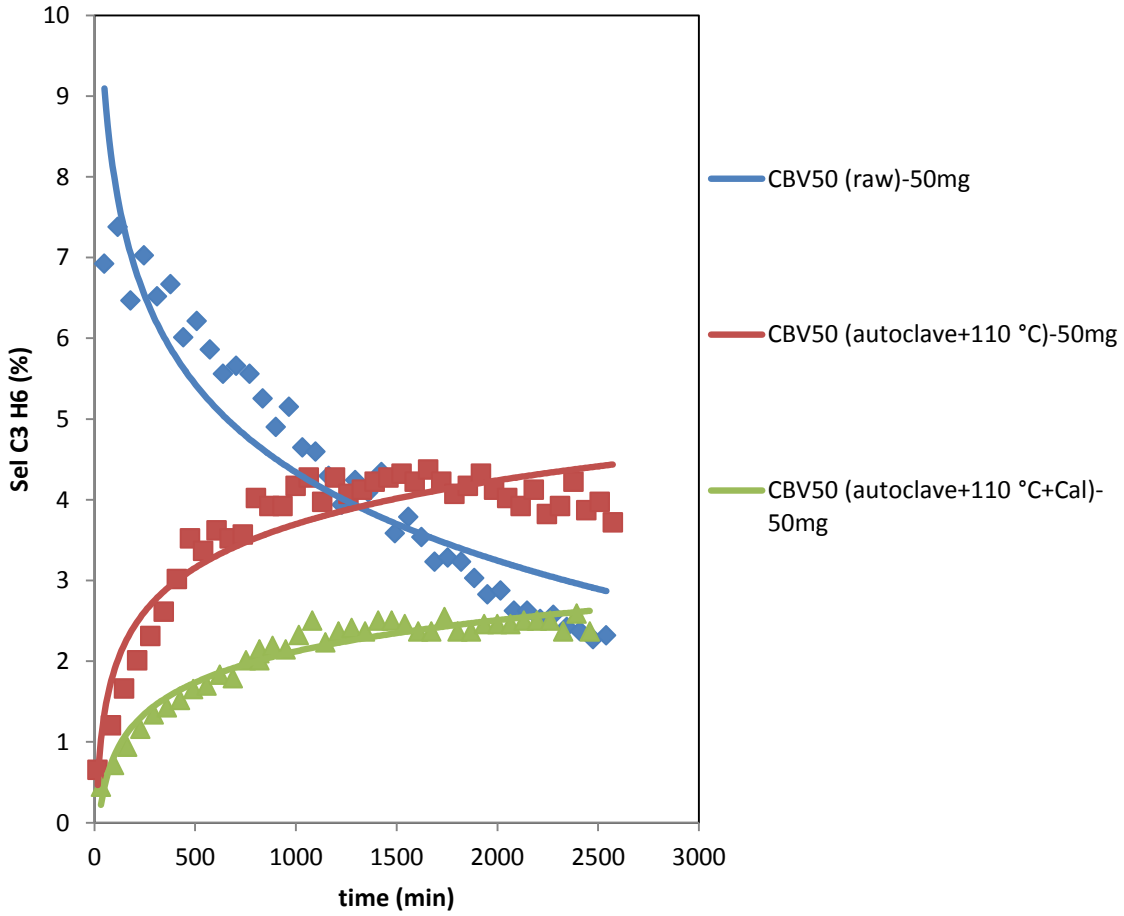

Figure 4.71. Propylene selectivity (%) versus time (min) for hydrothermally treated CBV50 (s). Reaction conditions : 0.0501 mL/min liquid ethanol flow (50% EtOH in gaseous phase), 21 mL/min inert gas flow ($He+N_2$) per reactor, 350 °C reaction temperature, and 50 mg catalyst mass. All conditions are per reactor.

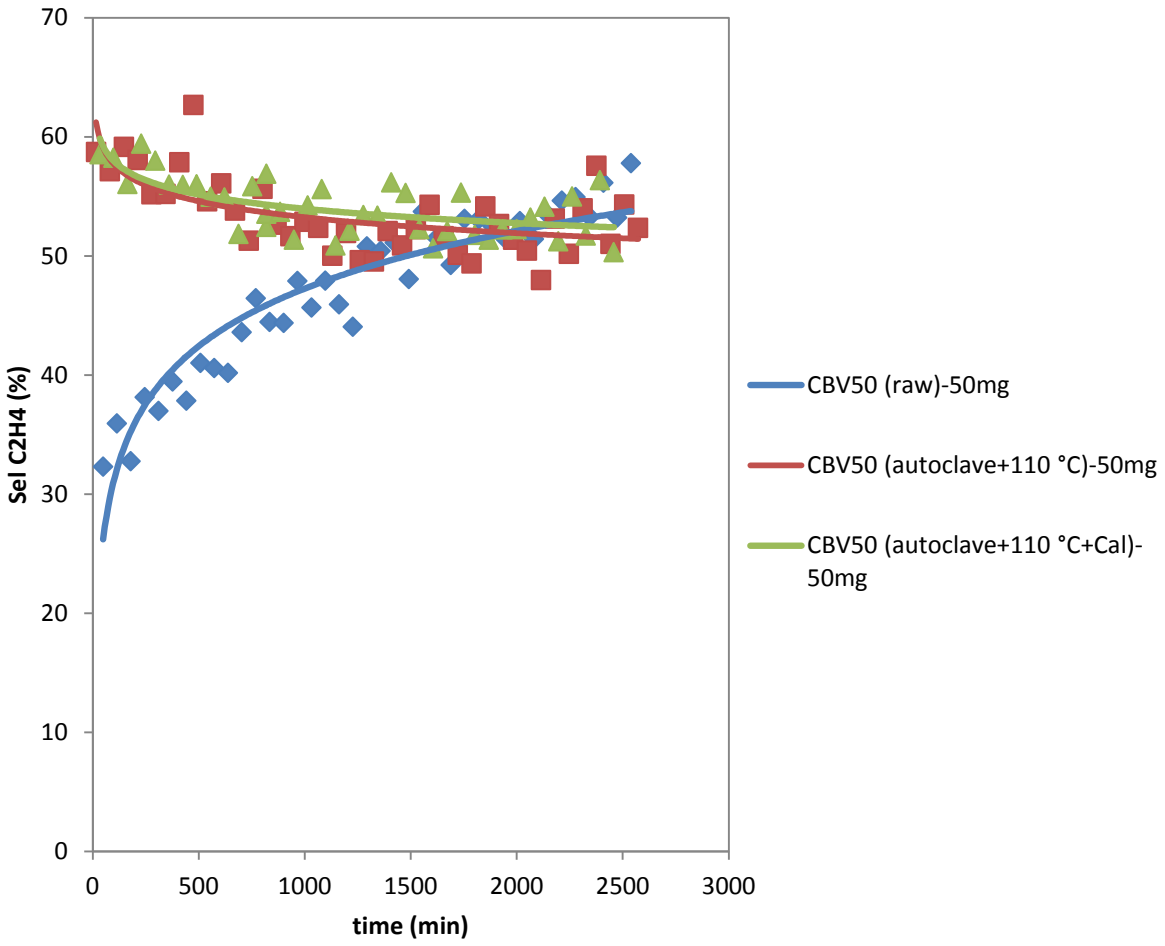

Figure 4.72. Ethylene selectivity (%) versus time (min) for hydrothermally treated CBV50 (s). Reaction conditions : 0.0501 mL/min liquid ethanol flow (50% EtOH in gaseous phase), 21 mL/min inert gas flow ($He+N_2$) per reactor, 350 °C reaction temperature, and 50 mg catalysts mass. All conditions are per reactor.

We discuss the effect of hydrothermal treatment on CBV50 for the mass 50mg. We present here only the results of the 50mg mass. All samples show a full conversion so the different treatment don't affect this parameter.

We move to propylene selectivity of hydrothermally treated catalysts. Highest selectivity was for 50mg raw CBV50 at 7% (Figure 4.71). But it was not stable and it sharply decreased to 2% after 2475 min. The highest and most stable propylene selectivity with time-on-stream was for hydrothermally treated 50mg CBV50 at 4%. This is followed by the calcined hydrothermally-treated 50mg CBV50 at 2%.

Concerning ethylene selectivity, all raw and treated CBV50 (s) show selectivities higher than or equal to 40% (except for the 50mg raw CBV50 which increased from 27 to 55%) [Figure 4.72]. We conclude from all above that hydrothermal treatment had an effect on stabilizing propylene selectivity.

4.1.3. Dealuminated catalysts

Microporous ZSM-5 zeolite was post-treated by dealumination with oxalic acid in order to finely tune the zeolite catalysts with hierarchically porous structure and varying acidity.

- Nitrogen Physisorption:

Similar nitrogen physisorption tests were done for the prepared materials as for the raw and metal-modified ones.

Table 4.20. Textural parameters of the dealuminated catalysts

Catalyst	BET Surface Area (m^2/g)	t-Plot Micropore Area (m^2/g)	Pore Volume (cm^3/g)	t-Plot Micopore Volume (cm^3/g)	Pore Size (Å)	Nanoparticle Size (Å)
CBV50 (raw)	328	255	0.06	0.13	75.85	183
CBV50 (oxalic acid+Cal)	378	233	0.07	0.12	71.80	159

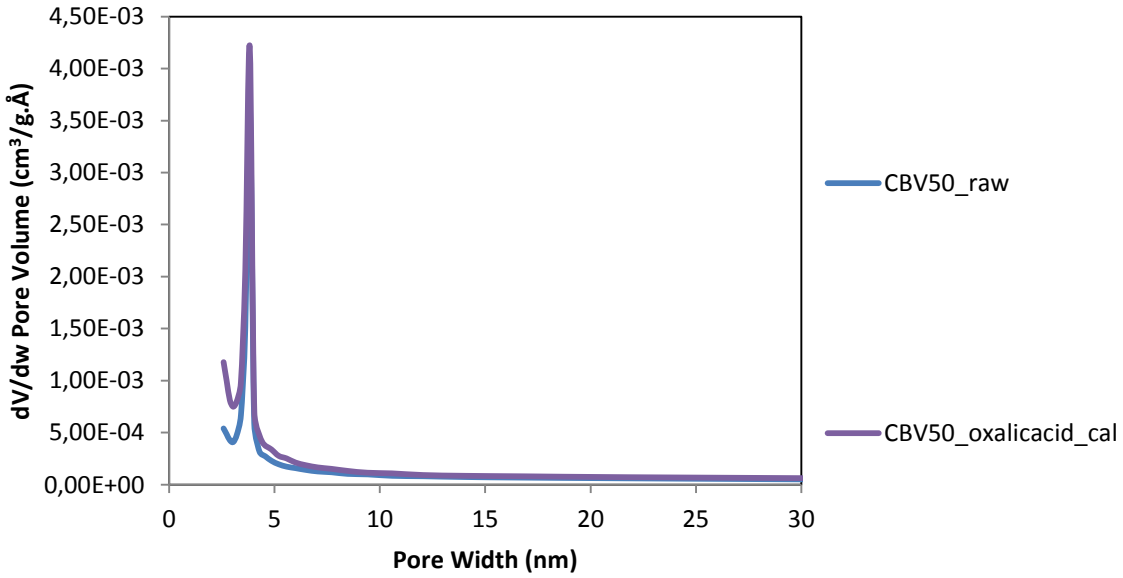

Figure 4.73. Pore distribution by BJH method (Harkins and Jura: Faas Correction) for dealuminated catalysts

Dealuminated catalysts show similar structural parameters as for the raw catalyst (Table 4.20). Nanoparticle size of the particles did not change much upon dealumination (183-159 Å for CBV50). Dealuminated CBV50 shows mono-model pore distribution characteristic for microporous CBV50s (Figure 4.73).

- XRD:

Whether the crystal system or crystallites size will change or not upon treatment with acid, will be seen in the following section.

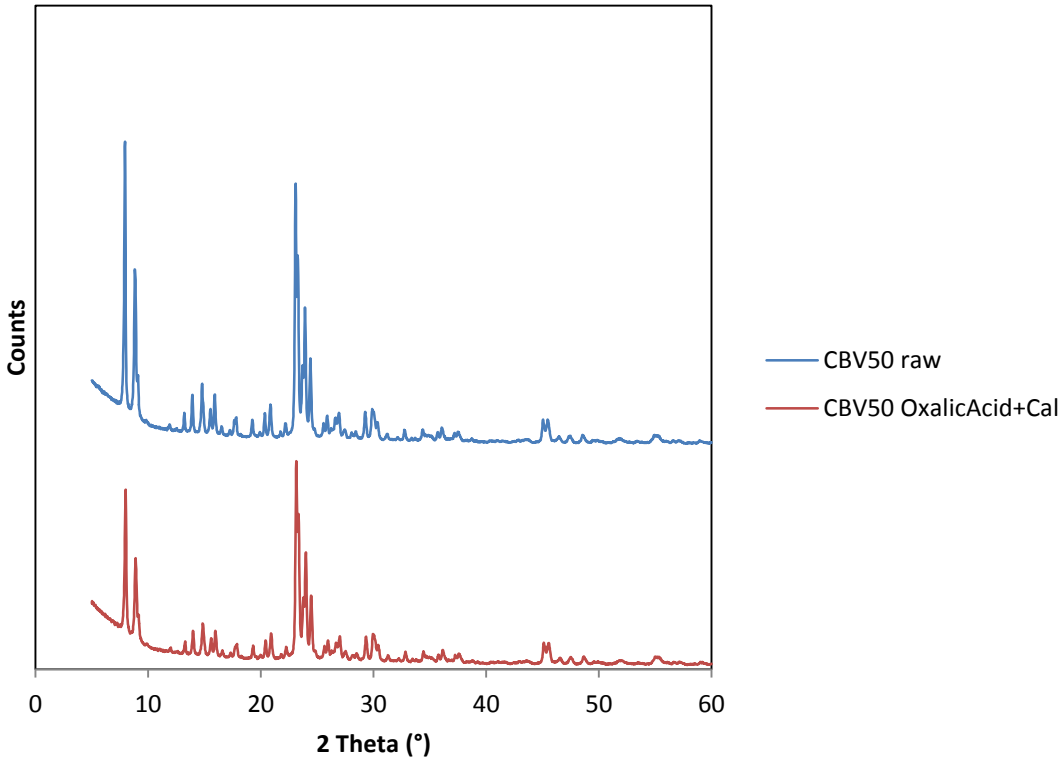

Figure 4.74. XRD pattern of dealuminated CBV50

Dealuminating the CBV50 preserved its crystal system (orthorhombic) [Figure 4.74]. Hence, there is not much to be relied on dealumination, in terms of propylene selectivity. The crystallites size of CBV50 was almost preserved upon the treatment (1.13-1.02 nm). ICDD cards match of the raw and the dealuminated CBV50.

- Catalytic Tests Results:

Relations were found between catalytic properties and activity. For us, our target is propylene molecule.

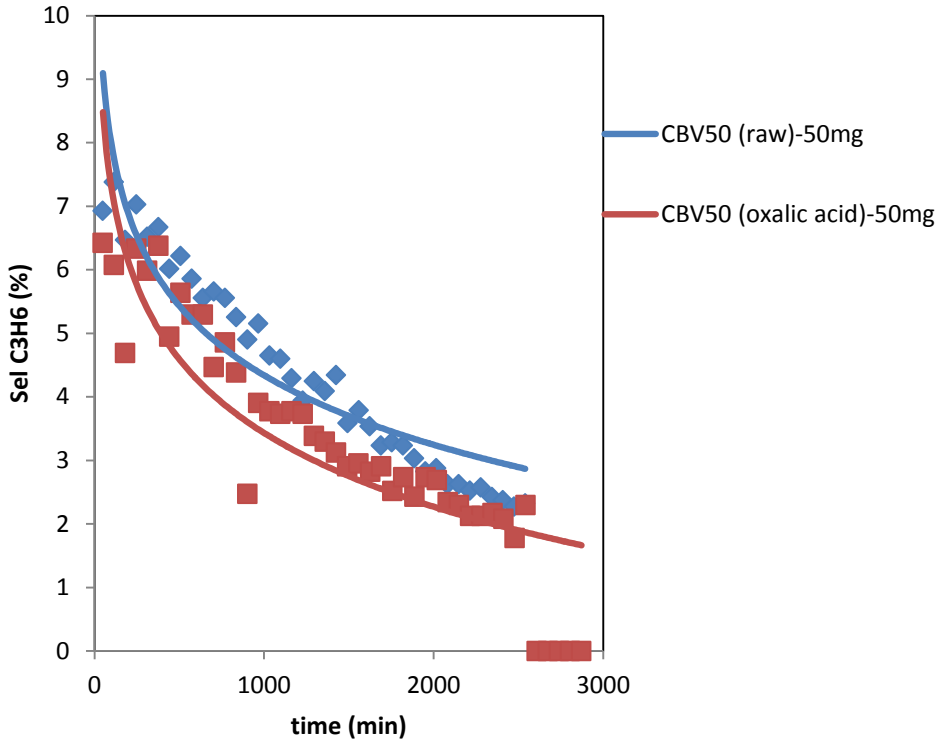

Figure 4.75. Propylene selectivity (%) versus time (min) for delaluminated catalysts. Reaction conditions : 0.0501 mL/min liquid ethanol (50% EtOH in gaseous phase), 21 mL/min inert gas flow ($He+N_2$) per reactor, 350 °C reaction temperature, and 50 mg catalyst mass. All conditions are per reactor.

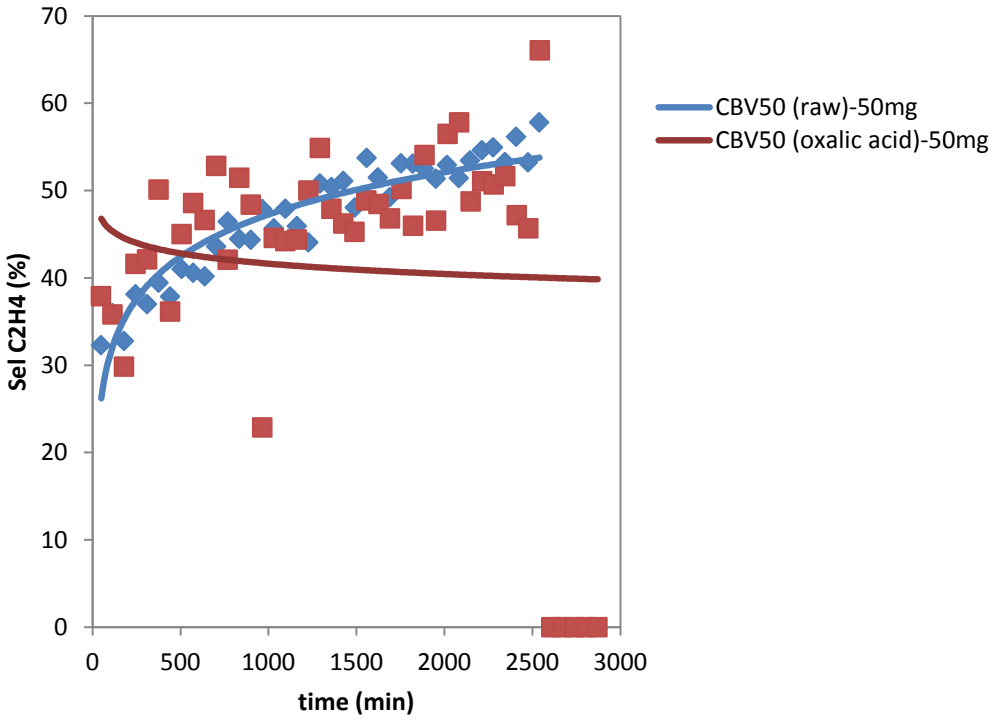

Figure 4.76. Ethylene selectivity (%) versus time (min) for delaluminated catalysts. Reaction conditions : 0.0501 mL/min liquid ethanol (50% EtOH in gaseous phase), 21 mL/min inert gas flow ($He+N_2$) per reactor, 350 °C reaction temperature, and 50 mg catalysts mass. All conditions are per reactor.

For ethanol conversion, dealumination didn't affect the conversion of 50mg raw CBV50 (100%). Propylene selectivity decreases linearly for 50mg raw CBV50 and dealuminated CBV50 (Figure 4.75). They decrease from 7 to 2%. Concerning ethylene selectivity, dealuminating the 50mg CBV50 decreased ethylene selectivity (gradual decrease up till 40%) while the raw CBV follow an inverse trend and is stable after a while at a selectivity superior to 50% (Figure 4.76).

We conclude that the dealuminated catalysts provide platform materials to compare the dehydration of ethanol into ethylene and diethyl ether, and consequently study the early stages of the ethanol-to-hydrocarbons reaction.

4.1.3. Desilicated catalysts

Microporous ZSM-5 zeolite was post-treated by desilication with sodium hydroxide in order to finely tune the zeolite catalysts with hierarchically porous structure and varying acidity.

- Nitrogen Physisorption:

Textural properties were determined for the catalysts treated with base.

Table 4.21. Textural parameters of the desilicated catalysts

Catalyst	BET Surface Area (m^2/g)	t-Plot Micropore Area (m^2/g)	Pore Volume (cm^3/g)	t-Plot Micopore Volume (cm^3/g)	Pore Size (Å)	Nanoparticle Size (Å)
CBV50 (raw)	328	255	0.06	0.13	75.85	183
CBV50 (NaOH+Cal)	400	234	0.15	0.12	64.71	150

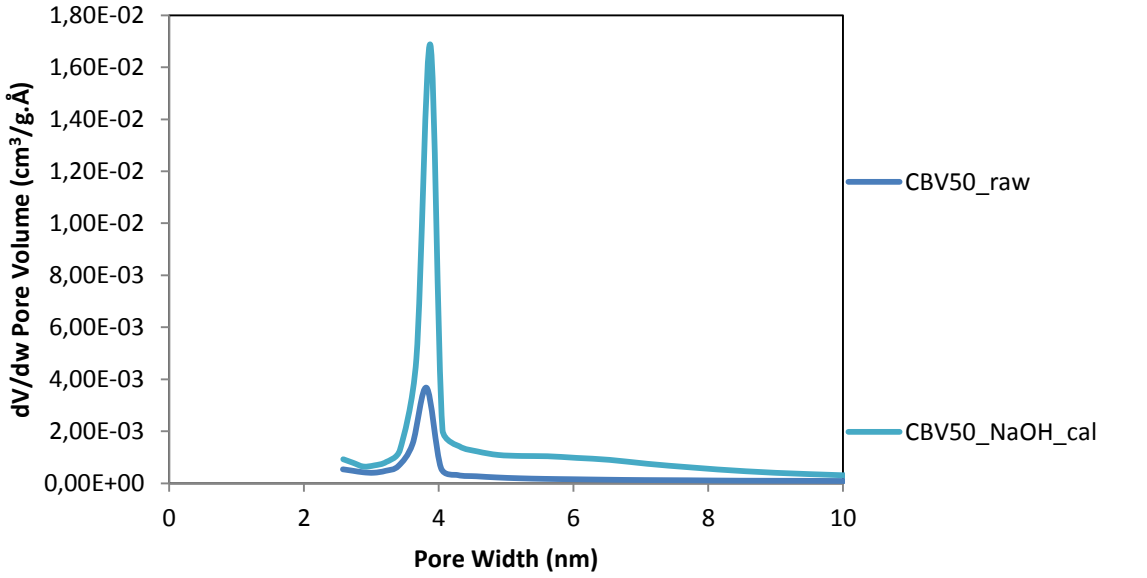

Figure 4.77. Pore distribution by BJH method (Harkins and Jura: Faas Correction) for desilicated zeolites

Desilicated catalysts show similar structural parameters as the raw catalysts, as well as similar pore distributions. This exempts the pore volume of desilicated CBV50, where it increases by 2.5 times upon desilication (increase from 0.06 to 0.15 cm^3/g) [Table 4.21]. BET surface area of desilicated CBV50 increased to 400 m^2/g, which is a relatively big surface area. The micropore area of desilicated CBV50 is nearly the half as that of the BET surface area (234 m^2/g). Desilication did not affect much the nanoparticle size of the particles (150 Å for desilicated CBV50). Desilicated CBV50 shows monomodel pore distribution (Figure 4.77).

- XRD:

The crystal system is important in the route of propylene formation.

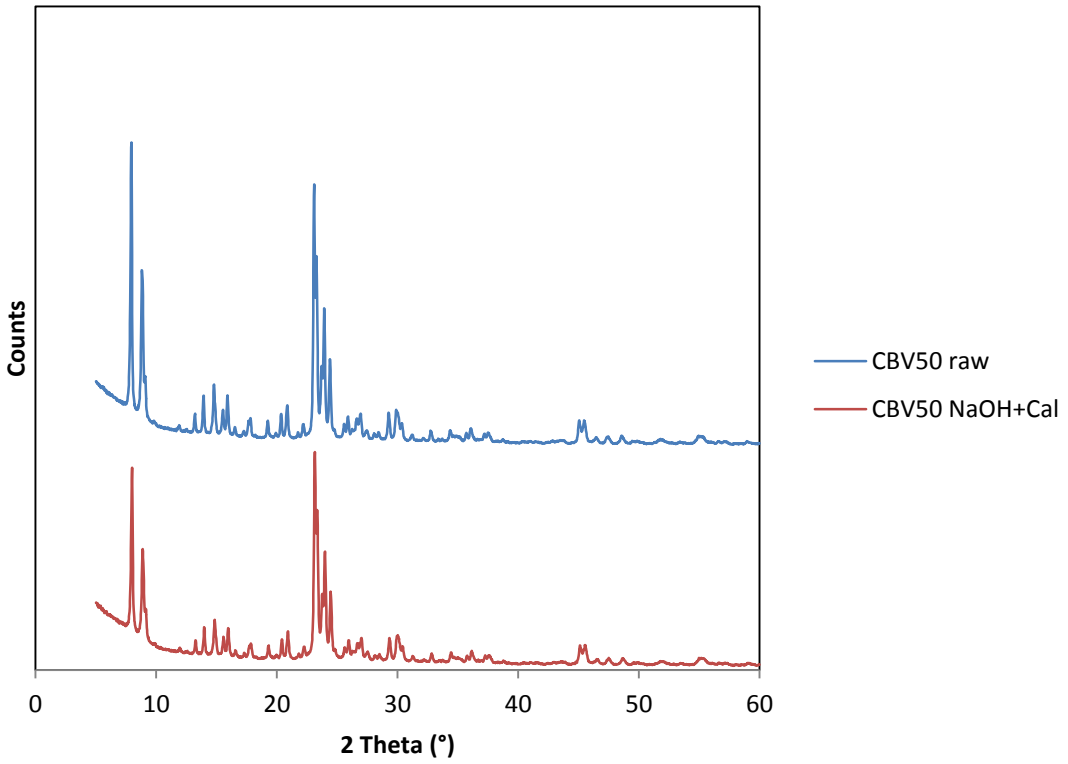

Figure 4.78. XRD pattern of desilicated CBV50

Upon all treatments of CBV50, the orthorhombic structure was preserved. Crystallites size of CBV50 decreases into half upon treatment (1.13-0.75 nm). The XRD pattern of the desilicated CBV50 highly matches with that of the raw one, with little differences in some reflection planes (Figure 4.78). The proposed structure of CBV50 is the same as that of silica.

- Catalytic Tests Results:

The aim behind all such treatments is to improve the catalyst activity.

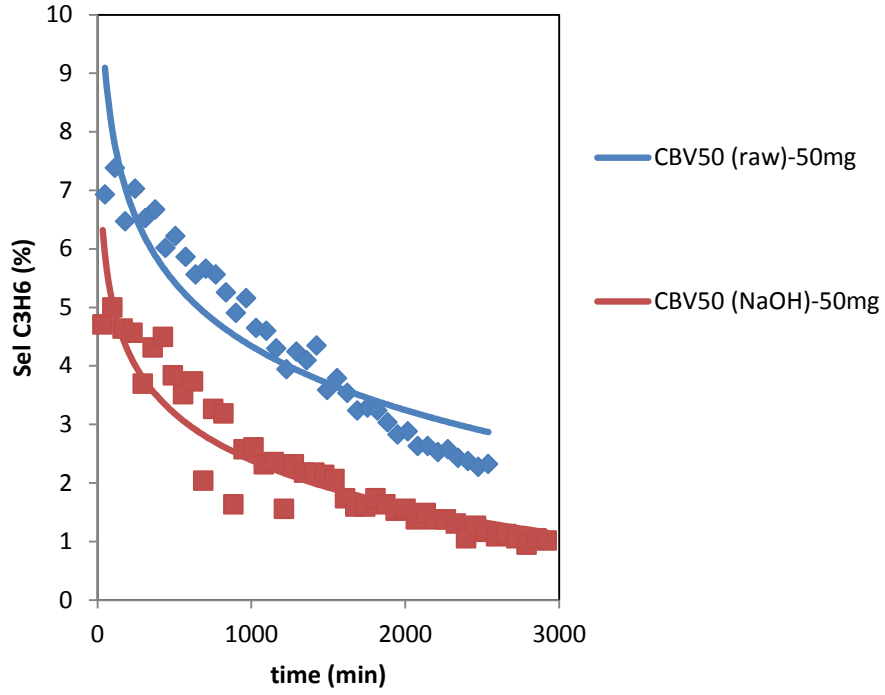

Figure 4.79. Propylene selectivity (%) versus time (min) for desilicated catalysts. Reaction conditions : 0.0501 mL/min liquid ethanol flow (50% EtOH in gaseous phase), 21 mL/min inert gas flow ($He+N_2$) per reactor, 350 °C reaction temperature, and 50 mg catalyst mass. All conditions are per reactor.

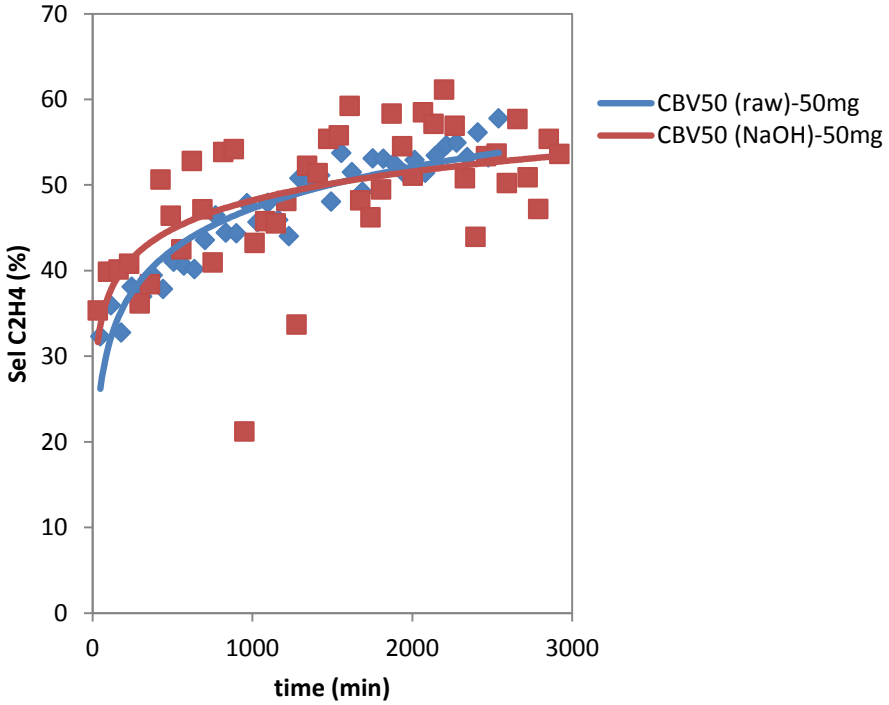

Figure 4.80. Ethylene selectivity (%) versus time (min) for desilicated catalysts. Reaction conditions : 0.0501 mL/min liquid ethanol flow (50% EtOH in gaseous phase), 21 mL/min inert gas flow ($He+N_2$) per reactor, 350 °C reaction temperature, and 50 mg catalyt mass. All conditions are per reactor.

Desilicating the 50mg CBV50 did not have an effect on conversion (remains at 100%). Moving to propylene selectivity, no peaks nor stabilizations were observed (Figure 4.79). Propylene selectivity decreases from 7 to 3% for the 50mg raw CBV50, while that of desilicated conjugate decreases from 5 to 1%. Thus, desilicating the 50mg CBV50 didn't have a positive effect on propylene selectivity. By viewing the effect of desilicating the 50mg CBV50 on ethylene selectivity, one realizes that it rendered the increase gradual (Figure 4.80).

If we consider that propylene is a target molecule, we find that the best performing catalyst is hydrothermally treated 50mg CBV50 (selectivity stable at 4%) among all hydrothermally treated, dealuminated and desilicated catalysts. Also in that it shows 100% ethanol conversion alongside. We conclude that the desilicated catalysts provide platform materials to compare the dehydration of ethanol into ethylene and diethyl ether, and consequently study the early stages of the ethanol-to-hydrocarbons reaction.

4.2. Conclusion

We conclude from all above that Brønsted acidity is the key player in propylene formation. Also, Both W- and Ag-CBV50 show to be effective in propylene formation, but the aromatic formation rate for the latter is higher. So it is important to get pure propylene without a full set of accompanying BTXs. On the other hand, it is useless to invest in Siral-1, as this was ineffective to form propylene even after impregnation. This one provides a good example of purely Lewis-acidity catalyst.

4.3. References

A. Takahashi, W. X. (2012). Effects of added phosphorus on conversion of ethanol to propylene over ZSM-5 catalysts. *Applied Catalysis A: General* , 162-167.

D. Goto, Y. H. (2010). Conversion of ethanol to propylene over HZSM-5 type zeolites containing alkaline earth metals. *Applied Catalysis A: General* , 89-95.

E. Selli, L. F. (1999). Comparison between the surface acidity of solid catalysts determined by TPD and FTIR analysis of pre-adsorbed pyridine. *Microporous and Mesoporous Materials* , 129-140.

F. Carniato, C. B. (2010). On the hydrothermal stability of MCM-41 mesoporous silica nanoparticles and the preparation of luminescent materials. *J. Mater. Chem.* , 5504-5509.

H. Oikawa, Y. S. (2006). Highly selective conversion of ethene to propene over SAPO-34 as a solid acid catalyst. *Applied Catalysis A: General* , 181-185.

K. Inoue, K. O. (2010). Metal modification effects on ethanol conversion to propylene by H-ZSM-5 with Si/Al2 ratio of 150. *Reac Kinet Mech Cat* , 477-489.

K. Inoue, M. I. (2010). Conversion of ethanol to propylene by H-ZSM-5 with Si/Al2 ratio of 280. *Cata Lett* , 14-19.

K. Murata, M. I. (2008). Effects of Surface Modification of H-ZSM-5 catalysts on direct transformation of ethanol into lower olefins . *Journal of the Japan Petroleum Institute* , 234-239.

M. Inaba, K. M. (2009). Effect of Fe-loading and reaction temperature on the production of olefins from ethanol by Fe/H-ZSM-5 zeolite catalysts. *React Kinet Catal Lett* , 19-26.

M. Inaba, K. M. (2011). Production of olefins from ethanol by Fe and/or P-modified H-ZSM-5 zeolite catalysts. *J Chem Technol Biotechnol* , 95-104.

M. Tamura, K. S. (2012). Comprehensive IR study on acid/base properties of metal oxides. *Appl. Catal, A* , 135-145.

M. Tamura, K. S. (2012). Comprehensive IT study on acid/base properties of metal oxides. *Appl. Catal, A* , 135-145.

On the hydrothermal stability of MCM-41 mesoporous silica nanoparticles and the preparation of luminescent materials. (2010). *J. Mater. Chem.* , 5504-5509.

Sivasanker, S. a. (1992). Influence of Zn- and Ga-doping on the conversion of ethanol to hydrocarbons over ZSM-5. *Catalysis Letters* , 413-418.

Y. Furumoto, Y. H. (2011). Effect of acidty of ZSM-5 zeolite on conversion of ethanol to propylene. *Catalysis A: General* , 262-267.

Chapter 5: Conclusion and Perspectives

Chapter 5. General Conclusion and Perspectives

5.1. General Conclusion

The production of propylene has received broad attention in recent years due to it increasing demand. An alternative for light olefins production from naphtha is alcohol chemistry, a segment of the chemical industry that uses ethanol as a raw material for manufacturing various chemicals. The development of catalysts and processes to increase the propylene/ethylene ratio is essential to meet the propylene demand. Different types of heterogeneous catalysts were employed in literature for the direct conversion of ethanol to propylene: microporous, mesoporous etc. Generally speaking, mesoporous catalysts give propylene in high selectivities but at low ethanol conversion. The reverse was encountered for microporous catalysts. It was reported also in literature that the acidity of HZSM-5 leads to a variety of products via oligomerization reactions, particularly aromatic compounds, causing coke deposition and catalyst deactivation.

From our work, we found that the most appropriate parameters are: CBV50 ZSM-5-type zeolite and Siral-1 mesoporous catalyst as catalyst supports, 50mg for the catalyst amount and 350 °C as reaction temperature. Raw Siral-1 (350 °C, 50mg) showed 13% selectivity in propylene at t_0 (43% ethylene), while CBV50 (350 °C, 50mg) showed full conversion and 5% propene. The addition of tungsten to CBV50 increased the selectivity in propene (16 versus 5% without tungsten). Tungsten was one of the best metals impregnated leading to a low aromatics formation rate. The addition of silver was also promising but resulted in a very low carbon balance (43%). This is due to the formation of non-identified products (*i.e.* aromatics). Regarding ZSM-5 (s) also, we deduce that aromatics formation is inevitable (*i.e.*, no pure propylene without aromatics). Furthermore, we did not observe an obvious deactivation of these catalysts with coke, even after 48 hours reaction in our reaction conditions.

We deduced that there exists a complex relationship between catalyst properties (*i.e.* porous structure and acidity) and performances. Since the distribution of products obtained in the zeolitic ethanol conversion process is strongly dependent on the acidity (acid strength and number of acid sites) as well as the channel structure of zeolites, our effort had been devoted to control the acidity of zeolites by manipulating them with a variety of metals. Ethanol conversion needs moderate density and strength of acid sites. The addition of tungsten to CBV50 increases the acidity (supplementary Lewis acid sites originating from WO_3); however, the addition of silver to CBV50 decreases the acidity. We modified ZSM-5 catalysts with different metals in order to reduce the density and strength of acid sites of HZSM-5. No constant relation was observed between the SiO_2/Al_2O_3 ratio and acidity.

We could also validate from acidity measurements that the pore size of the catalyst has to be comparable to the kinetic diameter of propylene, thus limiting the accumulation of aromatic species inside the zeolite pores and allow to obtain better propylene selectivity. We found as well that Brønsted acidity of ZSM-5 catalysts is the direct responsible for the formation of propylene. Whether Lewis acidity co-exists, this affects negatively on propylene

formation. Thus, as the highest selectivity of propylene was observed for CBV50, this has a correlation with the presence of Brønsted acid sites and microporosity. In addition, we have met the phenomenon of extra-framework alumina and structure rearrangement of some ZSM-5 catalysts, which sometimes can have a positive effect on propylene selectivity. This should be validated by further characterizations in the future.

From a small study done over Na-exchanged ZSM-5 (s), we could prove that the formation of propylene using these catalysts seems to follow the so-called hydrocarbon pool mechanism. By this route, ethylene oligomerizes into higher olefins which in turn crack to give propylene. Ethylene and propylene selectivities vary reversely. No traces of diethyl ether are detected for Na-exchanged ZSM-5 (s), so only intramolecular reaction takes place here.

From FTIR studies done over H-ZSM-5 samples, we found that there is a boost of carbon species adsorbed with the increase in ethanol concentration in the feed. We also deduced that high reaction temperature leads to fast desorption of light hydrocarbons. ZSM-5 was also exchanged with sodium, which had a direct effect on acidity. As the amount of sodium increases, there is a linear decrease of Brønsted acid sites. The reverse was observed for Lewis acid sites. The decrease of the Brønsted acidity leads to an increase of the target molecule propylene.

On the other side, SAPO-34 was as-synthesized in nano-crystallites sizes. We validated the occurrence of the "modified" hydrocarbon pool mechanism involving radicals over these materials. That is to say that propylene is formed indirectly from aromatics precursors, rather than directly from ethylene oligomerization. The ionic polyalkyl benzene (PAB) species would undergo a reaction of dealkylation potentially through a pairing route to generate propylene before being dehydrogenated by the PAB, becoming inactive. This was proved through tracking of precursors intermediates and the absence of diethyl ether intermediate. This mechanism was also observed over Na-exchanged ZSM-5 (s). Nano-crystallites showed faster removal of low molecular precursors for heavy aromatics to the external surface from the pores and shorter diffusion path lengths, thus preventing the formation of larger polyaromatics. This reduces the cage effect flaw observed over SAPO-34 zeotypes.

Hydrothermally-treated ZSM-5 (s) failed to produce propylene, despite that we tried to tune the pores of the catalyst by this procedure. However, comparing the selectivities in ethanol dehydration into ethylene and diethyl ether can help understand the early stages of this reaction. Focusing on diethyl ether will also be a future work.

Strong acid catalysts (Siral 1 and 40) promote the formation of ethylene. Raw Siral-1 showed the highest amount of acid sites and notably of strong acid sites (628 µmol/g). Concerning Siral-1 mesoporous catalysts, we thought at first that mesoporosity is the reason why propylene does not form efficiently for the raw support. So, we tried to narrow down the pores through metal modification. However, we found that the dominant Lewis acidity of this type of catalyst is the obstacle preventing the formation of propylene, despite that it is a good

catalyst for ethylene formation. Brønsted sites were only observed for the CBV50-based catalysts. So silica aluminas generally are ineffective for the ethanol-to-propylene reaction.

5.2. Perspectives

In future work, it is important to increase ethanol flow and thus the productivity. I suggest using a co-feed of hydrogen as well, as this was cited somewhere else to selectively hydrogenate-dehydrate the intermediate acetone into propylene. We should also assess hydrothermal stability of the catalyst. I suggest also analyzing the effect of stream treatment on HZSM-5 catalysts during the reaction. Furthermore, I suggest making a thermodynamic study of the ethanol conversion to propylene over HZSM-5s. Additionally, we should imitate the chemical composition of bio-ethanol, as this latter is more available and cheaper than synthetic ethanol. Bio-ethanol impurities include: 1.0% v water, 0.5% v methanol and 1.96-5.0% v denaturant gasoline according to ASTM® D4806 numbers. In addition, I suggest preparing mixed ZSM-5/SAPO-34 and mixed SSZ-13/SAPO-34 catalysts. SAPO-34 at least partially overlaps on HZSM-5, which results in the interfacial interaction of HZSM-5 and SAPO-34. Such interaction significantly modifies the texture and the acidity of the composite, which in turn affects its catalytic reactivity. SSZ-13/SAPO-34 composite was not ever reported before in literature. This can be prepared by hydrothermal synthesis and physical mixture. I suggest preparing co-metal impregnated ZSM-5s, to see the effect of the metals oxides on each other and how would this affect the lifetime of the catalyst. Also I suggest validating the metathesis mechanism occurring over mesoporous catalysts via spectroscopic measurements. Last but not least, I suggest increasing the weight percentage of the sole-metals impregnated than the theoretical 10%. Finally, we already formed high selectivity for C_5 alkanes and alkenes for specific catalysts under specific reaction condition, so I suggest industrializing this in order to produce these starting from bio-ethanol.

Abstract

This work is focused on the biomass valorization through the direct catalytic ethanol transformation into propylene. We have studied different types of ZSM-5 zeolites (*e.g.* CBV 55254G and CBV 3024E), SAPO zeotypes (*e.g.* SAPO-34) and mesoporous catalysts (*e.g.* Siral-1). ZSM-5s with relevant Brønsted acidity are known for their product size-tuning effect, SAPOs for their special chabazite structure, and mesoporous catalysts for the prevention of the shape selectivity flaw. Raw supports were screened for their convenience in terms of acidity and textural properties. CBV 5524G and Siral-1 were selected to be impregnated with metals. CBV 5524G was post-treated to induce mesoporosity in its structure. CBV3024E was exchanged with sodium to attenuate its acidity. SAPO-34 was as-synthesized to evaluate the effect of crystallites size. Different characterization techniques were employed as porosimetry, XRD, XPS, TGA-MS, TPR-MS, UV/Vis spectroscopy, ICP-MS, FT-IR and NH_3-TPD. Different reaction conditions were optimized as well such as the reactant flow rate, inert gases flow rate, GHSV, catalyst mass, reaction temperature and catalyst activation. Raw CBV50 showed 5% selectivity in propylene at full conversion. Besides, raw Siral-1 (350 °C, 50mg) showed 13% selectivity in propylene (44% ethylene). The addition of W to CBV50 increased the selectivity in propylene into 16%. Ag was also promising but resulted in a very low carbon balance (43%) suggesting the formation of non-identified aromatized products. Nano-sized SAPO-34 revealed a faster removal of aromatic precursors. Further, post-treated CBV 5524Gs provided an insight on the early-stage dehydration of ethanol.

Keywords: ethanol; ethylene; propylene; acidity; channel structure; selectivity; mechanism, solid acid catalyst.

Résumé

Ce travail est focalisé sur la valorisation de la biomasse par la transformation catalytique directe de l'éthanol en propylène. Nous avons étudié différents types de zéolites ZSM-5, des zéotypes SAPO (*e.g.* SAPO-34) et des catalyseurs mésoporeux (*i.e.* Siral-1). Les ZSM-5s présentant en majorité une acidité de type Brønsted sont connus pour permettre de contrôler la taille de chaines des produits formés, les SAPOs par leur structure chabazite et les catalyseurs mésoporeux permettent une sélectivité de forme. Les supports bruts ont été criblés pour cerner le rôle de l'acidité et des propriétés texturales. Une ZSM5 (*i.e.* CBV 5524G) et le Siral-1 ont été choisis pour être modifié par des métaux et subir différents traitements (*e.g.* post traité, échange au Na, …) permettant de modifier sélectivement les propriétés sus citées. Différentes techniques de caractérisation ont été employées telles que la porosimétrie, la DRX, l'XPS, l'ATG-MS, la RTP-MS, la spectroscopie UV-visible, l'ICP-MS, l'IRTF et la NH_3-TPD. Des conditions de réaction ont été optimisées en jouant sur différents paramètres comme le débit du réactif, le débit des gaz inertes, la GHSV, la masse du catalyseur, la température de la réaction et l'activation du catalyseur. Le CBV50 brut présente une sélectivité en propylène de 5%. En ajoutant différents métaux comme le W induit une augmentation de la sélectivité à hauteur de 16%. L'Ag était aussi prometteur mais a entrainé d'une diminution drastique du bilan carbone (43%) suggérant la formation de produits aromatiques non identifiés. Le SAPO-34 de taille nanométrique conduit à une élimination plus rapide des précurseurs aromatiques. De plus, les CBV50 (s) post-traités ont fourni un aperçu de la déshydratation au stade précoce de déshydratation de l'éthanol.

Mots-clés: éthanol; éthylène; propylène; acidité; structure de canal; sélectivité; mécanisme ; catalyseur acide solide.